地震研究所彙報
Bull. Earthq. Res. Inst.
Univ. Tokyo
Vol. 73 (1998) pp. 155-265

The Source Mechanism of B-type and Explosion Earthquakes and the Origin of N-type Earthquakes Observed at Asama Volcano, Central Japan

Munehisa SAWADA*

Earthquake Research Institute, University of Tokyo

Table of contents

* Present Address: Centro Nacional de Prevencion de Desastres, Delfin Madrigal 665, Coyoacan 04360, Mexico D.F., Mexico

Abstract

B-type, explosion and N-type earthquakes recorded by short period seismographs at Asama volcano, central Japan, are analyzed. Waveforms of B-type events are gradational from a high-frequency B-type (BH-type) to a low-frequency B-type (BL-type). Medium-frequency B-type events also exist. The focal depths of BH-type events are deeper than those of BM-type and BL-type events. The low-frequency contents (1-4 Hz) which predominate in explosion and typical BL-type events are probably Rayleigh waves. We investigated a model of body-force equivalent to explain both B-type and explosion events. Six candidates were chosen for the source model of volcanic earthquakes: 1) explosive source, 2) cylindrical model, 3) tensile crack model, 4) moment tensor M_{zz} component, 5) vertical single force F_z, and 6) CLVD source model. Among six candidates we found that the moment tensor M_{zz} component was the best fit model for the 1982 April explosion event. This implies that vibrations of the explosion event were the results of both upward and downward movement of volcanic gases. For BM-type and BL-type events, we chose a cylindrical model to explain the seismograms of these events. We conclude that waveforms of both BM-type and BL-type events are excited not only by the pressure increase, but also by the pressure decrease associated with the emission of volcanic gases.

N-type earthquakes were also analyzed and found to be characterized by high-frequency beginnings and long durations. From initial motions the hypocenters of N-type events were located under the crater. The spectra of N-type events at station SAN were much stronger than those at station MAE. Stations SAN and MAE are located 2.6 km and 1.3 km east of the crater, respectively. Moreover, an investigation of the particle motion of N-type events at station SAN showed that prograde motion is dominant. Conversely, particle motion at station MAE exhibits retrograde and prograde motion appearing alternately. These observations suggest that the source of the main motions of N-type events is located near station SAN. The spectra of high-frequency portions of N-type events are very similar to those of BH- or BM-type events. We found that hybrid events that had some wave characteristics of both N-type and B-type earthquakes appeared before the occurrence of typical N-type events. Hence we conclude that N-type earthquakes are triggered by B-type earthquakes.

1. Introduction

This paper discuses the wave characteristics and the source mechanism of B-type and explosion events observed at Asama volcano. We also discuss the wave characteristics of N-type events at Asama volcano.

Asama volcano is located in central Honshu, Japan. It is an active 2,568 m high, andesitic volcano. The first historically documented eruption of the volcano was in 685 AD (e.g., INOUE, 1987). In the 1783 eruption, the resulting large pyroclastic flows and mudflows destroyed villages, and killed many people (ARAMAKI, 1963; MINAKAMI, 1942 b). During the period from 1909 to 1914, Asama volcano was very active and typical Vulcanian eruptions occurred in the summit crater. Strong earthquakes around the volcano were also observed (OMORI, 1912, 1914 a, 1914 b, 1914 c, 1917, 1919; ABE, 1979). After the eruption of February 1922, the quiescent phase lasted until April 1926. During almost three decades from early 1930 s to the late 1950 s, strong explosions accompanied by loud detonations took place in the summit crater (MINAKAMI, 1935 a, 1935 b, 1935 c, 1936, 1937, 1942 a, 1950 a, 1950 b, 1956, 1959; SAKUMA, 1951; MINAKAMI and SAKUMA, 1953; MINAKAMI and MOGI, 1959; MINAKAMI *et al.*, 1959, 1960, 1970 a; TAKEYAMA *et al.*, 1959; SEKIYA, 1961; MIYAZAKI, 1990). Last two eruptions occurred

in 1982 and 1983 (SHIMOZURU *et al.*, 1982; EARTHQUAKE RESEARCH INSTITUTE, 1983 a, 1983 b).

Seismic observations at Asama volcano were started by OMORI (1912). He conducted temporary seismic observations at Yunotaira, which is located about 2.5 km south-west of the summit crater, in September 1910. He established a volcano observatory at Yunotaira in August 1911 with financial assistance from Nagano prefecture (OMORI, 1914 a, Fig. 1). Seismic observations were implemented only during the summer season due to the rigors of winter at Yunotaira. In those days Japan was a developing nation, and the Land Survey Department of Japan first published topographical maps around Asama volcano, scale 1: 50,000 in 1916. The Yunotaira observatory was equipped with a portable horizontal two-component tremor-recorder (natural period of 4 s and magnification of 100), a single horizontal tronometer (natural period of 15 s and magnification of 150), and a vertical motion of seismograph (natural period of 10 s and magnification of 50). Each of the instruments recorded signals usually on smoked-paper drum recorders with paper speeds of 1 to 2 cm per minute. However, on special occasions, for example at the time of eruptions the paper speed was increased to 5 to 7 cm per minute.

Parmanent seismic station was newly established in 1923. To implement seismic observations throughout the year, Nagano prefecture office constructed an observatory at Oiwake located 7.6 km southeast of the crater in November 1923. The observatory was equipped with Omori-designed tronometers (natural frequency of 6 s and magnification of 70 to 100). Both observatories at Oiwake and Yunotaira were

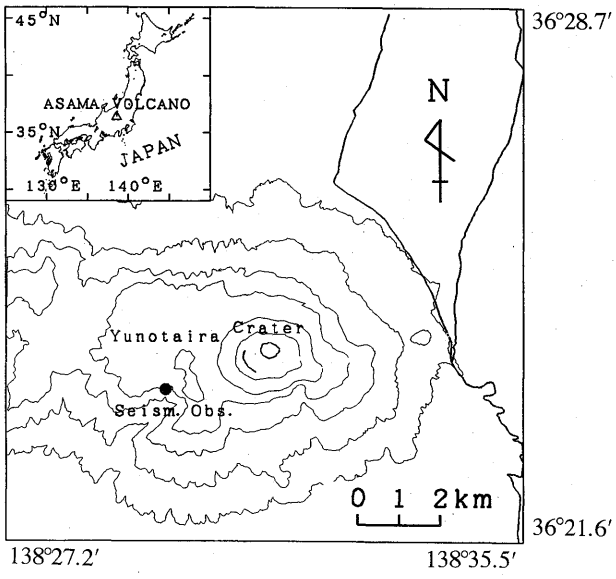

Fig. 1. Location map showing Asama volcano and the seismological observatory which was established by F. OMORI in 1911. The building was destroyed by fire in 1947, caused by volcanic bombs associated with the eruption.

transferred from Nagano prefecture to Japan Meteorological Agency (JMA) in 1926. JMA carried out the seismic observations at both observatories, and set up the Karuizawa weather station at Kutukake located 9.1 km south-east of the crater in January 1939. In August 1947, the Yunotaira observatory was destroyed by fire caused by volcanic bombs associated with the eruption. In western Japan, Kyoto University established Aso Volcanological Laboratory (AVL) in 1928. SASSA (1935, 1936 a, 1936 b) intensively investigated volcanic tremors and explosion earthquakes observed at Aso volcano.

The Asama Volcano Observatory (AVO) was set up 4.4 km east of the summit crater by Earthquake Research Institute, University of Tokyo in 1933. Seismic observations at AVO were carried out using seismographs of low sensitivity (magnification of 100 to 350) during the period from 1934 to 1952. In 1952, seismic stations of AVO were equipped with relatively high sensitivity seismographs (magnification of 4,000 to 7,000) of mechano-optical recorders having an optical lever of 1 m length. In 1954, AVO adopted a telemetering system with a transmission wire which was powered by a battery. In December 1958, electric power was supplied to AVO (MINAKAMI *et al.*, 1959). By 1963 the seismic stations of AVO had grown to 12 seismic stations. Seismic signals were telemetered by underground cables to AVO and recorded on smoked-paper drum recorders using a common time base (MINAKAMI *et al.*, 1970 a). Thus the prototype of the seismic network of AVO was set up in 1963.

Earthquake classification at Asama volcano was made by MINAKAMI (1960, 1974) based on smoked-paper records. He classified volcanic earthquakes observed at Asama into four types on the basis of smoked-paper records: 1) A-type earthquakes, 2) B-type earthquakes, 3) Explosion earthquakes, and 4) Volcanic tremor. OMORI (1912) had categorized volcanic earthquakes into two types: 1) type A earthquakes, which were associated with volcanic explosions, and 2) type B earthquakes which were not followed by explosions. OMORI's A-type events correspond to explosion earthquakes and B-type events coincided with MINAKAMI's A-type and B-type earthquakes. HAMADA *et al.* (1976) classified B-type events into two distinct categories: one was B-type event and the other was T-type event, which began with emergent P onsets followed by quasi-monochromatic oscillations of long durations. SHIMOZURU and KAGIYAMA (1989) alternately called this type of event a N-type event. TANAKA and JINGU (1979) classified volcanic earthquakes at Asama volcano into the five types including T-type earthquakes. In this study we call this type of earthquake a N-type event because the T of "T-type" event might be misunderstood as an abbreviation of "Tectonic" or "Volcano-tectonic" earthquake.

The most important observational facts in the earlier study of B-type events is that they increased in the number prior to explosive eruptions of Asama volcano (MINAKAMI, 1960). He found that the daily frequency of B-type events was the best indicator of the volcanic activity at Asama volcano. B-type events increased in number in the eruptive stage of Asama volcano and decreased in number in the calm stage. He introduced empirical formula to forecast eruption probability of Asama volcano from the daily frequency of B-type events. MINAKAMI's empirical formula

has validity today. TOKAREV (1971, 1983) carried out a similar trial to forecast eruptions of Bezymianny and other andesitic volcanoes from seismic data.

In MINAKAMI's earthquake classification at Asama volcano, B-type earthquakes occurred within a kilometer of the central crater (MINAKAMI *et al.*, 1970 a). However, his analysis was mainly based on smoked paper seismograms recorded at a paper speed of 1 mm/s. Accordingly, the hypocentral depths range of B-type events described by MINAKAMI *et al.* (1970 a) did not have good accuracy. In fact, the hypocenter depths of B-type events at Asama volcano are located in a range of 5 km to −2 km beneath sea level (e.g., KAGIYAMA *et al.*, 1985; SAWADA, 1994). Naturally, focal depths of B-type events defined by MINAKAMI *et al.* (1974) were inconsistent with those determined by high-quality seismic data recorded at other volcanoes (e.g., LATTER, 1981; ENDO *et al.*, 1981; MALONE, 1983; QAMAR *et al.*, 1983). Therefore, many volcanologists adopted a new classification based on the dominant frequencies of events, the hypocentral depths, and observable surface phenomena. However, in this study we follow MINAKAMI's earthquake classification with minor changes in the hypocentral depths range of B-type events. MINAKAMI's earthquake classification gives us comprehensive viewpoints in forecasting volcanic activity of andesitic volcanoes from seismic data (e.g., KAMO, 1978; ISHIHARA and IGUCHI, 1989; IGUCHI, 1994).

Volcanic earthquakes at Asama volcano (MINAKAMI *et al*, 1970 a; SHIMOZURU *et al.* 1975; IMAI, 1980, 1983 a, 1983 b; IMAI *et al.*, 1979; TAKEO *et al.*, 1984) share similarities in terms of seismic features to those recorded at other andesitic volcanoes, e.g., Sakurajima (MINAKAMI *et al.*, 1957; KAMO *et al.*, 1977; ISHIHARA and IGUCHI, 1989; IGUCHI, 1994; NISHI, 1980; YAMASATO, 1987), Tokachi (OKADA *et al.*, 1990; NISHIMURA *et al.*, 1990; NISHIMURA *et al.*, 1994), Suwanosejima (IGUCHI, 1991; IGUCHI and ISHIHARA, 1990; NISHI *et al.*, 1991), Pavlof (MCNUTT, 1986) and White Island volcano (SHERBURN and SCOTT, 1993).

The distribution of initial motions of explosion events is mostly compressional in all directions (MINAKAMI *et al.*, 1970 a; SHIMOZURU *et al.* 1975; YAMASATO, 1987). B-type events were classified into two subgroups: BH-type (high-frequency B-type) and BL-type (low-frequency B-type) events according to seismogram characteristics (SHIMOZURU and KAGIYAMA, 1989; ISHIHARA and IGUCHI, 1989). ISHIHARA and IGUCHI (1989) found that BH-type swarms occurred during the inflation stage with no significant changes of eruptive activity and that on the contrary, swarms of BL-type events took place during a period of rapid deflation of the summit area with the successive emission of volcanic ash and gases. IGUCHI and ISHIHARA (1989) studied the characteristics of B-type events recorded at Sakurajima volcano and found that the initial motions in both BH-type and BL-type events usually were all compressional as in the case of explosion events. Furthermore, the hypocenter depths of BL-type events were shallower than those of BH-type events. Seismic features and surface phenomena related to these events are summarized in Table 1.

The P-wave velocity structure model for Asama volcano was first proposed by MINAKAMI *et al.* (1970 b). SHIMOZURU (1979) estimated the P-wave velocity of the superficial layer at the eastern flank of Asama volcano using an air gun. SAWADA *et al.* (1983) revised the velocity structure model proposed by MINAKAMI *et al.* (1970 b).

Table 1. Observation of B-type and explosion earthquakes [Reproduced from SAWADA (1994) with permission from the Elsevier Science.]

Type of event	Distribution of initial motions	Surface phenomena
BH-type events	almost all compressional Sakurajima (IGUCHI, 1989)	not observed
BL-type events	almost all compressional Sakurajima (IGUCHI, 1989)	'soft' explosion Pavlof (MCNUTT, 1986) Strombolian eruption Sakurajima (ISHIHARA and IGUCHI, 1989)
Explosion events	almost all compressional Sakurajima (YAMASATO, 1987) Asama (MINAKAMI *et al.*, 1970a; SHIMOZURU *et al.*, 1975)	volcanic explosion

UEKI *et al.* (1982) estimated seismic Q under Asama volcano based on the coda waves of local earthquakes and BH-type events. They assumed the diffusion model (AKI and CHOUET, 1975), and found that the Q of the coda waves was frequency dependent with values increasing from 100 at 3 Hz and 150 at 6 Hz to 250–300 at 12 Hz. SUDO (1991) estimated Q_p under Aso caldera using local and regional earthquake data. He found that Q_p ranged from 50 to 100. UHIRA (1993) proposed a velocity structure model beneath Sakurajima volcano from the dispersion of surface waves excited by explosion earthquakes.

In Japan, analyses of volcanic tremors were presented by many authors. SASSA (1935, 1936a, 1936b) classified volcanic tremors at Aso volcano into four types. KIKUCHI (1962, 1964) and WADA and ONO (1963) found that volcanic tremors in the frequency range 2–5 Hz at Aso volcano were primarily surface waves. SHIMA (1958) and KUBOTERA (1964, 1974) modeled the second kind of volcanic tremor observed at Aso volcano as a spherically symmetrical fundamental mode of the vibration of a liquid sphere. SHIMOZURU *et al.* (1966) observed volcanic tremors at Kilauea volcano during the period from July to December 1963 and analyzed temporal changes in tremor spectra accompanied by eruptions. KAKUTA and IDEGAMI (1970) and NAGAMUNE (1975) analyzed C-type earthquakes that showed monochromatic sinusoidal waves at Sakurajima volcano and found that particle motion of C-type events exhibited a retrograde motion. KAMO *et al.* (1977) analyzed temporal changes in tremor spectra at Sakurajima volcano using digital filters and found that the peak frequencies of tremors varied over a very short time. MIKADA (1992) analyzed two types of volcanic tremor originating from Asama volcano. He suggested that one was probably caused by vibration of the magma conduit and the other was the result

of a successive occurrence of BL-type events.

Many papers give source models for volcanic earthquakes, especially low-frequency earthquakes and volcanic tremors. AKI *et al.* (1977) and CHOUET (1986) presented models based on random, jerky openings of fluid-filled tensile cracks driven by the excessive pressure of fluid. AKI and KOYANAGI (1981) used a fluid-filled crack model to explain seismic features of magma transport for deep tremors originating at depths around 40 km under Kilauea. FERRICK *et al.* (1982) proposed the theory that unstable fluid flows in a volcanic conduit was the common source mechanism of low-frequency earthquakes and volcanic tremors. SEIDEL *et al.* (1981) and SCHICK *et al.* (1982) presented a model involving hydraulic transients caused by escaping vapor and gas streams and resonance in a fissure and pipe network. CHOUET (1985) presented a model in which the source of tremors was the acoustic resonance of a fluid-filled volcanic pipe triggered by excess gas pressure. KOYANAGI *et al.* (1987), CHOUET *et al.* (1987) and CHOUET (1988) proposed a tremor source model based on the fluid-driven crack model.

AKI (1984) reviewed attributes and energetics of tremor occurrences and speculated on the lack of tremor occurrence at Mammoth Lakes. SHIMIZU *et al.* (1987) analyzed volcanic earthquakes associated with the 1983 Miyakezima eruption and found that the distribution of P-wave first motions could be explained by the tensile-shear crack model. GORDEEV (1992) explained that seismic signals associated with explosions consisted mostly of surface waves excited by buried P-wave sources.

UKAWA and OHTAKE (1987) analyzed a monochromatic earthquake which occurred about one year before the 1986 Izu-Oshima eruption and proposed a traction-force model for the earthquake, in which magma flowed through a conduit produced a unidirectional viscous force on the conduit wall. FERRAZZINI and AKI (1987) proposed normal modes trapped in a fluid layer sandwiched between two homogeneous elastic half spaces. KANAMORI and GIVEN (1982) and KANAMORI *et al.* (1984) analyzed the earthquake excited by the May 18, 1980 eruption of St. Helens volcano and concluded that the source was a nearly vertical single force. Since then many researchers have adopted a single force model to explain seismic waves excited by volcanic explosions (e.g., TAKEO *et al.* 1984; NISHIMURA and HAMAGUCHI, 1993; NISHIMURA *et al.*, 1994). KAWAKATSU *et al.* (1992) first observed volcanic earthquakes at Sakurajima volcano using broadband seismographs. KANESHIMA *et al.* (1996) observed long-period (15 s) volcanic tremors at Aso volcano using broadband seismographs. KANAMORI and MORI (1992) and WIDMER and ZURIN (1992) observed an unusually long Rayleigh wave train having a period of about 230 and 270 s during eruptions of Mt. Pinatubo. KANAMORI *et al.* (1994) found similar oscillations associated with the 1980 Mt. St. Helens and the 1883 Krakatau eruptions. Thus the sources of volcanic earthquakes vary widely.

Active andesitic volcanoes emit a large quantity of volcanic gases at the eruptive stage (HIRABAYASHI, 1982; OHTA *et al.*, 1988). For example, OHTA *et al.* (1988) estimated the quantity of SO_2 emissions from Asama volcano as 500 ton/day in the active stage of 1982. In the calm stage after the 1982 eruption, emission rates of SO_2 were 100 to

200 ton/day. ISHIHARA *et al.* (1983) observed explosions at Sakurajima volcano using a TV camera. They estimated the gas emission rate associated with explosions as 100–1,000 tons/s. ISHIHARA (1990) described the inflation-deflation process associated with the summit eruptions at Sakurajima volcano using water-tube tiltmeters and extensionmeters. Inflation before the eruptions was characterized by an abrupt increase of pressure at a depth 3–4 km beneath the crater; The deflation process started from the onset of eruptions with a rapid decrease of pressure at a shallow depth of 0–0.5 km.

IGUCHI (1994) analyzed the sources of B-type and explosion events at Sakurajima volcano. He concluded that the sources of explosion and B-type events were represented by a vertical expansion model. NISHIMURA *et al.* (1994) analyzed the source of BL-type events and volcanic tremor which occurred as swarms of BL-type events at Tokachi volcano. They reported that the source of BL-type events and tremor was represented by a single force model. UHIRA and TAKEO (1994) and UHIRA *et al.* (1995 a) investigated the source model for explosion earthquakes originating from Sakurajima volcano. In general, it is difficult to discriminate between the contribution from a single force F_z and that of a moment tensor M_{zz}, because Green's functions for F_z and M_{zz} are coupled (UHIRA and TAKEO, 1994). To estimate the contribution of a vertical single force of F_z, they compared two source models, i.e., a combination of six moment tensors (M_{xx}, M_{xy}, M_{xz}, M_{yy}, M_{yz}, M_{zz}) and that of a vertical single force and five moment tensors (F_z, M_{xx}, M_{xy}, M_{yz}, M_{yy}, M_{zz}). They concluded that the former model could satisfactorily explained the observed seismograms. They also found a rapid expansion followed by contraction occurred in the source regions of explosion earthquakes.

There are two ideas for the source of B-type events. One is that B-type events occurred in the edifice of the volcano due to brittle failure resulting from a strain-induced volcanic process and that emergent low-frequency waveforms of B-type events are the results of a path-effect (e.g., SHIMOZURU and KAGIYAMA, 1989; POWER *et al.*, 1994). The other idea is that B-type events occurred in the vent as a result of vesiculation or degassing process of magma in the conduit (e.g., IGUCHI, 1994; SAWADA, 1994).

The main purpose of this study is to elucidate the source process of B-type events at Asama volcano. This paper also describes the wave characteristics of B-type and explosion earthquakes at Asama volcano. We will discuss models of the equivalent body-force to explain these events. Untill now, various best-fit models of equivalent body-force have been proposed by many authors (cf. Table 8). We analyze the initial phase of seismograms of BM-type, BL-type, and explosion earthquakes and we choose six candidates for models of the equivalent body-force for B-type and explosion events: 1) explosive source, 2) cylindrical model (CHOUET, 1985; FUKUYAMA and TAKEO, 1990), 3) tensile crack model, 4) moment tensor M_{zz} component, 5) vertical single force F_z, and 6) CLVD source model. We will attemot to reduce the six candidates to two or three models in this paper. We will discuss seismic features of N-type events at Asama volcano. A discussion on seismic features of N-type

events will provide us with information of the source of B-type events. We also discuss the physical grounds why B-type events increase in number prior to eruption.

2. Seismic network of Asama volcano

Figure 2 shows permanent seismic stations operated by Asama Volcano Observatory (AVO) of the Earthquake Research Institute, the University of Tokyo (Table 2). The main recording instruments of AVO were smoked paper drum recorders until 1982. In 1982, a digital recording system was introduced to AVO. All the stations except station NAK are equipped with 1 sec short period seismometers with a damping coefficient of approximately 0.7. Frequency characteristics of the short period seismographs including amplifiers and filters are shown in Fig. 3 (curve A). Stations MAE, NAK, and SAN are three-component stations. Other stations are installed with two-component (one horizontal and one vertical) seismometers. Station NAK has 5 sec period, displacement type (magnification of 500) seismographs. The overall frequency characteristic of a 5 sec seismograph is also shown in Fig. 3 (curve B). Seismic signals from these stations are transmitted by underground cables to AVO. Seismic signals from the short period seismographs are recorded on both analog and digital magnetic tapes at AVO. Tape-recorders are controlled by an event-triggered on-line computer system. The digital system has a dynamic range of 72 dB. Analog tape recorders have a dynamic range of 42 dB. Seismic signals from these stations were also recorded by smoked drum recorders. All of the seismometers are placed on or near the ground surface.

In this study we used records from analog tape-recorders during the period from March 1982 to November 1983. As mentioned earlier, Asama volcano erupted in April 26, 1982 and April 8, 1983 and ejected a small quantity of volcanic ashes in

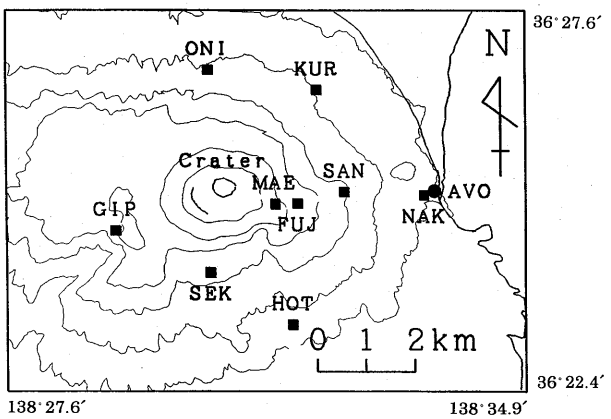

Fig. 2. Map of the permanent seismograph stations operated by Asama Volcano Observatory (AVO) of the Earthquake Research Institute.

Table 2. Stations coordinates and height.

stn No.	stn code	Latitude (N degree)	Longitude (E degree)	stn height (km)	R(km)
1	MAE	36.39905	138.53586	2.256	1.3
2	FUJ	36.39914	138.54111	2.232	1.7
3	SAN	36.40125	138.55170	1.825	2.6
4	NAK	36.40060	138.56983	1.381	4.2
5	HOT	36.37710	138.53983	1.462	3.3
6	SEK	36.38660	138.52100	1.869	1.9
7	GIP	36.39430	138.49993	2.033	2.3
8	ONI	36.42358	138.52076	1.710	2.2
9	KUR	36.41991	138.54550	1.557	2.7
10	AVO	36.40167	138.57222	1.381	4.4

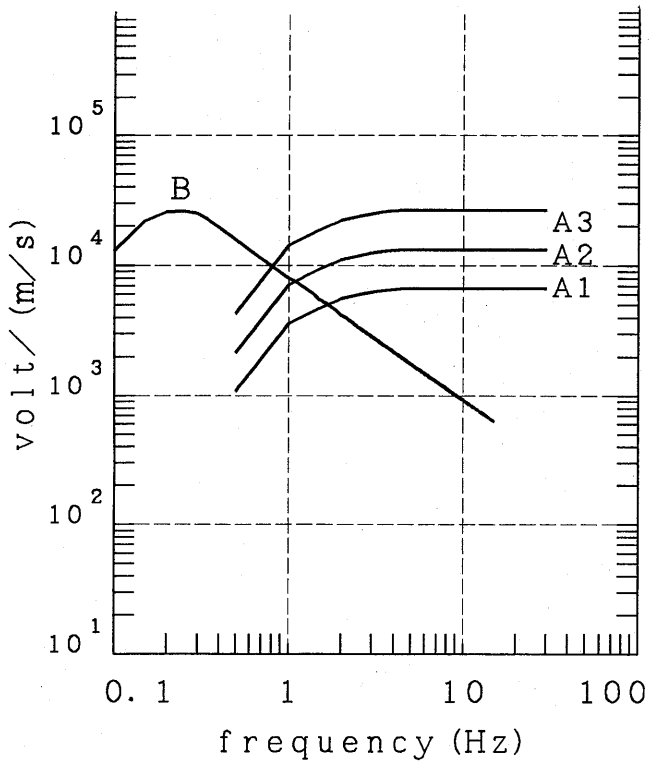

Fig. 3. Overall frequency characteristics of 1-sec natural period seismographs (curve A) and those of 5-sec natural period (curve B). A 1: station GIP (u-d: comp.); A 2: stations MAE (3-comp.), SAN (u-d: comp.), stations HOT, SEK and ONI (u-d: comp.); A 3: stations SAN (N-S, E-W: comp.), AVO (u-d: comp.) and KUR (u-d: comp). [Reproduced from SAWADA (1994) with permission from Elsevier Science.]

September 1983. The focal depths of B-type events at the eruptive stage are widely distributed from 5 km to −2 km below sea level (cf. Fig. 26, EARTHQUAKE RESEARCH INSTITUTE, 1983 a). Conversely, the hypocenter depths of B-type events at the calm stage of Asama volcano spread over a rather narrow range from 2 km to −1 km below sea level. The waveforms of volcanic earthquakes at the eruptive stage show a greater variety than those at the calm stage. Moreover, the underground cables that transmit the seismic signals from seismic stations to the AVO were constructed in 1979 and they have not been renewed until now. The cables were damaged by repeated lightning strikes. Recently seismic signals recorded on AVO have not been of good quality due to electric noise. This was the reason why we used data more than ten years earlier. However, the digital tapes during the period from March 1982 to November 1983 became obsolete and we could not read them using a computer. Therefore, we used analog magnetic tapes and the data on them were digitized at 250 samples per second for each channel using a 12-bit A/D converter. We also utilized smoked-paper records from 5 sec medium period seismometers to analyze explosion events.

3. Classification of volcanic earthquakes at Asama volcano

As mentioned previously, volcanic earthquakes observed at Asama volcano were classified into five groups according to seismogram characteristics (MINAKAMI, 1974; HAMADA *et al.*, 1976; TANAKA and JINGU, 1979). The goal of classifying volcanic earthquakes is to categorize events into classes on the basis of their source process. From this point of view, the present classification may not be the complete solution. However, except for volcanic tremors, we can distinguish four groups of seismograms. Furthermore, B-type and explosion events are considered to occur in the vent and the occurrence of B-type events has a close relation to the volcanic activity of Asama volcano (e.g., MINAKAMI, 1960). As for volcanic tremors, we have not yet finished elucidating their source process. However, we classified volcanic tremors into several types according to seismogram characteristics. Keeping in mind that most volcanic tremors appeared at the eruptive stage at Asama volcano (MINAKAMI, 1974; MIKADA, 1992), the present earthquake classification provides us with a good perspective view not only for understanding the present volcanic activity and but also for forecasting activity in the near future at Asama volcano. In the following, we describe the five types of volcanic earthquake observed at the volcano:

a) A-type earthquakes that have very similar waveforms to the tectonic earthquakes. Distribution of initial motions of A-type event is of the quadrant type (KAGIYAMA *et al.*, 1982). A-type earthquakes occur at the eastern flank (close to the station SAN) and the western flank (close to the station GIP) of Asama volcano. Fig. 4 a shows an example of seismograms of shallow A-type event that occurred at the eastern flank (close to the station FUJ). Fig. 4 b indicates those of the A-type event located beneath the western flank of Asama volcano. As shown in the seismograms, the initial motions are much clearer than those of B-type events (cf. Figs 7-9). Focal depths of A-type events that occurred at the eastern flank range from −0.5 to 4 km

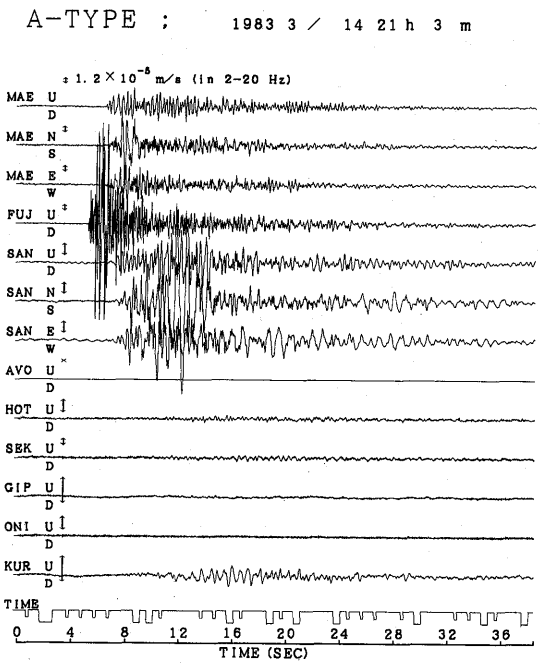

Fig. 4a. Seismograms of a A-type earthquake that occurred beneath the eastern flank of Asama volcano.

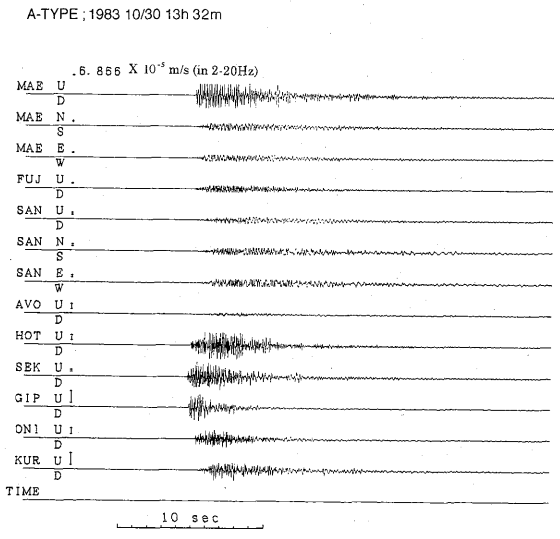

Fig. 4b. Seismograms of a A-type event located beneath the western flank of Asama volcano.

beneath sea level. Those occurring at the western flank range from 1.5 to 4 km (cf. Fig. 26). Thus A-type events seem to relate to faulting processes deep within the edifice of Asama volcano. A-type events occurring at the western flank often appeared as forerunning phenomena of volcanic eruption. In November 1958, two successive A-type events were recorded about one hour before an explosive eruption (MINAKAMI *et al.*, 1970 a). SHIMOZURU *et al.* (1975) pointed out that the seismicity of A-type events increased two months before the 1973 eruptions. However, the causality law between the seismicity of A-type events and the volcanic activity of Asama volcano is not clear at present.

b) B-type earthquakes that show wavetrains in a spindle-shaped envelope. The maximum amplitude of a B-type event is about 20μm at a distance of 2.6 km from the crater (station SAN, in Fig. 2). SHIMOZURU and KAGIYAMA (1989) classified B-type events into two subgroups: BH-type (high-frequency B-type) and BL-type (low-frequency B-type) events according to seismogram characteristics. The amplitude of the vertical component of BH-type events is smaller than that of the horizontal component. SHIMOZURU *et al.* (1975) first pointed out that in the case of dominant high-frequency B-type events (BH-type events) the maximum amplitude of the horizontal component is approximately two times larger than that of the vertical component (see Appendix). On the other hand the maximum amplitude of the vertical and the horizontal components of dominant of BL-type events show approximately the same value (cf. SHIMOZURU *et al.*, 1982).

c) N-type (T-type) earthquakes that began with emergent P onsets followed by low-frequency oscillations of long durations. This type of earthquake is categorized as a long-period earthquake (e.g., CHOUET *et al.*, 1994; CHOUET, 1996). The duration of N-type events ranges from approximately 20 seconds to 10 minutes (Fig. 5). HAMADA *et al.* (1976) first analyzed this type of volcanic earthquake. They named this type of event a T-type earthquake. SHIMOZURU and KAGIYAMA (1989) alternately called this type of event a N-type event. TANAKA and JINGU (1979) classified volcanic earthquakes at Asama volcano into the five types including N-type earthquakes. They investigated patterns of occurrence of individual types of event during the period from 1966 to 1977. They found that N-type events were not precursors to volcanic eruptions, because N-type events occurred not only at the eruptive stage, but also at the calm stage of Asama volcano.

d) Explosion earthquakes that are associated with volcanic explosions. The initial motions of explosion events are nearly all compressional at all stations at Asama volcano (MINAKAMI *et al.*, 1970 a; SHIMOZURU *et al.*, 1975). The lower limit of the amplitude of the explosion events is about 20μm at station SAN (MINAKAMI, 1960). The power spectra of explosion events have strong peaks at the fundamental frequency and at multiples of that frequency (IMAI, 1980, 1983 a). The wave characteristics of explosion earthquakes were not clear until quite recently. SHIMOZURU *et al.* (1975, 1982) estimated the magnitude of explosion events on the assumption of body waves. IMAI (1980) discussed the source process of explosion earthquakes under the assumption that seismic waves from explosion events consist of body

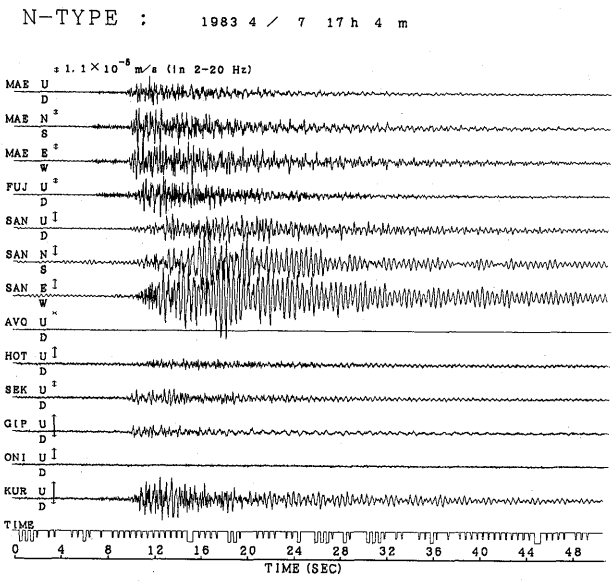

Fig. 5. An example of seismograms of a N-type earthquake.

waves.

e) Five distinct types of tremor were observed at Asama volcanoes (MINAKAMI, 1974; MIKADA, 1992): 1) volcanic tremor which BH-type events take place almost continuously (Fig. 6 a), 2) tremor with a succession of BL-type events (Fig. 6 b), 3) high-frequency continuous tremor whose spectral peaks are given by integer multiples of fundamental frequency of 0.88 Hz (MIKADA, 1992), 4) tremor having similar waveforms to C-type earthquakes observed at Sakurajima volcano, 5) volcanic tremor associated with the ejection of volcanic ashes.

4. Wave characteristics of B-type and explosion earthquakes observed at Asama volcano

4.1 B-type earthquakes

4.1.1 Seismograms of B-type events

Seismograms of B-type events have a wide variety of waveforms (Figures 7-9). B-type events begin with emergent P arrivals and show spindle-shaped envelopes. They have no distinct S phases (MINAKAMI, 1974). BH-type events start with relatively high-frequency (5-9 Hz) waves (Fig. 7). As mentioned earlier, the maximum trace amplitude of the horizontal components of BH-type events is approximately two times larger than that of the vertical component (SHIMOZURU *et al.*, 1975, 1982). Typical BL-type events are dominant low-frequency (approximately 1 Hz) waves (Fig. 8). They also show no clear S phases. B-type events with medium-frequencies start with low-frequencies (1-4 Hz), followed by high-frequency (5-9 Hz) waves (Fig. 9). This type of earthquake has so far been categorized as a BL-type event. Medium-frequency B-type events have some of the wave characteristics of both BL-type and

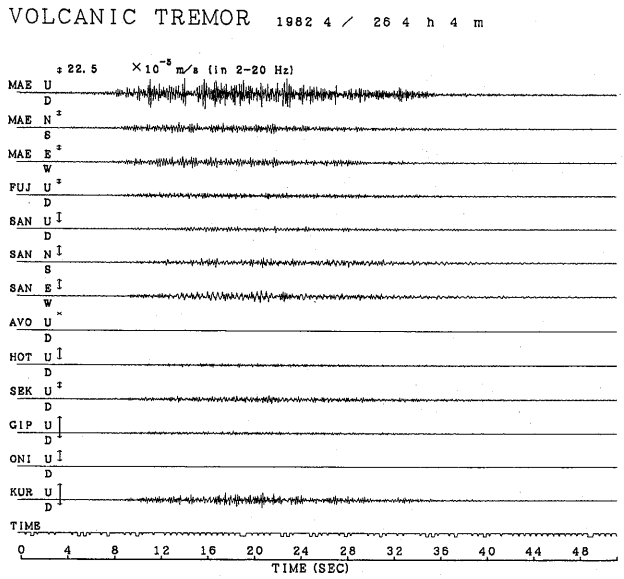

Fig. 6a. An example of seismograms of volcanic tremor a. volcanic tremor with a succession of BH-type earthquakes.

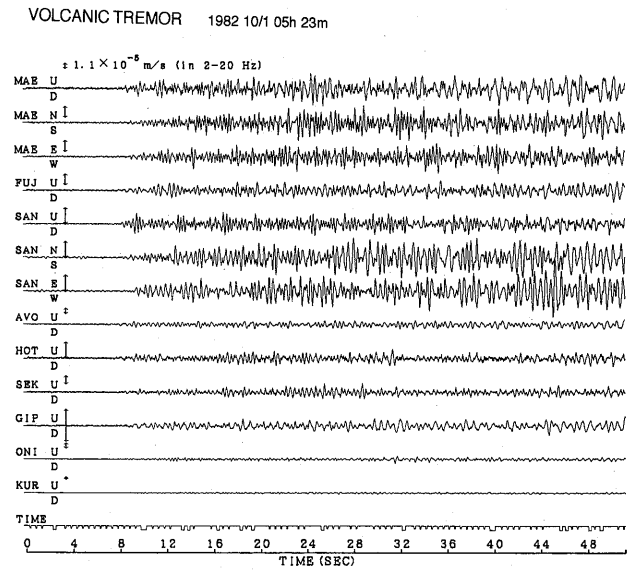

Fig. 6b. An example of seismograms of volcanic tremor with a succession of BL-type events.

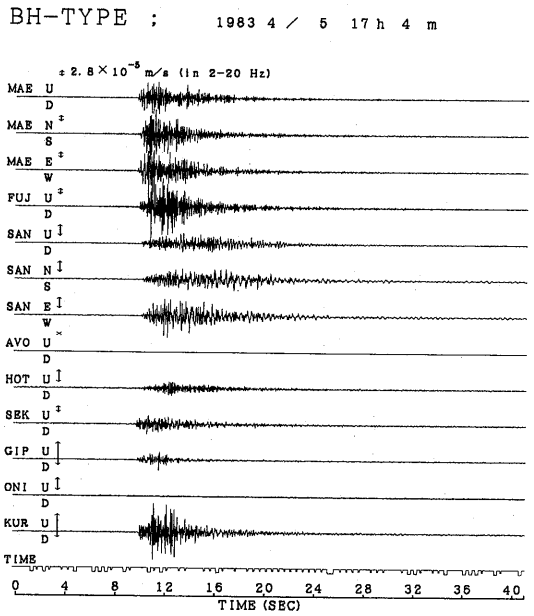

Fig. 7. Seismograms of BH-type (high-frequency B-type) event recorded by short period seismographs. Stations AVO and ONI malfunctioned. [Reproduced from SAWADA (1994) with permission from Elsevier Science.]

BH-type events, so we call these earthquakes BM-type events to distinguish them from typical BH-type and BL-type events.

4.1.2 Spectral analysis

We applied the Maximum Entropy Method (MEM) of the "one-sided Burg algorithms" (SAITO, 1978) to the spectral analysis of B-type events, because we can obtain good resolution using the maximum entropy method (e.g., KANASEWICH, 1981, p. 181; RADOSKI *et al.*, 1976). The comparison with the Sompi spectral analysis and the FFT method is shown in Appendix. To compare seismograms of B-type events (Fig. 7-9), no instrument corrections were made in the process of carrying out the spectral analysis and calculating the particle orbit diagrams.

Figure 10 gives an example of the maximum entropy (MEM) spectrum of a BH-type event for the vertical component recorded at station MAE, located approximately 1.3 km from the summit crater (see Table 2). The power spectrum has three prominent peaks at 6 Hz, around 8 Hz and 10 Hz, and a weak peak at 3 Hz. The spectrum for a typical BL-type event has strong peaks at frequencies of approximately 1, 4, 5, 7, and 8 Hz (Fig. 11). The dominant spectral peaks of a BM-type event at 1, 5, 7, and 9 Hz are shown in Fig. 12. The spectrum of a BM-type event shows a similar spectral structure in the high-frequency range (5-9 Hz) to that of BH-type events and in the low-frequency range (1-4 Hz) to that of BL-type events. However, the spectral peak of the BM-type event at the high-frequency range (5-9Hz) is

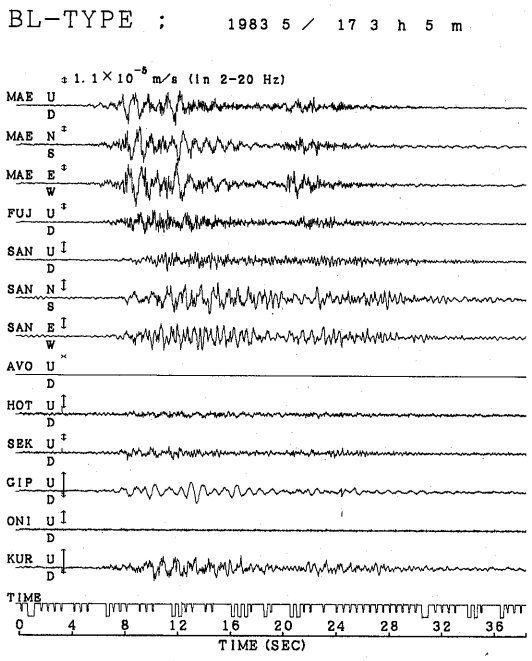

Fig. 8. Seismograms of a typical BL-type (low-frequency B-type) event recorded by short period seismographs. Stations AVO and ONI malfunctioned. [Reproduced from SAWADA (1994) with permission from Elsevier Science.]

approximately three times larger than that of a low-frequency one (cf. Fig. 12).

When we perform a spectral analysis of the volcanic earthquakes, we must keep in mind: 1) whether the peaks obtained peaks are produced by random noise or not, 2) whether those the peaks are produced at the source, or along the path, or near the station. A discussion on path or site effects can be found in FEHLER (1983), AKI (1988), CHIN and AKI (1991), FERRAZZINI and AKI (1992), and CHOUET *et al.* (1994). To discuss path or site effects we first performed a spectral analysis of non-volcanic near earthquakes. We show two examples of spectral analysis of near earthquakes (Table 3). Each data length used in the spectral analysis is 102.4 s. Fig. 13a shows the maximum entropy spectra of a near earthquake on April 18, 1982. The spectra from station KUR at the northeast foot of Asama volcano show clear peaks at 2, 4, 6, and 8 Hz. The common peaks from the three components at station MAE and the vertical component at station FUJ are at frequencies at 2, 4, and 6. Moreover, we can recognize that a very weak peak occurs at 8 Hz. The peak at 4 Hz from the vertical component from station SAN is enhanced in comparison with that from MAE, FUJ, and KUR. This is probably caused by a site effect. The spectra from station SAN show different spectral features from other stations. The energy spectra from the vertical component at station SAN are enhanced at 4 Hz. The maximum peak

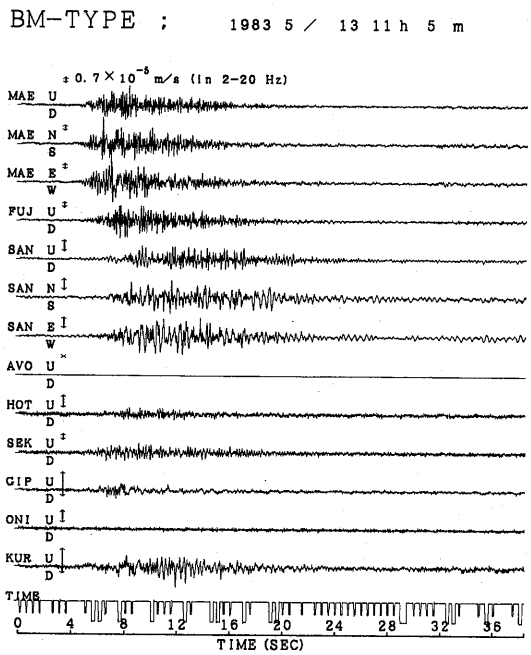

Fig. 9. Seismograms of BM-type (medium frequency B-type) event, which has the wave characteristics of both BL- and BH-type events. Stations AVO and ONI malfunctioned. [Reproduced from SAWADA (1994) with permission from Elsevier Science.]

frequencies from horizontal components of station SAN shifted to approximately 2.4 Hz. We cannot recognize the spectral peaks of 6 Hz from the east-west component at station SAN. Thus, we can see that except for station SAN the spectral peaks are common at station MAE, FUJ, and KUR. Fig. 13 b shows the maximum entropy spectra of a near earthquake on April 21, 1983. The spectra of the event on April 21, 1983 seem to be predominant of low-frequency content rather than those of the event on April 18, 1982. The spectra from station KUR and MAE and the vertical component and N-S component at station SAN show spectral peaks at 2, 3, and 5 Hz. However, spectra from the vertical components at station FUJ show no clear peak at 2 Hz. Thus we may conclude that the common peak frequencies at 2, 3, and 5 Hz of the three components at station MAE are probably not random noise but seismic signals. It should be noted that in the case of near-earthquakes the frequency range of seismic signals is less than 10 Hz (cf. Fig. 13).

We calculated stacked spectra for seismograms to eliminate the effects of random noise (e.g., FERRAZZINI and AKI, 1992). Figure 14 a shows five stacked spectra and individual seismograms of BH-type events at station MAE. For comparison, ten stacked spectra are shown in Fig. 15 b. We can see that except for a peak at 6 Hz both spectral peaks are approximately in the same frequency range below 10 Hz.

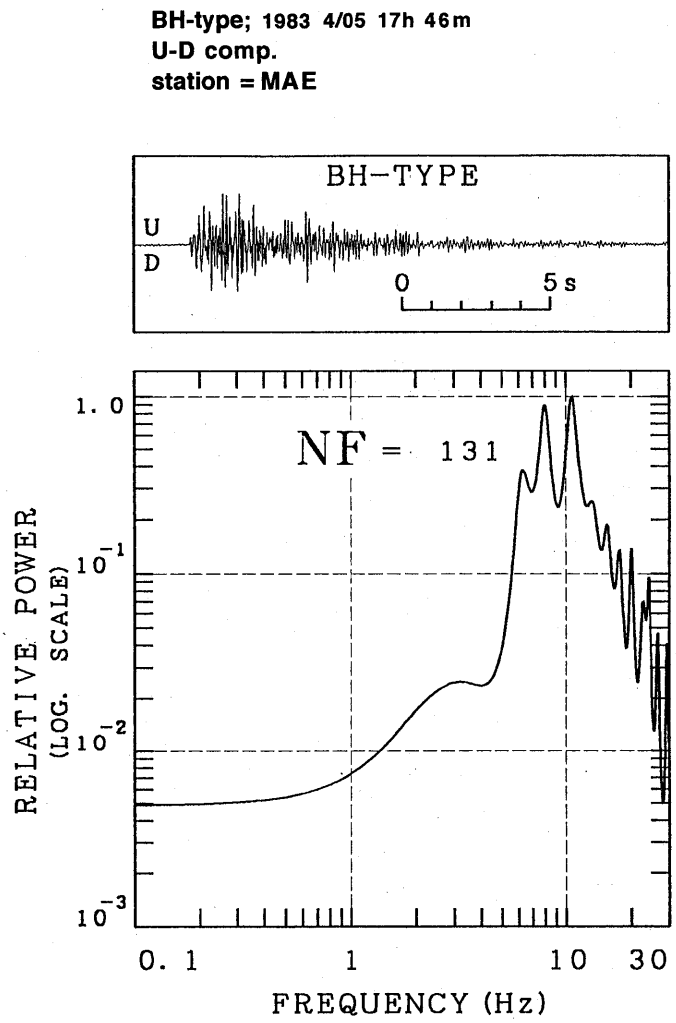

Fig. 10. Velocity spectrum of a typical BH-type event from the vertical component. "Nf" denotes filter coefficients to minimize the final prediction error (FPE) (KANASEWICH, 1981). [Reproduced from SAWADA (1994) with permission from Elsevier Science.]

Next we look at prominent peaks from ten stacked spectra. As shown in Fig. 14-15 in the cases of B-type events frequency range is much wider than that of near-earthquakes (< 30 Hz). We can distinguish four prominent peaks at about 3, 5, 7, and 9 Hz for a BH-type event (Fig. 14 b). Conversely, the stacked spectra of typical BL-type event have also five or six strong peaks at 1, 3, 4, 6, and 8 Hz (Fig. 14 c). The stacked spectra of BM-type events (Fig. 14 d) also show that spectral peaks in the high-frequency (5-9 Hz) range are very similar to those of BH-type events. Thus, the frequency ranges of spectral peaks of BH-type events and BL-type events are significantly different.

To estimate the effects of random noise and site effects we compared spectral

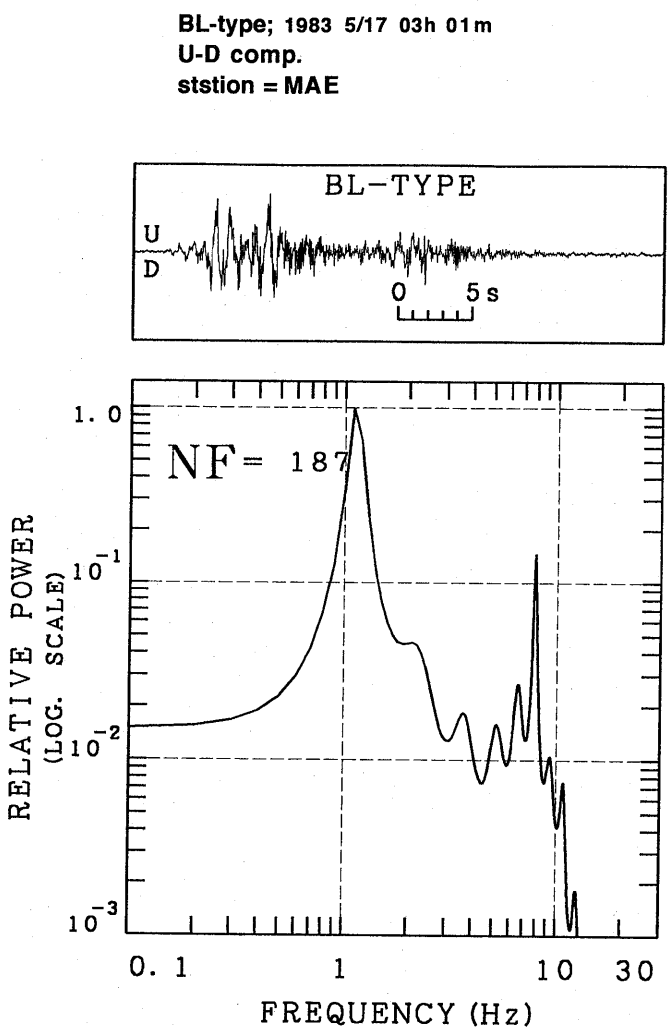

Fig. 11. Velocity spectrum of a typical BL-type event from the vertical component. [Reproduced from SAWADA (1994) with permission from Elsevier Science.]

peaks at stations FUJ and FUJ (Fig. 15). Stations FUJ and SAN are located approximately 0.4 km and 1.3 km east of station MAE, respectively (see Fig. 2 and Table 2). From Fig. 14 b and Fig. 15 a the common peak frequencies of BH-type events from three components at station MAE are at 3, 5, 7, and 9 Hz. The peak frequency at 5 Hz is not observed in the velocity spectra from the E-W component at station SAN. However, this peak frequency range at station SAN is very weak in the case of near-earthquakes. Therefore, the energy density at frequencies of 5 Hz is probably due to a source effect. We may think that peak frequencies at 3, 5, 7 and 9 Hz are attributed to the source process. As for BL-type events, the common peak frequencies of three components at station MAE are at 1, 3, 5, 7, and 9 Hz (Fig. 14 c and Fig. 15 b), and these

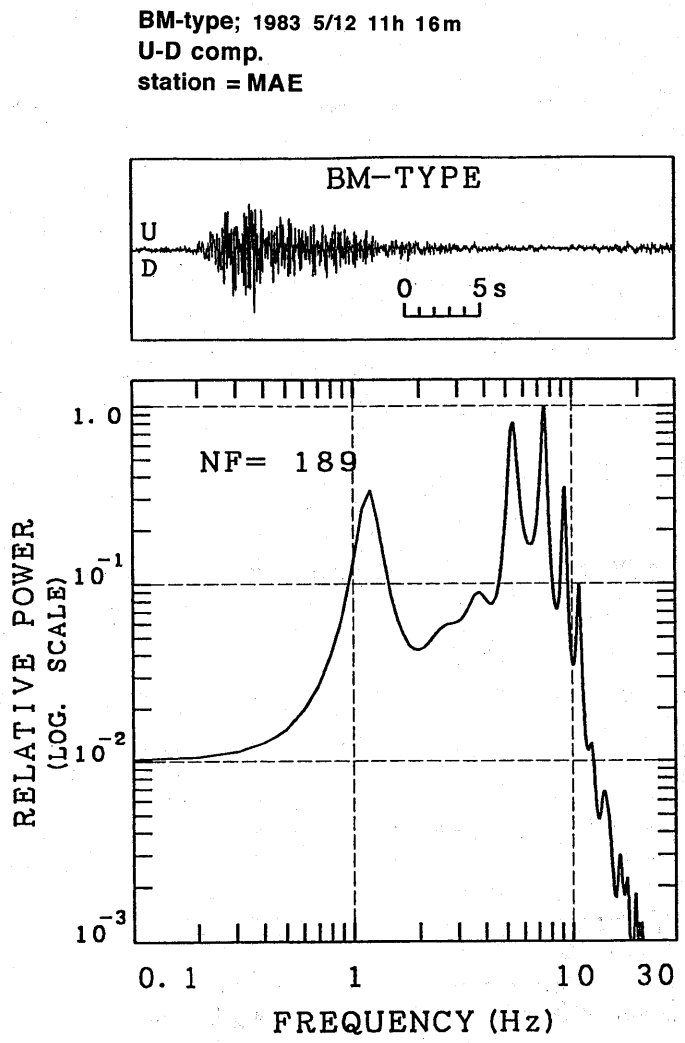

Fig. 12. Velocity spectrum of BM-type event from the vertical component. [Reproduced from SAWADA (1994) with permission from Elsevier Science.]

Table 3. List of near-earthquakes used in spectral analysis.

File name	origin time (Date Time)	latitude	longitude	hypocenter depth	magnitude
EXP824.07	'82 4/18 22h17m28.9s	37°04.0′	141°45.0′	40 km	4.2
AS8342.20	'83 4/21 13h49m10.2s	36°16.6′	140°19.3′	54 km	3.9

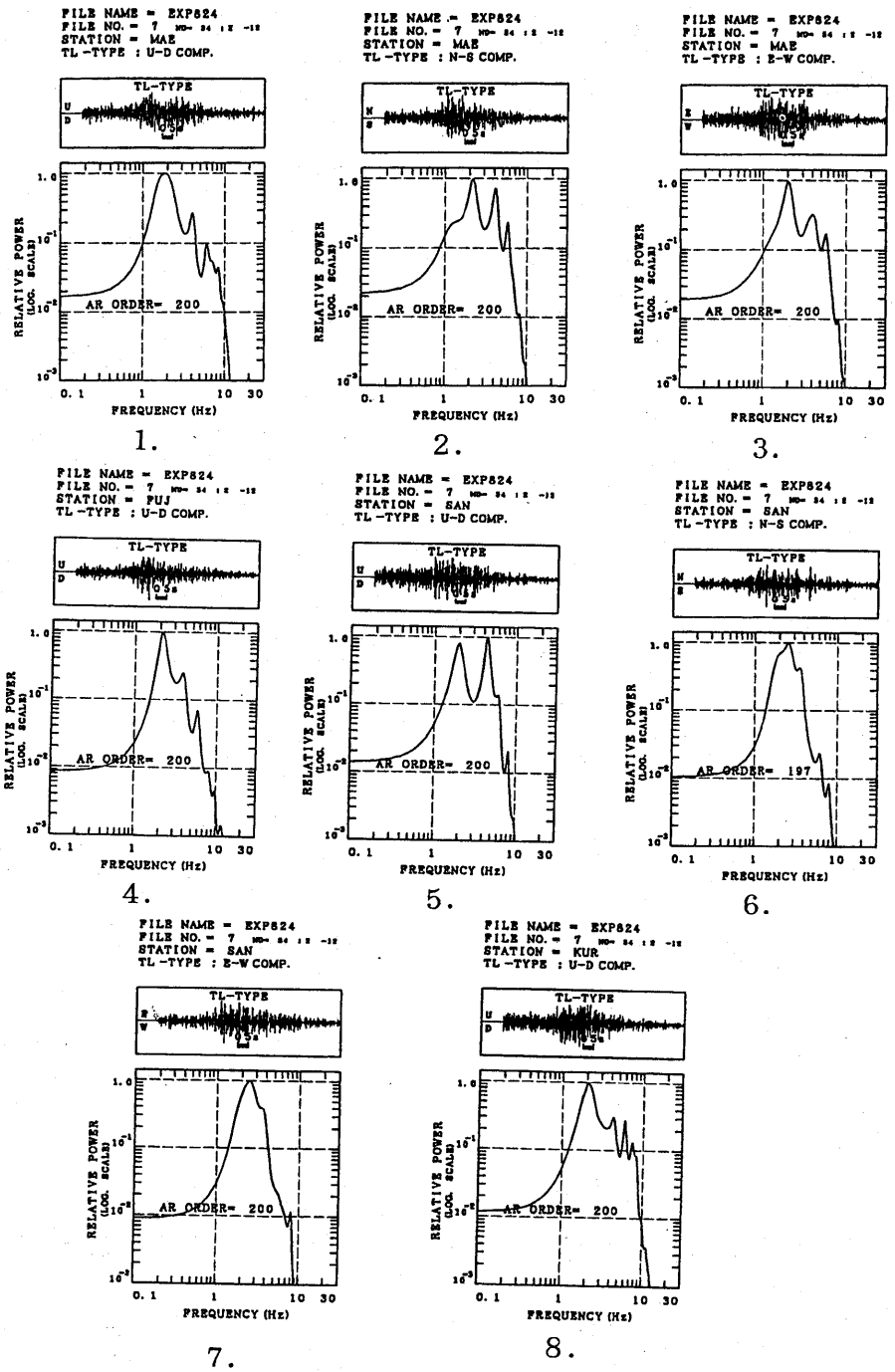

Fig. 13a. Velocity spectra of a near earthquake of Apr. 18, 1982 (1: U-D comp. of station MAE, 2: N-S comp. of station MAE, 3: E-W comp. of station MAE, 4: U-D comp. of station FUJ, 5: U-D comp. of station SAN, 6: N-S comp. of station SAN, 7: E-W comp. of station SAN, 8: U-D comp. of station KUR).

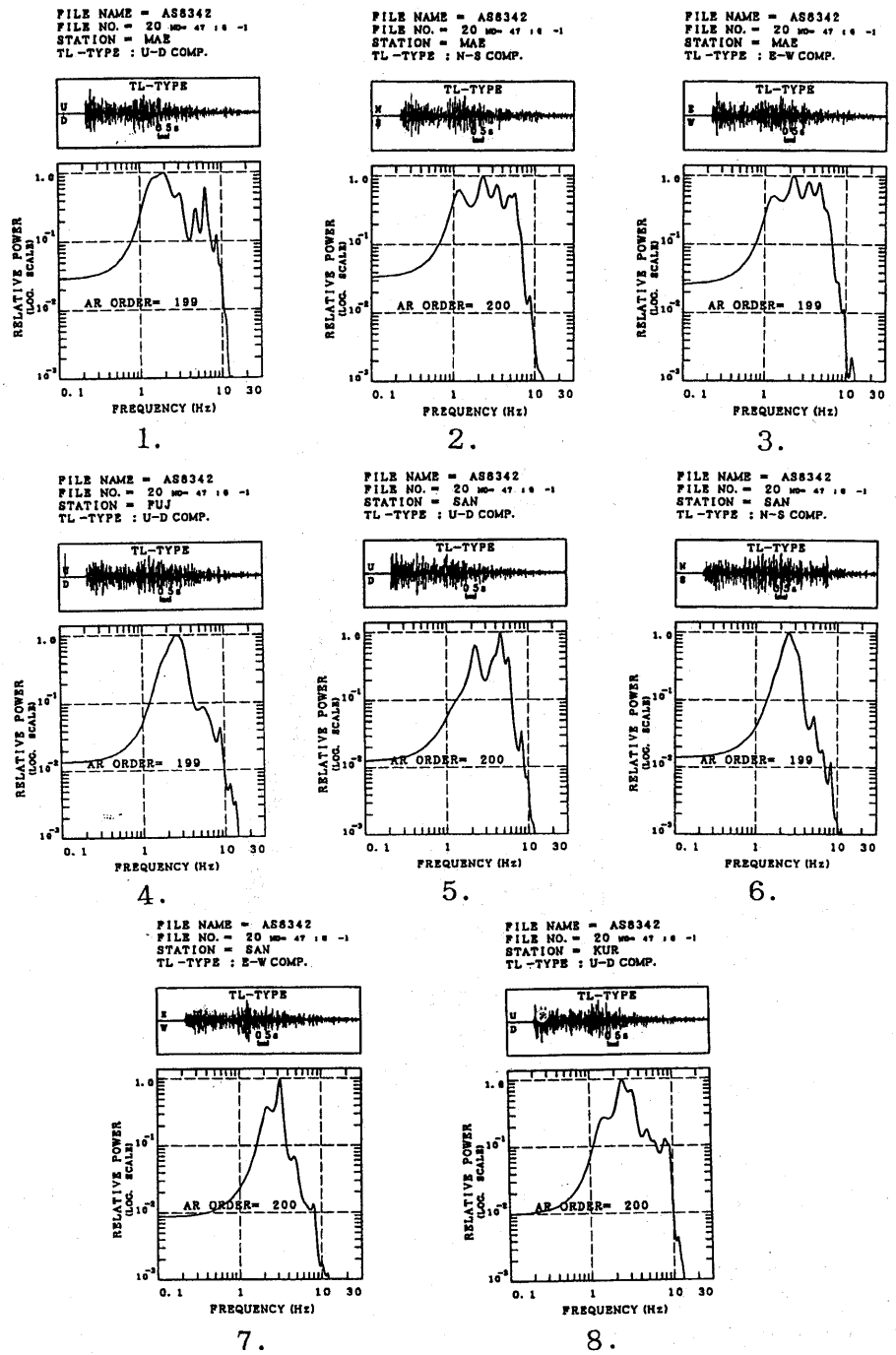

Fig. 13 b. Velocity spectra of a near earthquake of Apr. 21, 1983 (1: U-D comp. of station MAE, 2: N-S comp. of station MAE, 3: E-W comp. of station MAE, 4: U-D comp. of station FUJ, 5: U-D comp. of station SAN, 6: N-S comp. of station SAN, 7: E-W comp. of station SAN, 8: U-D comp. of station KUR).

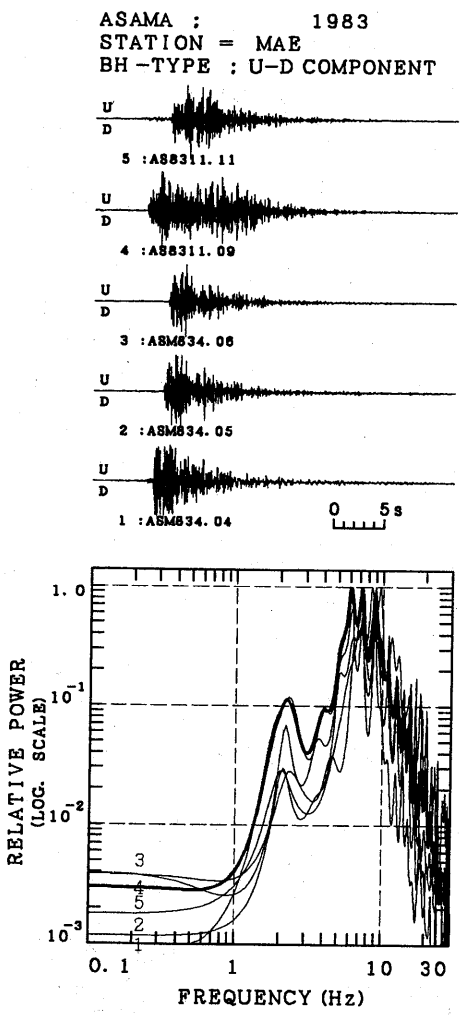

Fig. 14a. Five stacked velocity spectra of BH-type events from the vertical component at station MAE and individual seismograms of BH-type events used for velocity spectra (cf. Fig. 14b).

peak frequencies are also due to the source effects. We may conclude that these peak frequencies are excited by the source. In the same manner for BM-type events, peak frequencies at 1, 3, 5, and 7 Hz are seismic signals attributed to the source process (cf. Fig. 14b, Fig. 15c).

KAKUTA and NONAKA (1979) classified the patterns of running spectra of volcanic earthquakes into four types: 1) constant type, whose prominent peaks do not vary with time, 2) normal dispersion type, 3) reverse dispersion type 4) random type, whose prominent peaks change randomly with time.

Running spectra of BH-type events for vertical component were also examined

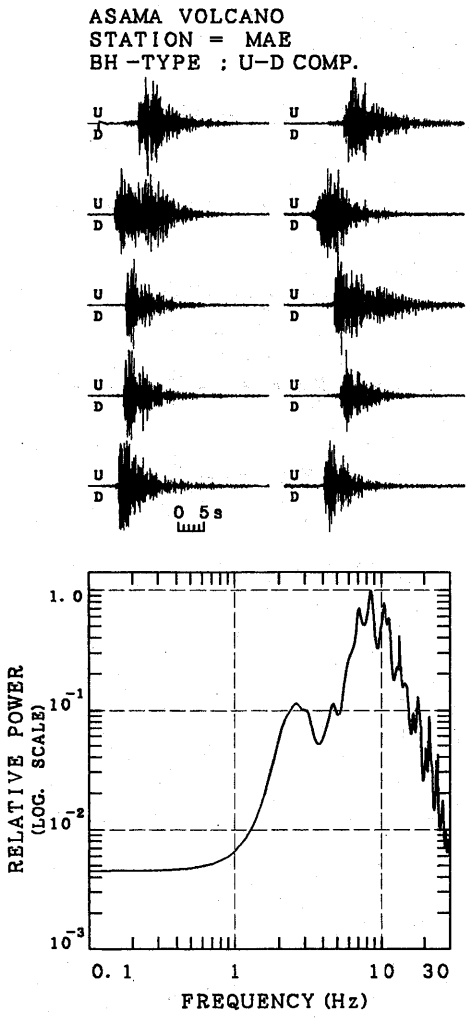

Fig. 14 b. Ten stacked velocity spectra of BH-type events from the vertical component at station MAE and individual seismograms of BH-type events used for velocity spectra (cf. Fig. 15 a).

(Fig. 16 a). One of the characteristics of the running power spectra for BH-type events is that prominent peaks randomly vary with time at the initial phase (cf. Appendix). Dominant frequency of relatively high-frequency range (5–9 Hz) wave packets lasted until a later phase (between solid arrows in Fig. 16 a). The frequency range of BH-type events is approximately from 2 to 30 Hz (cf. Fig. 16 a and Fig. 14 b). The running spectra of a BL-type event show that stable peaks appear at about 1–2 Hz and continue to a later phase (Fig. 16 b). The running spectra of a BM-type (medium-frequency B-type) event show that low-frequency (1–2 Hz) waves and high-frequency wave trains (5–9 Hz) appear first and low-frequency content soon

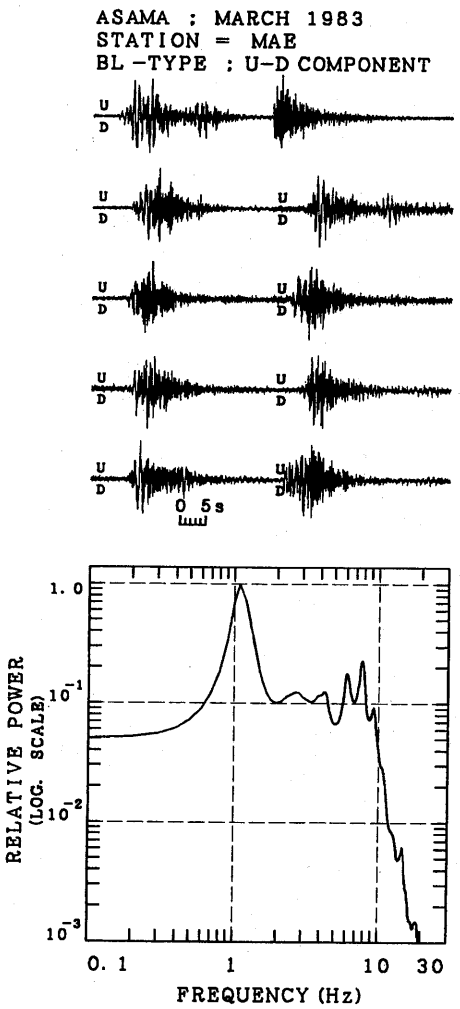

Fig. 14c. Ten stacked velocity spectra of BL-type events from the vertical component at station MAE and individual seismograms of BH-type events used for velocity spectra (cf. Fig. 15b).

dies away (between solid arrows in Fig, 16c) and high-frequency wave trains lasted a shorter time than that of BH-type events (between solid arrows in Fig. 16c). The spectral structure of the high-frequency content of BM-type events is similar to that of BH-type events. The frequency range of BM-type events of the vertical component at station MAE is approximately from 1 Hz to 20 Hz (cf. Figs. 16c and 14d). Thus, three-types of B-type events are clearly distinguishable from running power spectra.

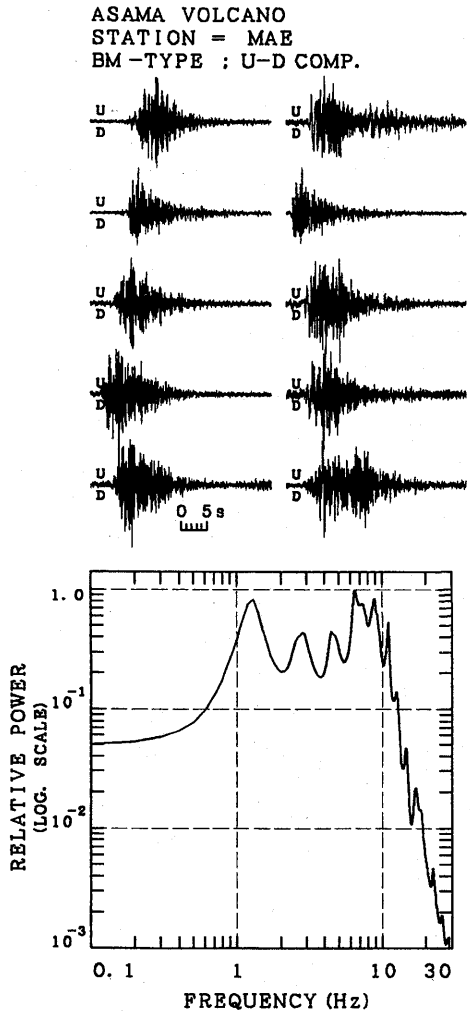

Fig. 14d. Ten stacked velocity spectra of BM-type events from the vertical component at station MAE and individual seismograms of BH-type events used for velocity spectra (cf. Fig. 15c).

4.1.3 Polarization analysis

A polarization analysis was carried out in to distinguish three types of B-type events. In particle motion diagrams the displacement amplitude was calculated from velocity amplitude by numerical integration. The displacement amplitude was filtered using a digital Butterworth band-pass filter with a zero phase shift (KANASEWICH, 1981; SAITO, 1975). The zero phase shift band-pass filter is obtained by running forward and backward over the data in the same time domain (e.g., TAKEO and ABE, 1981). Thus obtained seismic signals are normalized by the maximum amplitude of three component records.

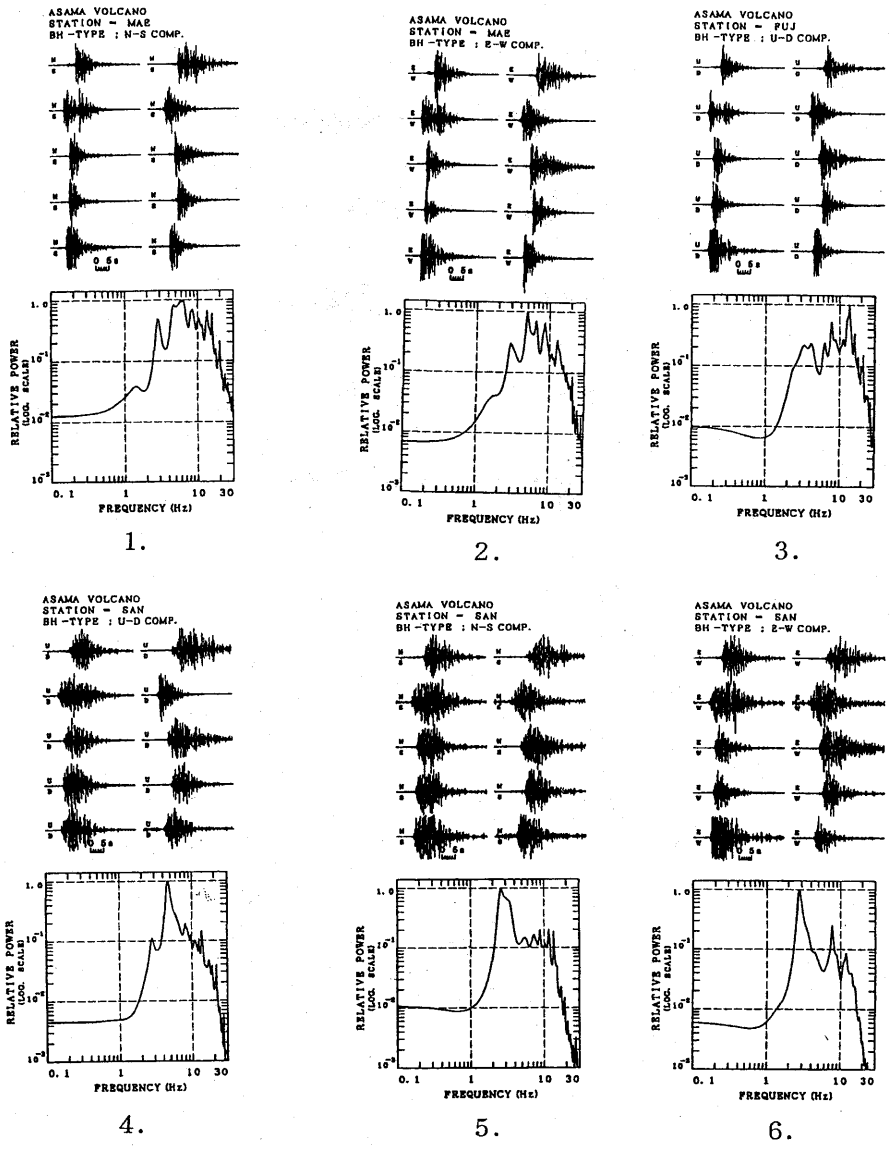

Fig. 15a. Ten stacked velocity spectra of BH-type events from other components at stations MAE, FUJ, and SAN (1: N-S comp. of station MAE, 2: E-W comp. of station MAE, 3: U-D comp. of station FUJ, 4: U-D comp. of station SAN, 5: N-S comp. of station SAN, 6: E-W comp. of station SAN).

Figures 18-20 show particle motion diagrams at the station MAE. The station MAE is situated east of the summit crater, and the seismic sources are located under the crater. Therefore, the N-S and the E-W directions approximately correspond to the transverse and the radial directions, respec-tively. The time window for the diagram is plotted in Figures. The bottom trace indicates the sense and rate of

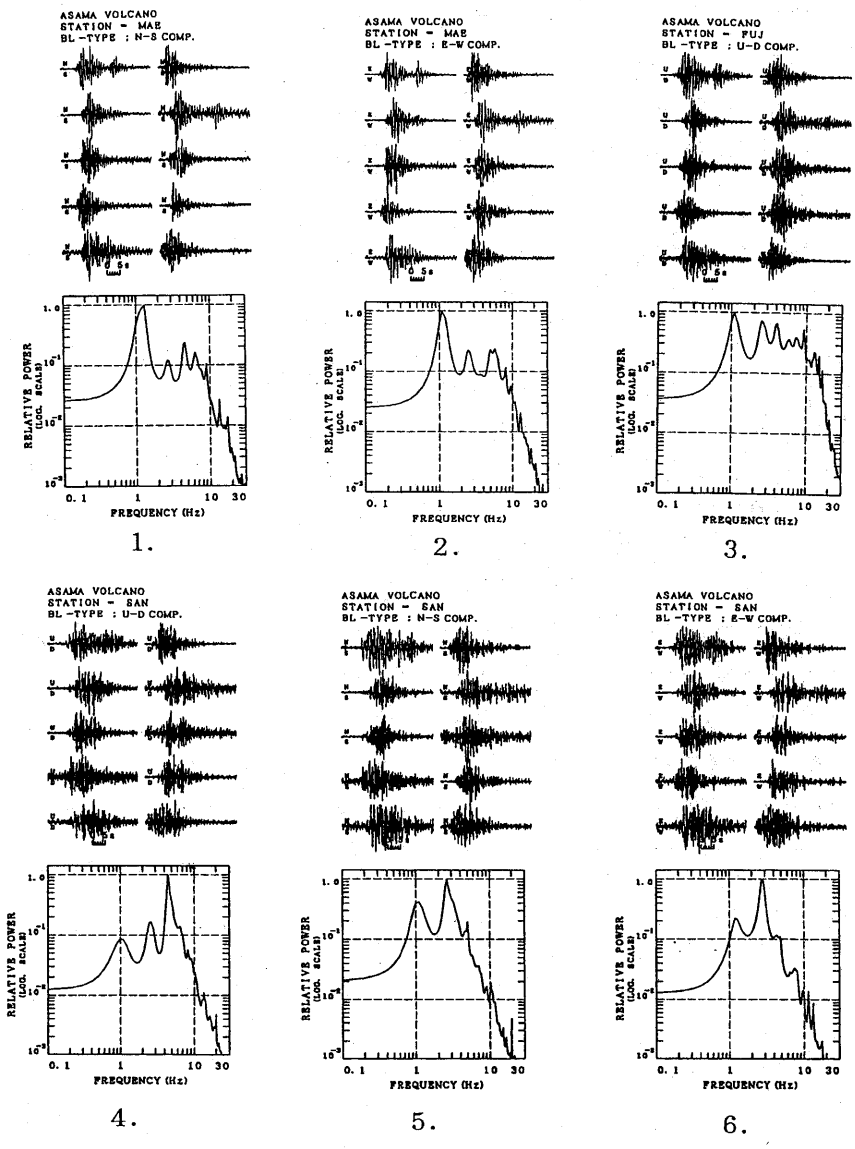

Fig. 15 b. Ten stacked velocity spectra of BL-type events from other components at stations MAE, FUJ, and SAN (1: N-S comp. of station MAE, 2: E-W comp. of station MAE, 3: U-D comp. of station FUJ, 4: U-D comp. of station SAN, 5: N-S comp. of station SAN, 6: E-W comp. of station SAN).

rotation. Let us consider the two-dimensional polar coordinates (Fig. 17). P_i is the ith position of the particle motion diagram. $P_i=(R_i, \Phi_i)$, (i=1, ..., n), where R_i is the distance from the origin of the particle motion diagram, n is the total number of data, and Φ is the angle taken counterclockwise p for the direction of propagation. We define the rate of rotation as $y_i=R_i \sin(\Phi_i)$, (i=1, ..., n). In the bottom trace, the rate

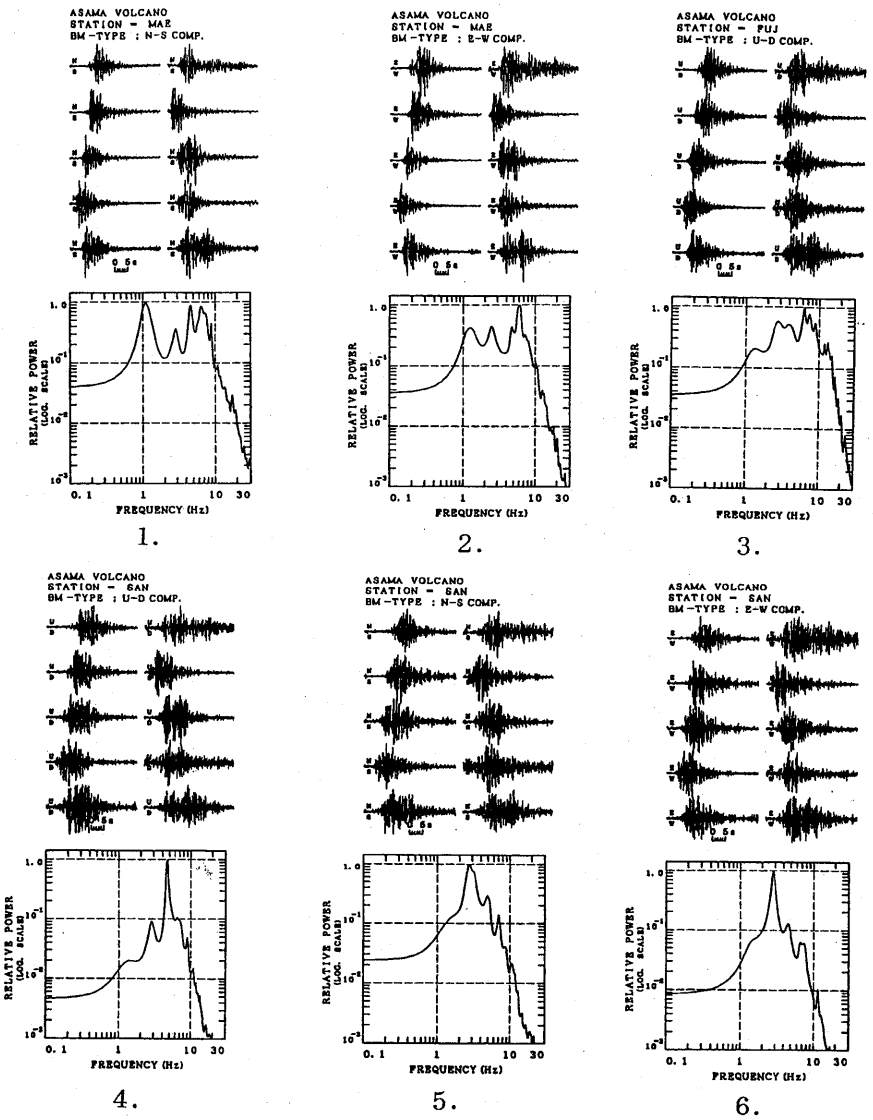

Fig. 15c. Ten stacked velocity spectra of BM-type events from other components at stations MAE, FUJ, and SAN (1: N-S comp. of station MAE, 2: E-W comp. of station MAE, 3: U-D comp. of station FUJ, 4: U-D comp. of station SAN, 5: N-S comp. of station SAN, 6: E-W comp. of station SAN).

of rotation is defined as $y_i = R_i \sin(\Phi_i - \Phi_{i-1})$, where y_i is normalized by the maximum value. Thus we can easily discriminate the sense of rotation of the seismic signals.

In the particle motion diagrams from the high-frequency content (5-9 Hz) of the BH-type event prograde and retrograde motions appear alternately. The low-frequency portions (1-4 Hz) of BH-type events also show the alternate appearance of

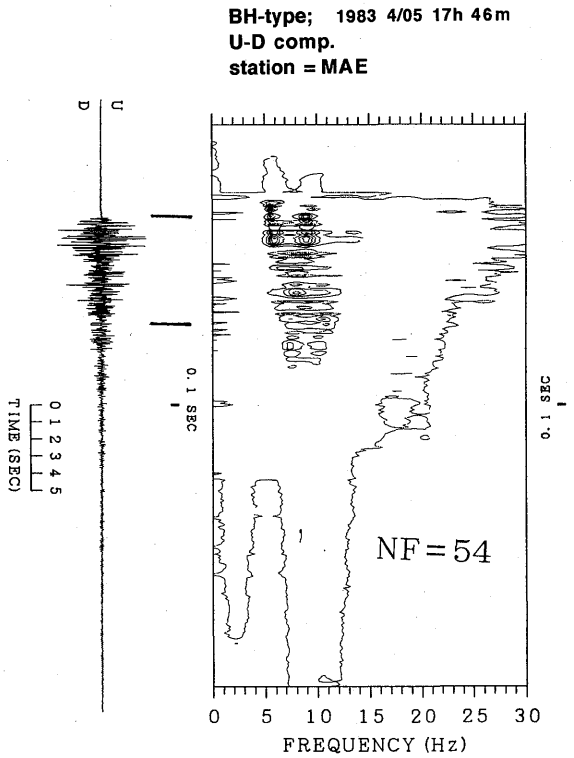

Fig. 16a. Running spectra of a BH-type event recorded at station MAE. The spectra were calculated for a 3-s time window at 0.1 s time intervals. Power spectral density is graded into ten classes on a linear scale. [Reproduced from SAWADA (1994) with permission from Elsevier Science.]

both prograde and retrograde motions, and the retrograde motion is dominant (Fig. 18b). The amplitude of the vertical component of BH-type events is smaller than that of the horizontal component. SHIMOZURU *et al.* (1975) first pointed out that in the case of BH-type events the amplitude of the horizontal component is approximately two times larger than that of the vertical component. Figure 19a shows the particle motion of high-frequency (5-9 Hz) portions of BL-type events have alternate prograde and retrograde motions. Low-frequency portions (1-4 Hz) of BL-type events exhibit that the retrograde motion is dominant. Running power spectra and particle orbit diagrams of low-frequency content suggest that the maximum amplitude portions of low-frequency contents of BL-type events probably consist of Rayleigh waves. The high-frequency portions (5-9 Hz) of BM-type events show that a prograde motion appears first then retrograde and prograde motions alternately appear (Fig. 19a). The particle motions of the low-frequency portions (1-4 Hz) of BM-type events show that the retrograde motion is dominant (Fig. 20b).

Figures 21 and 22 represent particle motion diagrams of BH- and BL-type events

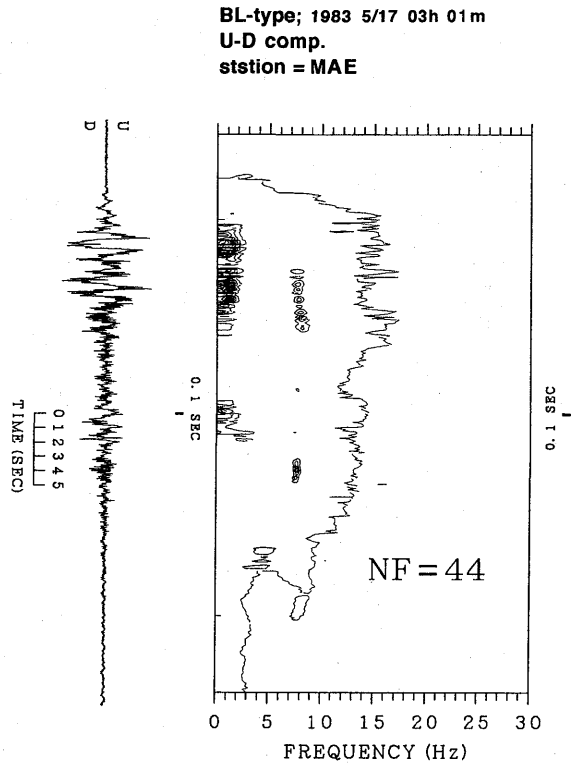

Fig. 16 b. Running spectra of a BL-type event recorded at station MAE. The spectra were calculated for a 3-s time window at 0.1 s time intervals. Power spectral density is graded into ten classes on a linear scale. [Reproduced from SAWADA (1994) with permission from Elsevier Science.]

from station SAN for a comparison with those of N-type events (cf. Fig. 56). Fig. 21 a shows particle motions for the high-frequency content of a BH-type event at station SAN. Prograde and retrograde motions alternately appear. Fig. 21 b shows particle motions for the low-frequency content of a BH-type event at station SAN. Prograde and retrograde motions also alternately appear.

4.2 Explosion earthquakes

4.2.1 Seismograms of an explosion event

An explosion earthquake was recorded by both short and medium period seismographs on April 26, 1982 (SHIMOZURU *et al.*, 1982). Seismograms from station NAK were smoked-drum records with a recording speed of 1 mm per second. Seismograms were enlarged using photographs and hand digitized. Seismic signals were corrected for mechanical distortions due to the finite pen-arm length of galvanometers (Fig. 23). This event was also recorded by short period seismographs (Fig. 24).

4.2.2 Polarization analysis

The particle motion of an explosion event also exhibits retrograde elliptical

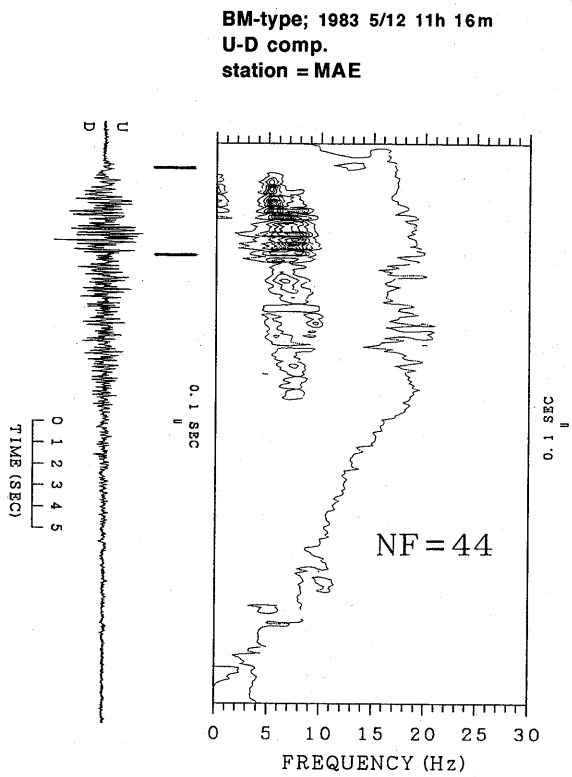

Fig. 16c. Running spectra of a BM-type event at station MAE. The spectra were calculated for a 3-s time window at 0.1 s time intervals. Power spectral density is graded into ten classes on a linear scale. [Reproduced from SAWADA (1994) with permission from Elsevier Science.]

motions (Fig. 25). The particle motions of the explosion event are similar to those of BL-type events (Fig. 19). Running spectra of explosion events at station NAK had a tendency to show a normal dispersion (IMAI, 1980, 1983 a). Therefore, we can conclude that Rayleigh waves predominate in explosion events as in the case of BL-type events. A polarization analysis of the explosion event at station MAE was also made. The seismic signals from MAE station were saturated. However, we can utilize the record to check the sense of rotation of the signals. The seismic signals start with retrograde motion, followed by prograde motion. However, the retrograde motion is dominant.

5. Hypocenter distribution of B-type and explosion earthquakes

The P-wave velocity structure under Asama volcano used for hypocenter determination is shown in Table 4. These structure parameters were based on work by MINAKAMI *et al.* (1970 b) and SAWADA *et al.* (1983). Fig. 26 shows the hypocenter distribution of A-type, B-type, and explosion events. Hypocenters of BH-type

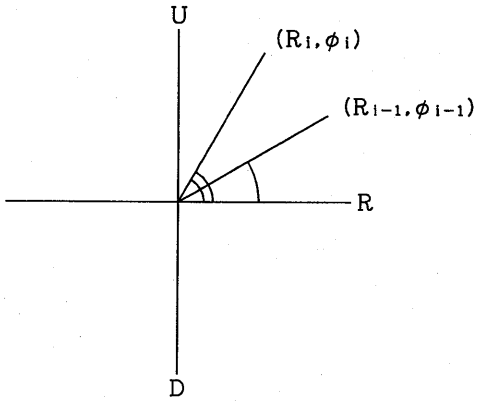

Fig. 17. Particle motion diagram. R and U respectively show the radial and the vertical components of seismic waves. R_i and Φ_i denote the distance from the origin of i-th position of particle motion and the angle taken counterclockwise for its propagation direction, respectively.

events tend to be located more deeply than BL-type and BM-type events (Fig. 26). The distribution of hypocenters suggests that these events are located in the vent, and that probably B-type events occur in relation to magma transport phenomena. MINAKAMI *et al.* (1970 a) suggested that the focal depths of B-type events were shallower than 1 km. However, his estimation was based on smoked-paper records taken at a paper speed of 1 mm/s. Thus his suggestion on the hypocenter depths of B-type events should be revised.

Fig. 27 shows the relation between dominant frequencies of B-type events and focal depths (cf. Table 5). We used the same data with those depicted in Fig. 26. At a glance we can see that BH-type events are located more deeply approximately 0.5 km below sea level. BL-type events are located shallower than about 1 km below sea level. On the other hand BM-type events are located shallower than about 2 km beneath sea level. However, as cited in Chap. 2, the seismeters of the Asama Volcano Observatory are placed at the surface of the ground and the accuracy of hypocenter determination is not so good.

Fig. 28 shows the hypocenter distribution routinely determined by Asama Volcano Observatory (modified from TSUJI *et al.*, 1990). P-wave velocity is assumed to be 2.5 km/s. We can recognize that B-type events are located under the vent in a small region at a depth range of -2 km to 0 km. A-type events are located at the western flank at a depth range of approximately 1 to 4 km, and eastern flank at a depth range of -1 to 4 km.

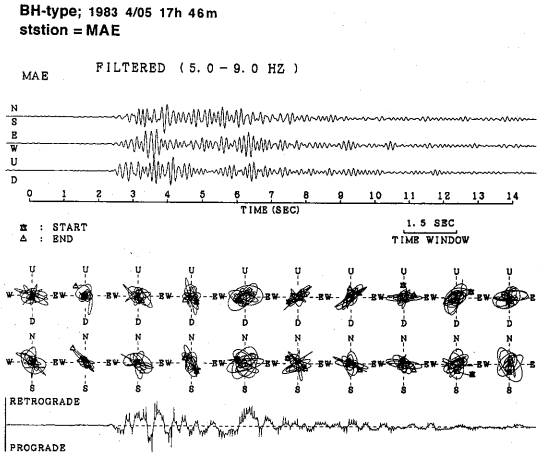

Fig. 18a. Particle motion diagram of high-frequency portion (5–9 Hz) of a BH-type event at station MAE. [Reproduced from SAWADA (1994) with permission from Elsevier Science.]

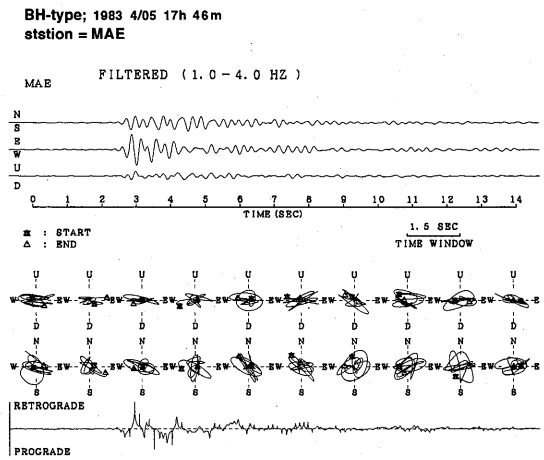

Fig. 18b. Particle motion diagram of low-frequency portion (1–4 Hz) of a BH-type event at station MAE. [Reproduced from SAWADA (1994) with permission from Elsevier Science.]

6. Source mechanism of B-type and explosion earthquakes

6.1 Waveform inversion

We discuss a model of the equivalent body-force (e.g., AKI and RICHARDS, 1980, p. 40) to explain both B-type and explosion events. Waveform inversion is very useful for investigating the source process of volcanic earthquakes (TAKEO *et al.*, 1984, 1990; HAMAGUCHI *et al.*, 1992; UHIRA and TAKEO, 1994; NISHIMURA *et al.*, 1995; UHIRA *et al.*, 1995 a, 1995 b). Here we follow TAKEO *et al.* (1990), UHIRA and TAKEO (1994), UHIRA *et al.*

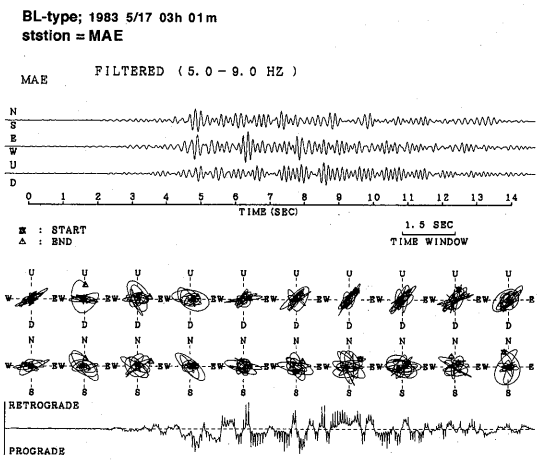

Fig. 19a. Particle motion diagram of high-frequency portion (5–9 Hz) of a BL-type event at station MAE. [Reproduced from SAWADA (1994) with permission from Elsevier Science.]

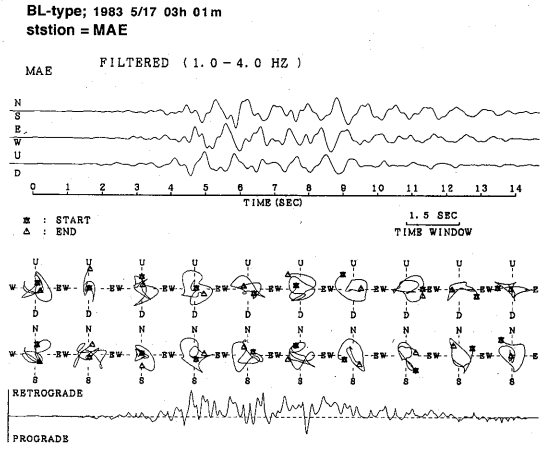

Fig. 19b. Particle motion diagram of low-frequency portion (1–4 Hz) of a BL-type event at station MAE. Retrograde motion is dominant. [Reproduced from SAWADA (1994) with permission from Elsevier Science.]

(1995a) and CHOUET (1996b).

6.1.1 Method

We assume that the observed wavelengths of B-type and explosion events are much longer than the linear dimensions of source sizes. Then, the source is effectively a point source (AKI and RICHARDS, 1980, p.50). If the l-th point source is located at ξ_l, the n-th component of the displacement at station $\mathbf{x}$ can be expressed as

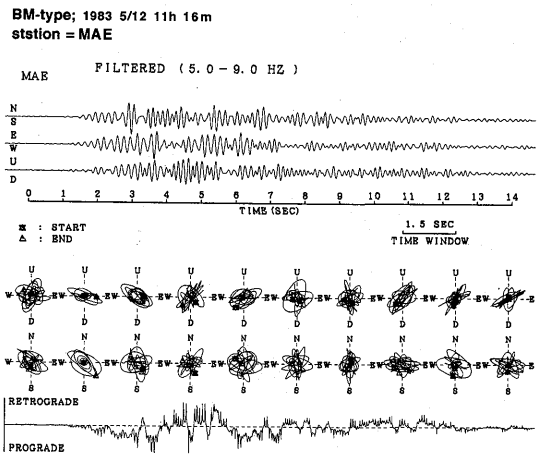

Fig. 20a. Particle motion of high-frequency content (5-9 Hz) of a BM-type event at station MAE. Prograde motion is dominant at initial phase.

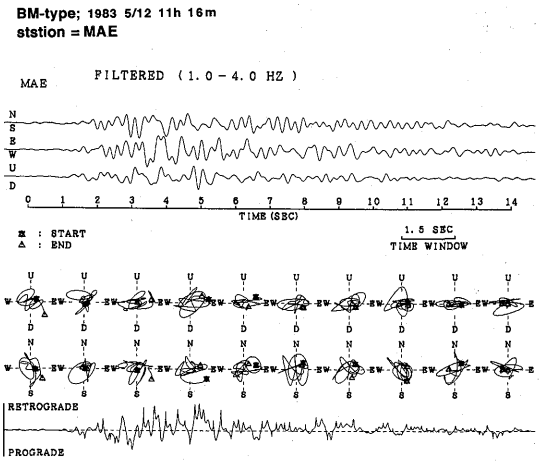

Fig. 20b. Particle motion of low-frequency content (1-4 Hz) of a BM-type event.

$$u_n(\boldsymbol{x},\ t)=\sum_l\left\{\sum_{p,q} m_l^{pq}(\tau)*G_{np,q}(\boldsymbol{x},\ t;\ \xi_l\tau)+\sum_p f_l^p(\tau)*G_{np}(\boldsymbol{x},\ t;\ \xi_l\tau)\right\}, \tag{1}$$

where * denotes a convolution of $m_l^{pq}(\tau)$ and $G_{np,q}(\boldsymbol{x},t;\ \xi_l\tau)$ or $f_l^p(\tau)$ and $G_{np}(\boldsymbol{x},t;\ \xi_l\tau)$. $G_{np,q}(\boldsymbol{x},t;\ \xi_l\tau)$ is the derivative of the Green's function $G_{np}(\boldsymbol{x},t;\ \xi_l\tau)$ with respect to the q-th component of the source coordinate ξ_l. $G_{np}(\boldsymbol{x},t;\ \xi_l\tau)$ is the Green's function for the n-th component when a unit impulse is applied at $\boldsymbol{x}=\xi_l$ at time $t=\tau$ and in the p-th direction. The components $m_l^{pq}(\tau)$ and $f_l^p(\tau)$ respectively define the time histo-

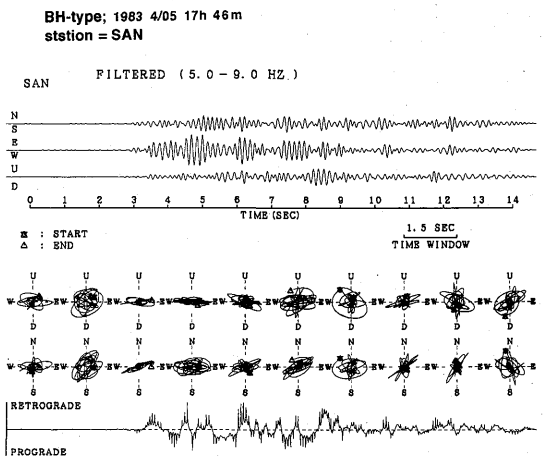

Fig. 21 a. Particle motion of high-frequency content of a BH-type event at station SAN. Prograde and retrograde motion alternately appears.

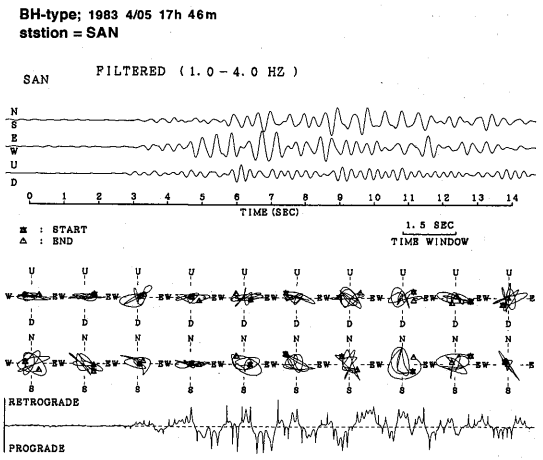

Fig. 21 b. Particle motion of low-frequency content of a BH-type even at station SAN.

ries of the (p, q) component of the moment tensor (m_{pq}) and p-th component of the single force (F_p).

The unknowns in equation (1) are the source time functions of moment tensor or force components. To solve these unknowns, synthetic seismograms of $u_n(x, t)$ are calculated for each station using simple assumed source time functions, and the errors between synthetic and observed seismograms are minimized (TAKEO, 1987; KIKUCHI and KANAMORI, 1982, 1991; TAKEO, 1992). $u_{jnl}(t; p)$ denotes the synthetic seismograms of the n-th component at station x_j due to the l-th point source, where p is a parameter that collectively represents the onset time, the location, and any other

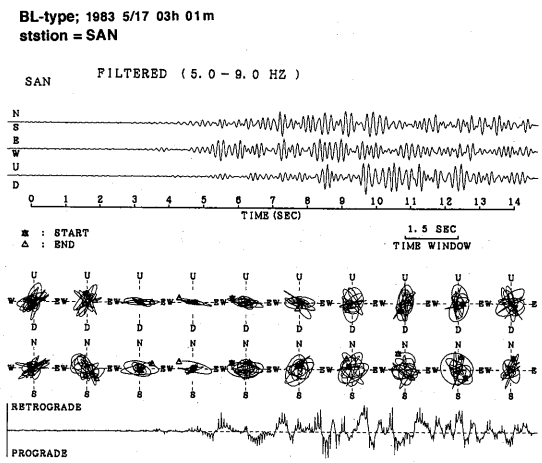

Fig. 22a. Particle motion of high-frequency content of a BL-type event at station SAN.

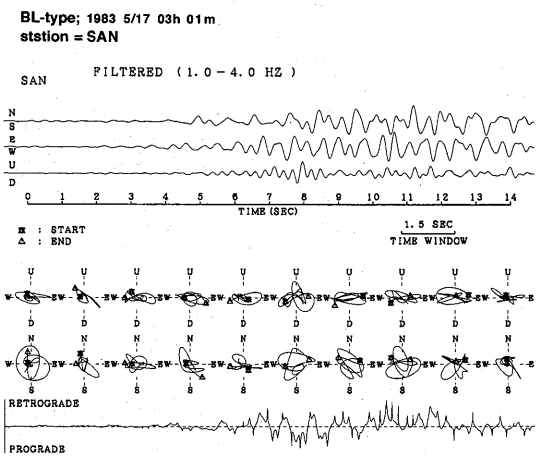

Fig. 22b. Particle motion of low-frequency content of a BL-type even at station SAN.

attributes of the source. Using $obs_{jn}(t)$ of the n-th component at station x_j for the observed seismogram, the best estimate of the coefficients for $m_l^{pq}(\tau)$ or $f_l^p(\tau)$ can be obtained from (KIKUCHI and KANAMORI, 1982, 1991).

$$\Delta = \sum_{j=1}^{N_s} \sum_{n=1}^{N_c} \int w_{jn} [obs_{jn}(t) - \sum_{l=1}^{N_b} a_l u_{jnl}(t; p)]^2 dt$$

$$= R_x - 2\sum_{l=1}^{N_b} a_l G_l + \sum_{m=1}^{N_b} \sum_{l=1}^{N_b} R_{lm} a_l a_m$$

$$= \text{minimum}, \qquad (2)$$

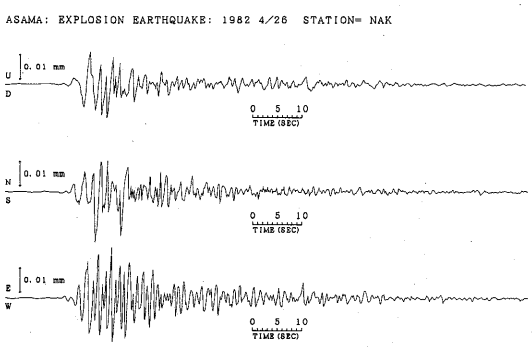

Fig. 23. Seismograms of the 1982 April explosion event recorded by medium period seismographs at station NAK. The station NAK is located about 4.2 km east of the summit crater (see Fig. 2). [Reproduced from SAWADA (1994) with permission from Elsevier Science.]

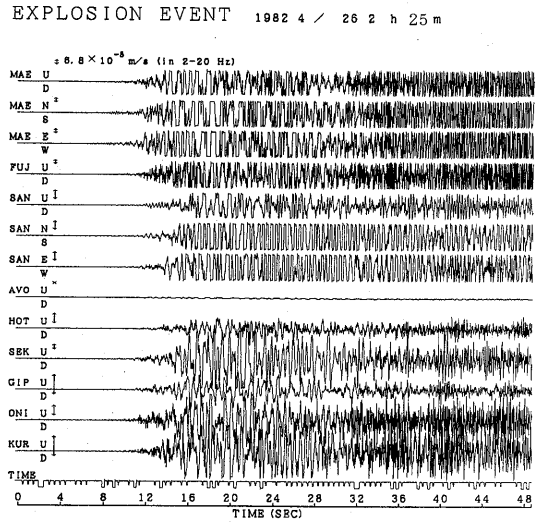

Fig. 24. Seismograms of the 1982 April explosion event recorded by short period seismographs.

where N_b is the combination of moment tensor and force components used, N_S is the number of stations, N_c is the number of components and w_{jn} is the weighting factor for seismogram.

$$R_x = \sum_{l=1}^{N_s} \sum_{n=1}^{N_c} w_{jn} [obs_{jn}(t)]^2 \, dt,$$

$$\mathrm{R_{jm}}(p) = \sum_{j} \sum_{n} \int w_{jn} [u_{jnl}(t; p)\, u_{jnm}(t; p)]^2 \, dt, \tag{3}$$

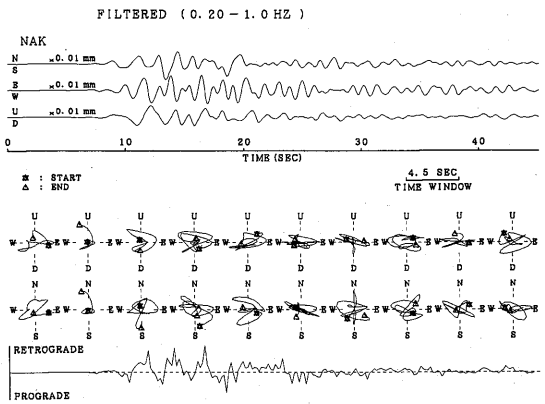

Fig. 25. An example of particle motion foran explosion event at station NAK. Prograde and retrograde motions appear alternately, though retrograde motions are dominant. [Reproduced from SAWADA (1994) with permission from Elsevier Science.]

Table 4. Asama volcano velocity model.

Layer No.	Depth to top of the layer (km)	P wave velocity (km/s)
1	-2.5	2.4
2	3.5	5.2

$$G_l(p)=\sum_j \sum_n \int w_{jn}[u_{jnl}(t;p)obs_{jn}(t)]^2dt.$$

The minimization of Δ can be obtained

$$\frac{\partial \Delta}{\partial a_l}=0;\ l=1,\cdots\cdots,N_b.$$

Then, the normal equation can be written

$$\sum_{m-1}^{Nb} R_{lm}a_m=G_l,\ l=1,\ \cdots\cdots,\ N_b. \tag{4}$$

The solution of the above equation is

$$a_l=a_l^0\equiv\sum_m R_{lm}^l G_m \tag{5}$$

where R_{lm}^l is the inverse of the matrix R_{lm}. The residual is

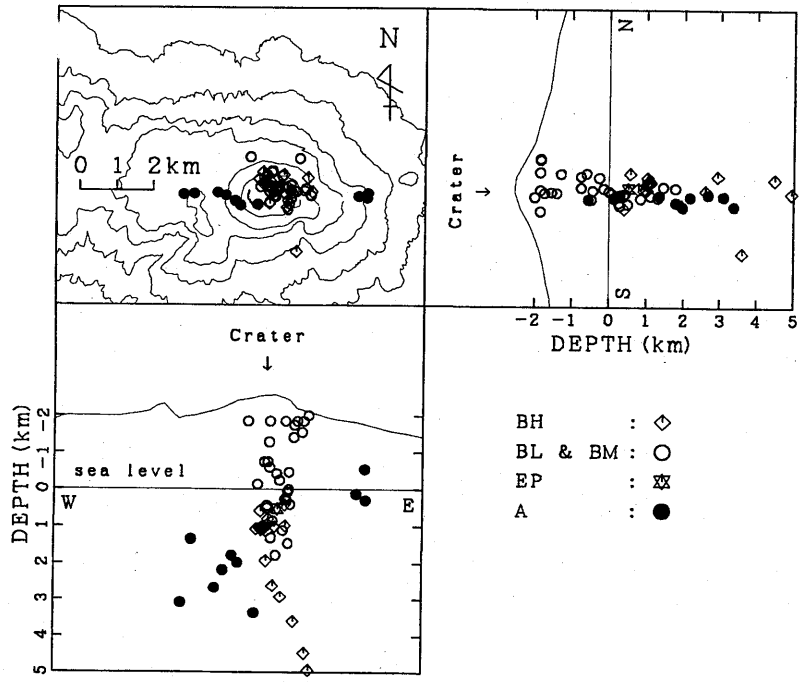

Fig. 26. Hypocenter distribution of B-type and explosion events. Velocity structure used for hypocenter determination (SAWADA *et al.*, 1983) is shown in Table 2. The asterisk denotes the hypocenter of an explosion event determined from the short period seismograms. Locations of both BL-type and BM-type events are plotted with the same symbol. The accuracy of hypocenter determination for BH-type events was about ±0.2 km for epicenters and 0.5 km for depth. That for BM-type and BL-type (including explosion earthquake) was about ±0.3 km for epicenters and ±0.8 km, respectively. [Reproduced from SAWADA (1994) with permission from Elsevier Science.]

$$\Delta = R_x - \sum_l G_l a_l^0. \tag{6}$$

The coefficients a_l and Δ depend on the parameter p. The optimum p is determined from the criterion of "minimum Δ", or

$$\Psi_M(p) = \frac{\sum_l G_l a_l^0}{R_x} = \frac{\sum_l \sum_m R_{lm}^l G_m G_l}{R_x} = \text{maximum}, \tag{7}$$

where Ψ_M is the correlation between the observed and synthetic seismograms. After the solution has been obtained, the residual waveforms are defined as

$$obs_{jn}{}^l(t) = obs_{jn}(t) - \sum_l a_l u_{jnl}(t;\, p).$$

Then the above procedure is iterated until no more significant decrease in the

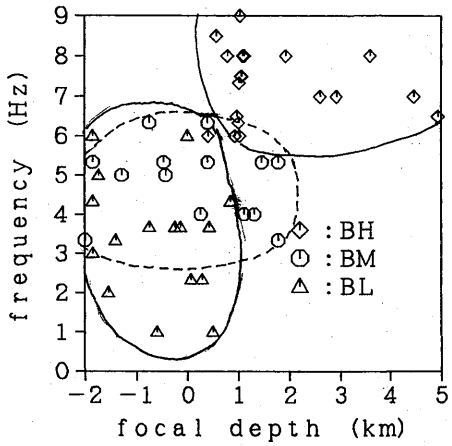

Fig. 27. Relation between dominant frequencies of events and focal depths.

error occurs. Therefore, N denotes the number of iterations (i.e., number of sub events). The squared error with N iterations is defined as

$$\Delta = \sum_n \sum_j \int w_{jn}[obs_{jn}^N(t) - \sum_l a_l u_{jnl}(t; p_n)]^2 dt.$$

6.1.2 Source models

To estimate the seismic sources of B-type and explosion events, we chose the following six candidates for the source model (cf. Table 6, KAWAKATSU, 1991):

1) Explosive source model. Explosion earthquakes at Asama volcano are almost all compressional. This model can explain the initial motions of explosion earthquakes.

2) Tensile crack model. TAKEO *et al.* (1990) investigated long-period seismic events excited by the 1987 Izu-Oshima eruptions, and they concluded that one event could be explained by horizontal tension crack opening. UHIRA *et al.* (1995 a) analyzed explosion earthquakes at Sakurajima volcano using short-period seismograms, and found that the ratio among the diagonal components (M_{xx}, M_{yy}, M_{zz}) was about 1: 1: 3. This ratio suggests that the shape of the source region is compatible with a horizontal crack opening in the vertical direction. In this study we used a model compatible with a vertical crack opening in the horizontal direction (see Table 6).

3) Cylindrical model. We consider that the shape of the vent is approximately cylindrical. CHOUET (1985) modeled the acoustic resonance of a fluid-filled cylindrical pipe triggered by excess gas pressure. FUKUYAMA and TAKEO (1990) adopted the contraction of a cylindrical model for the 1987 Izu-Oshima explosion earthquake. UHIRA and TAKEO (1994) analyzed two examples of explosion earthquakes at Sakurajima volcano using a long period (natural period of 10 s) and found that the ratio among the diagonal components (M_{xx}, M_{yy}, M_{zz}) of explosion earthquakes of October

Table 5. Relation between dominant frequencies of events and hypocenter locations.

file name	date	type of event	dominant frequencies (Hz)	hypocenter (km)		
				X	y	z
ASM834.05	Apr. 5 '83 17h46m	BH	9,6	0.23	0.56	1.06
ASM834.06	Apr. 5 '83 21h41m	BH	7,6,9	0.20	0.54	1.02
ASM834.08	Apr. 6 '83 12h50m	BH	8	0.18	0.58	1.09
ASM8342.07	Apr. 5 '83 21h50m	BH	8,7	0.05	0.64	1.07
ASM8342.11	Apr. 6 '83 15h29m	BH	9,8	0.16	0.83	0.57
ASM8342.14	Apr. 7 '83 22h12m	BH	10,8	0.15	0.52	1.04
AS8210.09	Sept. 30' 82 18h11m	BH	6,10	0.36	0.42	0.79
AS8210.16	Sept. 30' 82 18h30m	BH	4,9	0.82	0.42	0.98
AS8210.18	Sept. 30' 82 19h57m	BH	8,4	0.35	0.38	0.94
AS8210.19	Sept. 30' 82 20h07m	BH	7,4,8	0.53	0.39	1.01
EXP824.16	Apr. 26 '82 02h21m	BH	7	0.72	0.76	2.92
EXP824.17	Apr. 26 '82 02h32m	BH	8	1.07	-1.32	3.60
EXP824.18	Apr. 26 '82 02h51m	BH	6	0.28	0.72	1.03
EXP824.19	Apr. 26 '82 02h58m	BH	8	0.32	-0.02	1.93
EXP824.20	Apr. 26 '82 03h03m	BH	7	1.38	0.67	4.47
EXP824.26	Apr. 26 '82 03h02m	BH	7	0.50	0.37	2.60
AS8241.16	Apr. 26 '82 04h12m	BH	6,7	1.49	0.29	4.94
AS8342.16	Apr. 7 '83 04h34m	BH	8	0.33	0.59	1.12
AS8311.11	Nov. 26 '83 22h06m	BH	8	0.81	-0.12	0.41
ASBL1.01	Mar. 12 '83 15h44m	BL	1,8,9	1.16	1.19	-1.85
ASBL1.07	Mar. 13 '83 12h03m	BL	1,9,3	0. 41	0.86	-1.85
ASBL1.09	Mar. 13 '83 14h56m	BL	1	0.33	0.01	0.50
ASBL1.10	Mar. 13 '83 19h29m	BL	1,7,3	0.08	0.43	-0.14
ASBL1.11	Mar. 14 '83 03h58M	BL	1,2,8	0.35	0.43	-0.75
ASBL1.12	Mar. 14 '83 11h29m	BL	2,1,6	-0.18	1.23	-1.85

(To be continued)

Table 5. (continued)

file name	date	type of event	dominant Frequencies (Hz)	hypocenter (km)		
				X	Y	Z
ASBL1.15	Mar.14 '83 13h28m	BL	1,2,7	1.06	0.30	-1.41
SBL1.18	Mar.15 '83 12h11m	BL	8,1,4	0.49	0.16	0.85
ASBL1.20	Mar.16 '82 21h39m	BL	1,3,7	0.33	0.29	0.43
ASBL1.24	Mar.17 '83 01h41m	BL	1,8,9	0.92	0.35	0.00
ASBL1.25	Mar.17 '83 03h01m	BL	1,4,2	0.89	0.30	0.07
ASBL1.27	Mar.17 '83 05h46m	BL	2	1.29	0.32	-1.55
ASBL1.28	Mar.17 '83 08h06m	BL	1,3,7	0.67	0.72	-0.25
ASBL2.02	Mar.13 '83 15h49m	BL	1,4,2	0.87	-0.03	0.29
ASBL2.05	Mar.13 '83 19h29m	BL	1	0.40	0.83	-0.60
ASBL2.14	MAR.14 '83 18h14m	BL	2,8	1.08	0.30	-1.74
ASBL1.04	Mar.13 '83 11h16m	BM	8,5,3	0.92	0.47	1.46
ASBL1.05	Mar.13 '83 11h34m	BM	6,1,3	0.58	0.44	1.78
ASBL1.06	Mar.13 '83 11h43m	BM	8,5,1	0.96	0.25	0.40
ASBL1.14	Mar.14 '83 12h31m	BM	6,4,2	0.76	0.23	1.11
ASBL1.17	Mar.14 '83 23h05m	BM	7,1,4	0.82	0.05	0.26
ASBL1.21	Mar.16 '83 23h21m	BM	6,1,3	1.46	0.19	-2.00
ASBL1.23	Mar.17 '83 00h46m	BM	8,1,3	0.45	0.18	1.31
ASBL2.13	Mar.14 '83 13h28M	BM	5,2,8	0.59	0.37	-0.43
ASBL2.21	Mar.15 '83 04h06m	BM	5,2,9	1.33	0.38	-1.85
ASBL2.22	Mar.15 '83 04h56m	BM	8,6,1	0.39	0.82	-1.29
A.SBL2.23	Mar.15 '83 07h37m	BM	5,8,3	0.83	-0.19	-1.85
AS8241.02	Apr.16 '82 23h24m	BM	7,9,3	0.26	0.75	-0.75
AS8311.05	Oct.24 '83 15h59m	BM	6,8,2	0.93	0.13	-0,47
AS8311.06	Oct.24 '83 23h38m	BM	7,8,1	0.58	0.44	1.78
AS8311.08	Oct.25 '83 04h50m	BM	2,9,8	0.96	0.25	0.40
Expl.	Apr.26 '82 02h04m	Exp.		0.61	0.43	0.53

30, 1986 was approximately 1.8 : 1.8 : 1. This ratio suggested that the shape of source region was approximately cylindrical.

4) Vertical expansion model. IGUCHI (1994) analyzed B-type and explosion earthquakes and showed that M_{zz} component was dominant and the contribution of M_{xx} and M_{yy} was very small. UHIRA *et al.* (1995 a) also confirmed the predominance of M_{zz}. However, they pointed out that M_{xx} and M_{yy} were not small enough to be ignored.

5) Vertical single force model. KANAMORI and GIVEN (1982) first adopted a vertical single force model for the explosion earthquakes of the 1980 eruption of St. Helens volcano. Many researchers discussed the source model for volcanic earthquakes based on a vertical single force model (TAKEO *et al.*, 1984, 1990; HAMAGUCHI *et al.*, 1992; NISHIMURA and HAMAGUCHI, 1993; NISHIMURA, 1995).

6) CLVD source model (see Table 6). KNOPOFF and RANDALL (1970) named earthquake source moments of the kind which have no volume change, no net force, and no net torque, a compensated linear vector dipole (CLVD). In the principal-axis coordinate system, it consists of three orthogonal force-dipoles with moments in the ratio $2 : -1 : -1$. Earthquakes generated by injecting fluid into a crack are expressed by CLVD mechanisms. This type of earthquake was observed at Long Valley caldera, California in 1980 and geothermal areas, Iceland (JULIAN and SIPKIN, 1985; FOULGER and LONG, 1992).

6.1.3 Source time function

We assumed three functional forms for the source time functions for $m_t^{pq}(\tau)$ and $f_t^p(\tau)$: 1) a parabolic triangle function, 2) a triangle function, and 3) a ramp function. To determine the number of iterations (e.g., the number of sub-events), we compared the results of waveform inversion using parabolic triangle, triangle and ramp functions for the source time function. Then we performed the iterations under the condition that no significant differences were recognized for the cumulative source time function. Thus we determined the number of iterations to be five. The waveform match was not significantly improved after the fifth iteration. After we determined the number of iterations, we compared the residual for these three functional forms of source time functions. Finally, we used a parabolic triangle function as the source time function, because the residual is th smallest. The peak values were determined by inversion for assumed duration time.

6.1.4 Green's functions

We calculate Green's functions for free surface displacement using reflection-transmission matrices (KENNET and KERRY, 1979), and the discrete wave number method (BOUCHON, 1979, 1981) assuming a velocity structure represented by an anelastic layered half-space. The effective Q values, which are dimensionless measures of anelasticity, are assumed to be constant over the range of observed frequencies. Then, the effects of anelasticity are introduced using dispersive complex velocity (LIU *et al.*, 1976; AKI and RICHARDS, 1980, p.180; TAKEO, 1985).

The geometry and the coordinate systems are given in Fig. 29. The source is located in the layered half-space at Cartesian coordinates (R, T, U), where R, T, and

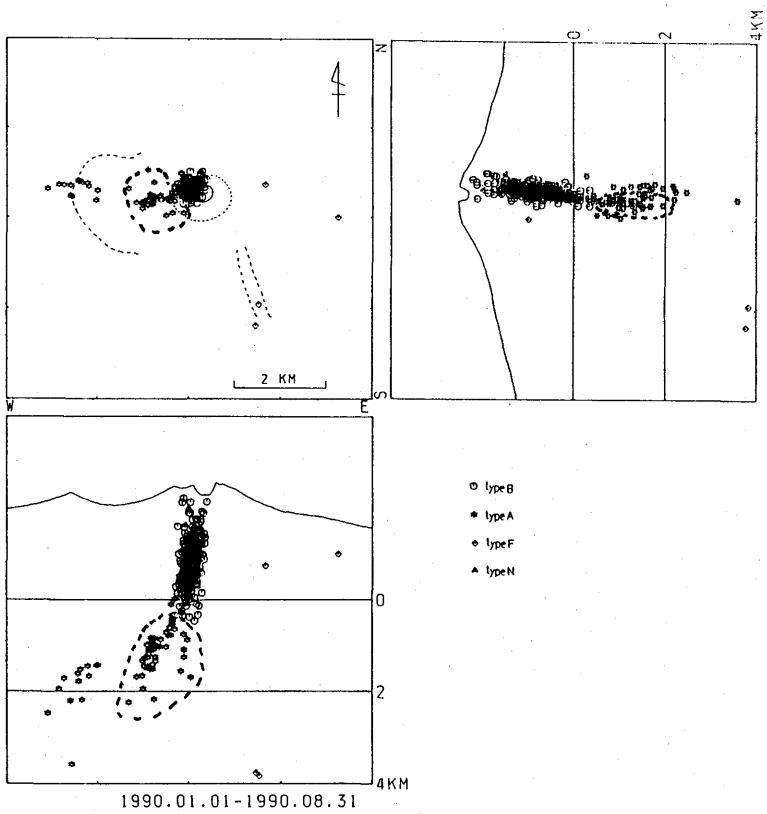

Fig. 28. Hypocenter distribution of volcanic earthquakes routinely determined by Asama Volcano Observatory (From TSUJI *et al.*, 1992). P-wave velocity is assumed to be 2.5 km/s. Symbols of A-type events in hatched regions should be corrected by replacing with them of B-type (BH-type) events. Type F earthquake denotes A-type event occurring beneath the east flank of Asama volcano.

U represent radial, transverse, and vertical components. The receivers are located on a ree surface at Cartesian coordinates (X, Y, Z), where X, Y, and Z denote east-west, north-south, and the vertical components, respectively. The direction of the source is defined from the dip angle and the azimuth. In Fig. 29, THET and PHI denote the dip and the azimuth for the source, which are measured clockwise from the Z-axis to the U-axis along the X-axis and anticlockwise from the X-axis to the R-axis along the Z-axis, respectively. Units of THET and PHI are represented by degrees.

The layered structure used for Green's functions calculations is shown in table 7. UHIRA and TAKEO (1994) used the Q_p value of 70 for the uppermost layer at Sakurajima volcano, and UHIRA *et al.* (1995 a) adopted Q_p value of 60 at Unzen volcano. IGUCHI (1994) used Q_p value of 20 at Sakurajima volcano. SUDO (1991) estimated Q_p at Aso caldera to be ranging from 50 to 100. Therefore, the Q_p values used in this study are comparable to the other volcanoes.

To determine the optimal source mechanism, we used AIC criterion (e.g.,

Table 6. Source model used in this study.

No.	source model	moment tensor or force
1	explosive source:	$\mathbf{M}=M_0\begin{pmatrix}1&0&0\\0&1&0\\0&0&1\end{pmatrix}$
2	cylindrical model:	$\mathbf{M}=M_0\begin{pmatrix}2&0&0\\0&2&0\\0&0&1\end{pmatrix}$
3	tensile crack:	$\mathbf{M}=M_0\begin{pmatrix}3&0&0\\0&1&0\\0&0&1\end{pmatrix}$
4	moment tensor *Mzz* comp.:	$\mathbf{M}=M_0\begin{pmatrix}0&0&0\\0&0&0\\0&0&1\end{pmatrix}$
5	single force model *Fz*:	$\mathbf{F}=F_0(0\quad 0\quad 1)$
6	CLVD	$\mathbf{M}=M_0\begin{pmatrix}-1&0&0\\0&-1&0\\0&0&2\end{pmatrix}$

NAKAGAWA and OYANAGI, 1982) and residuals. The AIC criterion is defined as

$$\mathrm{AIC}=n_d\times l_n(\Delta_N)+2\mathrm{R}, \tag{8}$$

where n_d is the volume of data and R is the rank of the Jacobian matrix.

6.2 Source mechanism of B-type events

We analyzed the initial phases of B-type earthquakes. As cited in Chap. 4, dominant frequencies of BH-type events ranged from 5 Hz to 9 Hz. Because BH-type events were dominated too much by high frequencies to obtain reliable results, we did not treat BH-type events in this study. Therefore, we analyzed BM-type and BL-type events. We analyzed six examples of BM-type and five examples of BL-type events, which were used in stacked spectra (Figs. 14d and 14c). Examples of source models for volcanic earthquakes of various volcanoes are listed in Table 8.

We calculated synthetic seismograms using five parameters for the assumed source time function and the source: 1) duration or rise time for the assumed source time function, 2) length of time window for the source time function, 3) depths of the

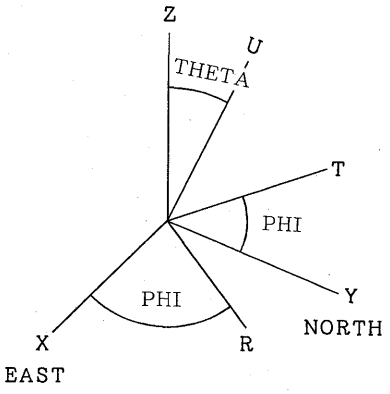

Fig. 29. The geometry and the coordinate system used in this study. The source is located at Cartesian coordinates (R, T, U), where R, T and U denote radial, transverse, and upward directions. The receivers are located at the coordinates (X, Y, Z). THET and PHI denote dip angle and azimuth, which are measured clockwise from Z-axis to U-axis along X-axis and anticlockwise from X-axis to R-axis along Z-axis, respectively.

Table 7. Velocity structure of Asama volcano.

Layer No.	Vp (km/s)	Vs (km/s)	ρ	Depth (km)	Qp	Qs
1	2.40	1.40	2.00	0.00	50.0	25.0
2	3.50	2.10	2.40	2.50	100.0	50.0
3	5.20	3.10	2.60	4.50	200.0	100.0
4	7.10	4.10	2.70	100.0	300.0	150.0

source, 4) dip angle of the source, 5) azimuth of the source.

Parabolic triangle, triangle, and ramp functions were assumed for the source time function. We chose eight examples of duration or rise time for three functional types of source ranging from 0.2 s to 1.6 s every 0.2 s. Then we calculated the synthetic seismograms for 3 examples of time window: 2, 3, and 4 sec. The dominant frequencies and the waveforms of the synthetic seismograms depend on duration or rise time of the assumed source time function and length of time window. Finally, we adopted the functional type of a parabolic triangle and a 4 s time window.

We assumed that the epicenters of B-type events were located at the center of the crater. The direction of the source is defined by the dip angle and the azimuth. We calculated synthetic seismograms for six source depths from −1.0 km to 1.5 km at every 0.5 km below sea level. We calculated the synthetic seismograms for six examples of focal depths. Changes of hypocenter depth effectively affect amplitude ratios of the vertical to the horizontal component of the synthetic seismograms. The amplitude of the vertical component becomes larger as focal depths are at

Table 8. The source models of volcanic earthquakes.

Volcanoes	Types of event	Source models	References
Sakurajima volcano	Explosion events	Cylindrical model Tensile Crack	UHIRA and TAKEO(1994)
	Explosion events	Combination of moment tensor	UHIRA et al. (1995)
	Explosion events	Vertical expansion model	IGUCHI(1994)
	BH- and BL-type events	Vertical expansion model	IGUCHI(1994)
Tokachi volcano	BL-type events	Single force	NISHIMURA et al.(1994)
	Tremor (BL-type)	Single force	
Asama volcano	Explosion event	Single force	TAKEO et al.(1984)

shallower locating because Rayleigh waves build up. We calculated synthetic seismograms at each focal depth for every 10 degree for the range of PHI=0° to PHI=360°, and THET=−30° to 80°. A change in the dip angle of the source has also an effect the amplitude ratios of the vertical to the horizontal component of the synthetic seismograms. A change in the azimuth of the source results in amplitude ratios of the E-W component to the N-S component of the synthetic seismograms.

We filtered observed and synthetic seismograms using a Chebyshev band-pass filter whose passband and stop band was 1 Hz to 3 Hz and 5 Hz, respectively. A zero-phase shift filter was used. Observed seismograms were shown for displacement amplitude which was calculated from the velocity amplitude by performing a numerical integration.

The analysis of B-type events was essentially based on three-component seismograms from station MAE in this study. We also analyzed B-type events from other stations. The station MAE is located 1.3 km east of the crater. The seismograms of B-type events from station MAE were much clearer than those from other stations. Therefore, the comparison of the synthetic seismograms with observed ones from other stations was depicted as additional information. As cited in Chap. 4, the dominant frequencies of seismic signals from stations MAE, FUJ, and SAN were slightly different (cf. Fig. 13). MINAKAMI *et al.* (1970 a) described the geological formations on which seismic stations were built. The geological formations at stations FUJ and SAN are recent pumice. However, those at station MAE are volcanic bombs and ash on lava flows. Therefore, it is natural for the dominant frequencies of B-type events to be slightly different at these stations.

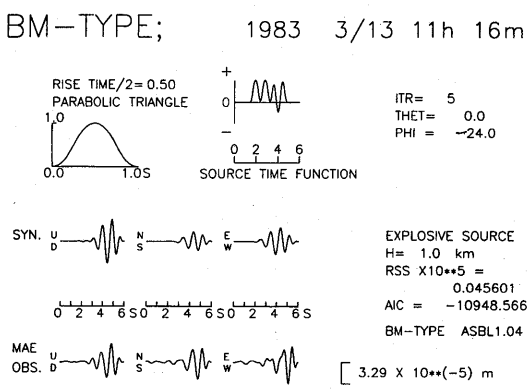

Fig. 30 a. Model check of explosive source model. Comparison of observed seismograms of a BM-type event at 11 h 16 m March 13, 1983 with synthetic ones at station MAE for the explosive source model. A parabolic triangle function is assumed for the source time function. At top left is an assumed source time function. At top right is cumulative source time function obtained with five iterations. AIC indicates AKAIKE' s Information Criterion. H denotes the hypocenter depths of synthetic seismograms. We can see that the amplitude of the N-S component of synthetic seismograms is smaller than that of observed ones.

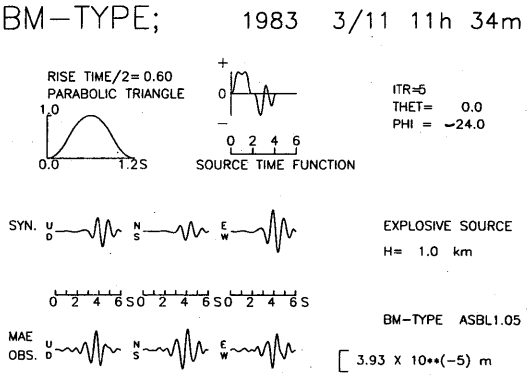

Fig. 30 b. Model check of explosive source model. Comparison of observed seismograms of a BM-type event at 11 h 34 m March 13, 1983 with synthetic ones at station MAE for the explosive source model. A parabolic triangle function is assumed for the source time function. At top left is an assumed source time function. At top right is cumulative source time function obtained with five iterations. AIC indicates AKAIKE's Information Criterion. H denotes the hypocenter depths of synthetic seismograms. We can see that the amplitude of the N-S component of synthetic seismograms is smaller than that of observed ones.

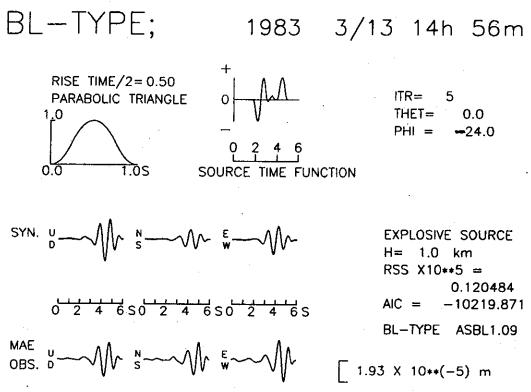

Fig. 30 c. Model check of explosive source model. Comparison of observed seismograms of a BL-type event at 14 h 56 m March 13, 1983 with synthetic ones at station MAE for the explosive source model. A parabolic triangle function is assumed for the source time function. At top left is an assumed source time function. At top right is cumulative source time function obtained with five iterations. AIC indicates AKAIKE's Information Criterion. H denotes the hypocenter depths of synthetic seismograms. We can see that the amplitude of the N-S component of synthetic seismograms is smaller than that of observed ones.

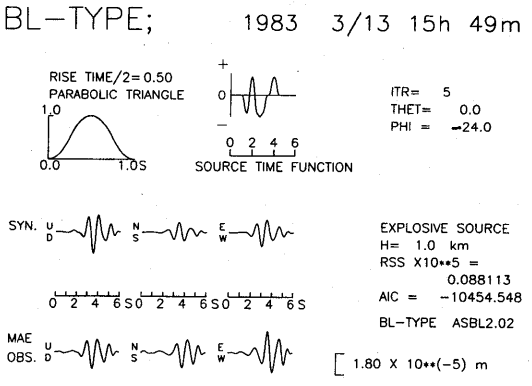

Fig. 30 d. Model check of explosive source model. Comparison of observed seismograms of a BL-type event at 15 h 49 m March 13, 1983 with synthetic ones at station MAE for the explosive source model. A parabolic triangle function is assumed for the source time function. At top left is an assumed source time function. At top right is cumulative source time function obtained with five iterations. AIC indicates AKAIKE's Information Criterion. H denotes the hypocenter depths of synthetic seismograms. We can see that amplitude of the N-S component of synthetic seismograms is smaller than that of observed ones.

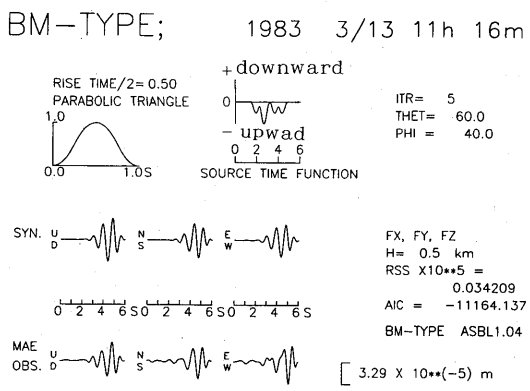

Fig. 31 a. Model check of the vertical single force model. Comparison of observed seismograms of a BM-type event at 11 h 16 m March 13, 1983 with synthetic ones at station MAE for the single force model. A parabolic triangle function is assumed for the source time function. At top left shows an assumed source time function. At top right is cumulative source time function obtained with 5 iterations. RSS shows squared error. THET and PHI indicate the best-fit angle of the dip and the azimuth, which was measured clockwise and anticlockwise, respectively (cf. Fig. 29). Angle is measured in degrees.

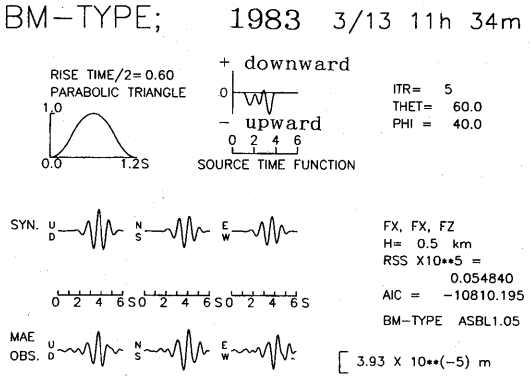

Fig. 31 b. Model check of vertical single force model. Comparison of observed seismograms of a BM-type event at 11 h 34 m March 13, 1983 with synthetic ones at station MAE for the single force model. A parabolic triangle function is assumed for the source time function. At top left is an assumed source time function. At top right is cumulative source time function obtained with five iterations. RSS shows squared error. THET and PHI indicate best-fit angle of the dip and the azimuth, which was measured clockwise and anticlockwise, respectively (cf. Fig. 29). Angle is measured in degrees.

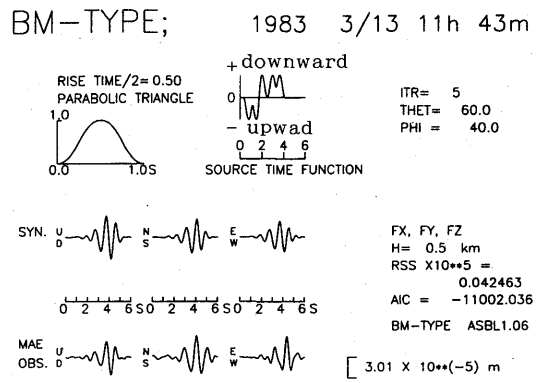

Fig. 31 c. Model check of vertical single force model. Comparison of observed seismograms of a BM-type event at 11 h 43 m March 13, 1983 with synthetic ones at station MAE for the single force model. A parabolic triangle function is assumed for the source time function. At top left is an assumed source time function. At top right is cumulative source time function obtained with five iterations. RSS shows squared error. THET and PHI indicate best-fit angle of the dip and the azimuth, which was measured clockwise plus and anticlockwise plus, respectively (cf. Fig. 29). Angle is measured in degrees.

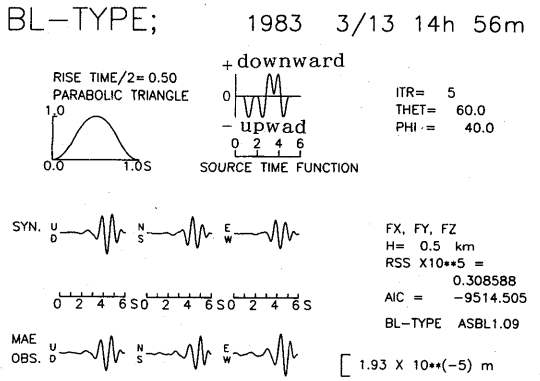

Fig. 31 d. Model check of vertical single force model. Comparison of observed seismograms of a BL-type event at 14 h 56 m March 13, 1983 with synthetic ones at station MAE for the single force model. A parabolic triangle function is assumed for the source time function. At top left is an assumed source time function. At top right is cumulative source time function obtained with five iterations. RSS shows squared error. THET and PHI indicate best-fit angle of the dip and the azimuth, which was measured clockwise and anticlockwise, respectively (cf. Fig. 29). Unit of the angle is degree.

Table 9. The source of BM-type event.
▲: Cylindrical model □: Tensile crack model

N	fi name	depth (km)	dip (degree)	azimuth (degree)	source
1	ASBL1.04	1.0	30 30	120 20	(1) ▲ (2) □
2	ASBL1.05	1.0	30 40	120 120	(1) ▲ (2) □
3	ASBL1.06	1.0	30 40	120 120	(1) ▲ (2) □
4	ASBL1.14	1.0	30 30	120 120	(1) ▲ (2) □
5	ASBL1.17	1.0	30 30	130 120	(1) ▲ (2) □
6	ASBL1.23	0.5	40 40	30 30	(1) ▲ (2) □

6.2.1 Model check for explosive source model

First we made a simple verification of the validity of an explosive source model. We assumed that the source is located under the center of the crater. Then the azimuth of station MAE is approximately −24 degrees from the east (Fig. 29). Fig. 30 shows the comparison of the synthetic seismograms for the explosive source model and the observed ones of BM-type and BL-type events. In Fig. 30 ITR, THET, and PHI denote the number of iterations, the dip angle and the azimuth of the source, respectively. H shows the assumed source depth. RSS and AIC indicate squared residuals and AKAIKE's Information Criterion, respectively. At a glance we can see the displacement amplitude of the N-S component (approximately transverse direction) from the synthetic seismograms are fairly smaller than those of observed ones. Therefore, we may conclude that the isotropic explosive source model cannot explain the observed seismograms.

6.2.2 Model check for vertical single-force model

Next, we verify the validity of the single force model. A vertical single force is inclined with the dip angle THET and the azimuth PHI. We broke a vertical single force down into three components in the Cartesian coordinate. Fig. 31 shows a comparison of the synthetic seismograms for the vertical single force model and the observed seismograms of BM- and BL-type events. Fig. 31 a and 31b show a comparison of the synthetic seismograms and observed ones of a BM-type event at 11 h 16 m March 13, 1983 and a BM-type event at 11 h 34 m March 13, 1983, respectively. In these cases, cumulative source time functions show that the upward motion is dominant in the source region. Fig. 31 c and 31 d show the results of a BM-type event at 11 h 43 m March 13, 1983 and a BL-type event at 14 h 56 m March 13, 1983. Both show that the pward motion is dominant in the initial phase. In these four cases, the residuals were the smallest in the six candidates of source models and the match between synthetic waveforms and observed ones is the best among the six candidates. However, an upward single force is represented by the counterforce of

the actual source process. Hence, the upward single force corresponds to the downward movement of volcanic gases or downward ejecta motion. Therefore, we do not adopt the single force model which has a dominant upward motion (e.g., UHIRA and TAKEO, 1994; SAWADA, 1994). Thus we discuss the waveform match of B-type events for the remainder of the four source models: 1) a cylindrical source model, 2) a tensile crack model, 3) moment tensor component *Mzz*, and 4) CLVD source model.

6.2.3 BM-type events

As mentioned earlier, we assumed that the hypocenters of BM-type events were located under the crater and the source depths are placed from −1.0 km to 1.5 km at every 0.5 km beneath sea level. Weighting factor is assumed to be 1.0 for stations

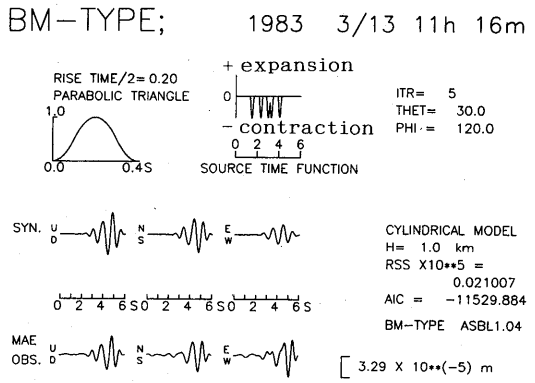

Fig. 32a. The source process for a BM-type event at 11 h 16 m March 13, 1983. Comparison of observed seismograms with the synthetic ones at station MAE for a cylindrical model. The parameters are same as Fig. 31.

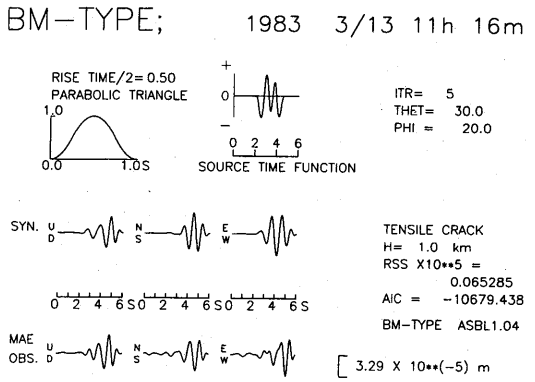

Fig. 32b. The source process for a BM-type event at 11 h 16 m March 13, 1983. Comparison of observed seismograms with the synthetic ones at station MAE for a tensile crack model. The parameters are same as Fig. 31.

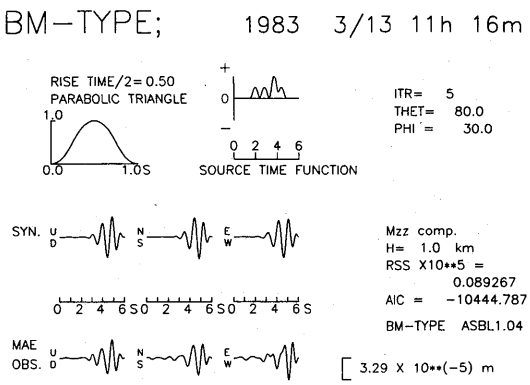

Fig. 32c. The source process for a BM-type event at 11 h 16 m March 13, 1983. Comparison of observed seismograms with the synthetic ones at station MAE for a moment tensor component *Mzz* model. The parameters are same as Fig. 31.

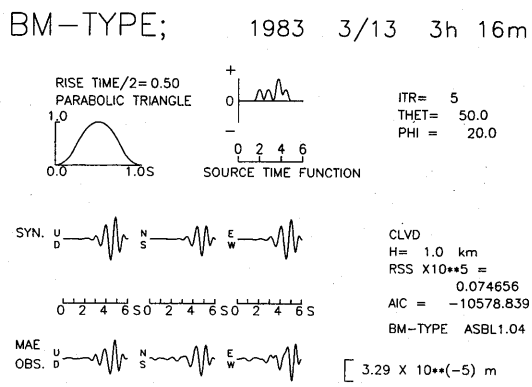

Fig. 32d. The source process for a BM-type event at 11 h 16 m March 13, 1983. Comparison of observed seismograms with the synthetic ones at station MAE for a CLVD model. The parameters are same as Fig. 31.

MAE, FUJ, and SAN and 0.5 for stations SEK, HOT, GIP, ONI, and KUR, respectively. We filtered observed and synthetic seismograms using a Chebyshev band-pass filter whose passband was 0.8 Hz to 1.5 Hz and stop band of 4 Hz. A zero-phase shift filter was used. Observed seismograms were shown in the displacement amplitude, which was calculated from the velocity amplitude by performing a numerical integration. In Fig. 32-43. ITR shows the number of iterations and H denotes the source depth of the synthetic seismograms. THET and PHI indicate the dip angle and the azimuth of the source. As discussed in 6.1.1, the parameter of p was determined to maximize the correlation between the observed and the synthetic seismograms (cf. eq. (7)). We calculated p for three components and compared the

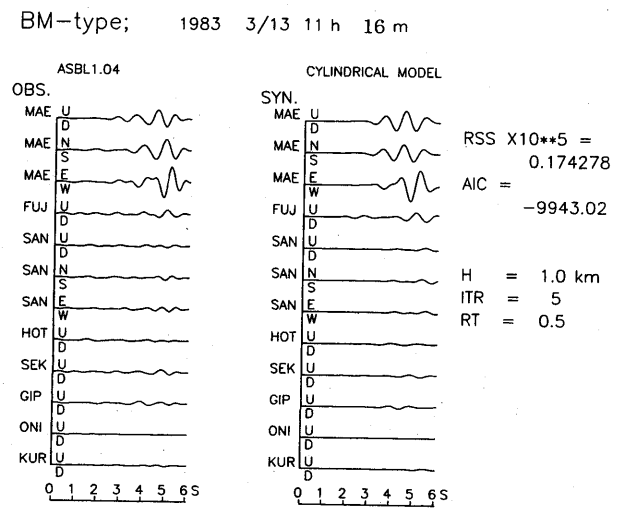

Fig. 33. The source process for a BM-type event at 11 h 16 m March 13, 1983. Comparison of observed seismograms with the synthetic ones for a cylindrical source model. A parabolic triangle function is assumed for the source time function.

residuals for the three components. We adopted p determined from the vertical component seismograms because the residuals were the smallest. However, the phases of the horizontal components, especially in the E-W component, between the observed seismograms and the synthetic ones are slightly different from each other. We analyzed six examples of BM-type events. The results are summarized in Table 9. For six examples of BM-type events the best-fit model was a cylindrical model and the second best fit model was a tensile crack model. Here we discuss three examples of BM-type events.

6.2.3.1 Example 1: a BM-type event at 11 h 16 m March 13, 1983

The source process of a BM-type event at 11 h 16 m March 13, 1983 was investigated for four candidates source models. The comparison between the observed seismograms and the synthetic ones for the four candidates source models at station MAE is shown in Fig. 32. Among the four source models a cylindrical model gives the minimum squared residuals and the minimum AIC (Fig. 32 a). The source depth was assumed to be 1.0 km beneath sea level. The cumulative source time function for the cylindrical model shows that the contraction component is dominant. This suggests that the seismic signals of BM-type events are the results of contractions in the source region. A tensile crack model gives the second minimum AIC (Fig. 32 b). Compared to the results of a cylindrical model the matching of phases in the E-W component is not so good in the case of a tensile crack model (Fig. 32). Moment tensor M_{zz} component and CLVD models are larger in the squared residuals (Fig. 32 c and Fig. 32 d). Fig. 33 shows a comparison between the observed seismograms and the synthetic ones of a cylindrical source model from eight seismic stations of AVO. Seismic signals from station MAE were clear. However, those

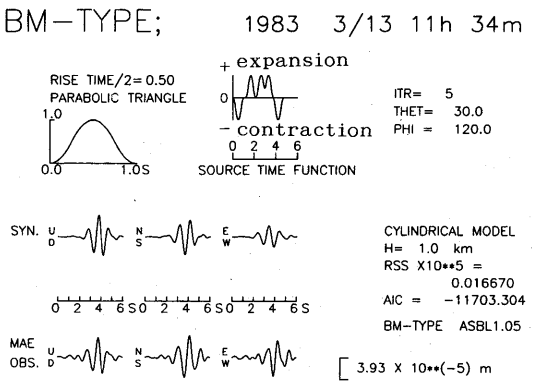

Fig. 34 a. The source process for a BM-type event at 11 h 34 m March 13, 1983. Comparison of observed seismograms with the synthetic ones at station MAE for a cylindrical model.

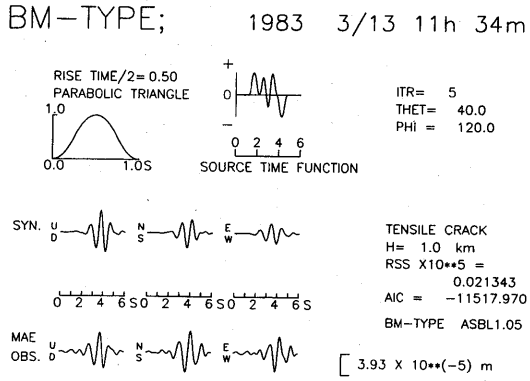

Fig. 34 b. The source process for a BM-type event at 11 h 34 m March 13, 1983. Comparison of observed seismograms with the synthetic ones at station MAE for a tensile crack model.

from other station were very noisy. Therefore, we depicted Fig. 33 to provide additional information.

6.2.3.2 Example 2: a BM-type event at 11 h 34 m March 13, 1983

A BM-type at 11 h 34 m March 13, 1983 was investigated. Fig. 34 shows a comparison between the observed seismograms and the synthetic ones at station MAE. The source depth was assumed to be 1.0 km beneath sea level. A cylindrical model gives the minimum squared residuals and the minimum AIC (Fig. 34 a). The cumulative source time function for the cylindrical model shows that the expansion component is slightly dominant in the source region. A tensile crack model gives the second minimum AIC (Fig. 34 b). Fig. 35 shows a comparison of observed seismograms from eight seismic stations of AVO with synthetic seismograms.

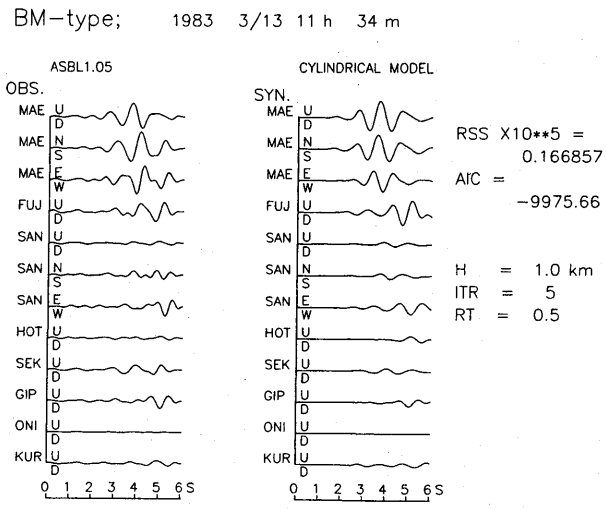

Fig. 35. The source process for a BM-type event at 11 h 34 m March 13, 1983. Comparison of observed seismograms with the synthetic ones for a cylindrical source model. A parabolic triangle function is assumed for the source time function.

6.2.3.3 Example 3: a BM-type event at 11 h 43 m March 13, 1983

A comparison between the observed seismograms of a BM-type event at 11 h 43 m March 13, 1983 and the synthetic ones at station MAE is shown in Fig. 36. A cylindrical model gives the minimum squared residuals and the minimum AIC (Fig. 36 a). In this case the expansion component is dominant in the source region. A tensile crack model offers the second minimum AIC (Fig. 36 b). Comparison of the observed seismograms from eight seismic stations of AVO with the synthetic ones of a cylindrical model is shown in Fig. 37.

Thus we can see that in the case of BM-type events cylindrical and tensile crack models match the observed seismograms (cf. Table 9). As for the source time function for a cylindrical model, the expansion component is dominant. However, we cannot ignore the contraction component. Therefore, the seismograms of BM-type events are the results of vibrations excited by the pressure increase of cylindrical form, as well as the pressure decrease.

6.2.4 The BL-type events

We analyzed five examples of BL-type events that were used in stacked spectra (Fig. 13 c). We assumed that the hypocenters of BL-type events were also located under the crater and six source depths from −1.0 km to 1.5 km at every 0.5 km beneath sea level. We investigated the source process of BL-type events for four candidates source models. As was in the case of BM-type events, the cylindrical model and the tensile crack model give the minimum and the second minimum squared residuals and AIC. Therefore, we omitted the results for the M_{zz} component and the CLVD source. In Fig. 38–43 ITR and H denote the number of iterations and

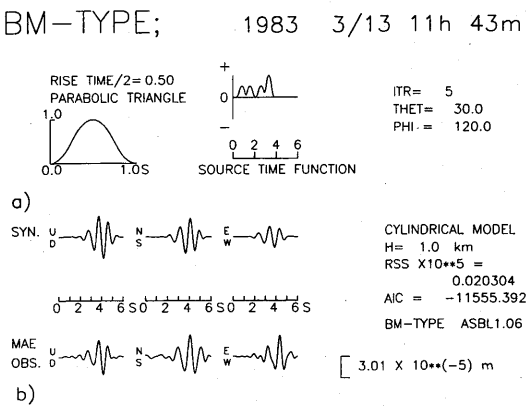

Fig. 36a. The source process for a BM-type event a 11h 43m March 13, 1983. Comparison of observed seismograms with the synthetic ones at station MAE for a cylindrical model.

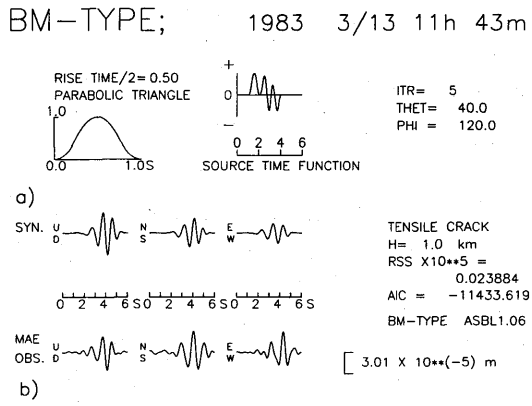

Fig. 36b. The source process for a BM-type event at 11h 43m March 13, 1983. Comparison of observed seismograms with the synthetic ones at station MAE for a tensile crack model.

the source depth of synthetic seismograms. THET and PHI indicate the dip angle and the azimuth of the source. As discussed in the previous section, we calculated p for three components and compared the residuals for the three components and adopted p determined from vertical component seismograms because the residuals were smallest. Actually, in the case of a BL-type event, the amplitude of the vertical component is fairly large. The results are summarized in Table 10. As in the cases of BM-type events, the best-fit model for BL-type events was a cylindrical model and the second best-fit model was a tensile crack model.

6.2.4.1 Example 1: a BL-type event at 14h 56m March 13, 1983

Comparison between the observed seismograms and the synthetic ones of a

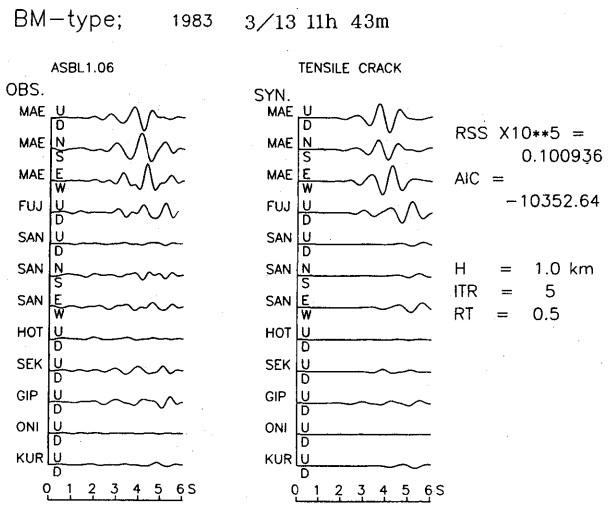

Fig. 37. The source process for a BM-type event at 11 h 43 m March 13, 1983. Comparison of observed seismograms with the synthetic ones for a cylindrical source model. A parabolic triangle function is assumed for the source time function.

Table 10. The source of BL-type event.
▲: Cylindrical model □: Tensile crack model

No.	file name	depth (km)	dip (degree)	azimuth (degree)	source
1	ASBL1.09	1.0	30 30	130 30	(1) ▲ (2) □
2	ASBL1.11	0.5	30 60	20 60	(1) ▲ (2) □
3	ASBL1.24	0.5	30 30	20 20	(1) ▲ (2) □
4	ASBL1.25	0.5	30 20	20 20	(1) ▲ (2) □
5	ASBL2.02	0.5	30 30	20 20	(1) ▲ (2) □

cylindrical and a tensile crack models at station MAE is shown in Fig. 38. The cumulative source time function for the cylindrical model shows that the expansion component is slightly dominant. The matching of waveforms in the horizontal components is not as good as that in the vertical components. A tensile crack model gives the second minimum AIC (Fig. 38 b). Fig. 39 shows a comparison of the observed seismograms from eight seismic stations of AVO with the synthetic ones of the cylindrical model.

6.2.4.2 Example2: a BL-type event at 15 h 19 m March 13, 1983

Fig. 40 shows a omparison between the observed seismograms and the synthetic

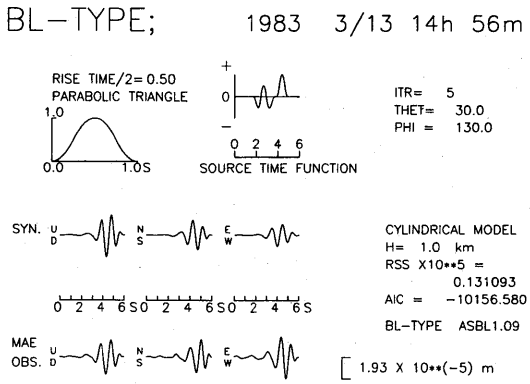

Fig. 38 a. The source process for a BL-type event at 14 h 56 m March 13, 1983. Comparison of observed seismograms with the synthetic ones at station MAE for a cylindrical model.

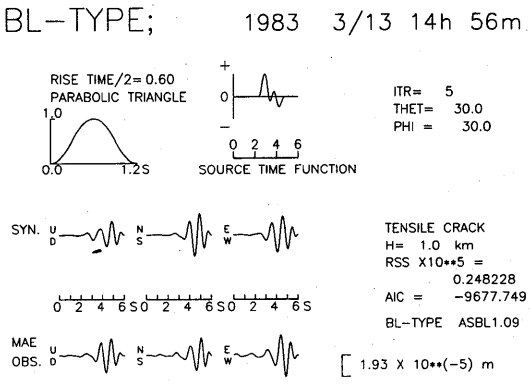

Fig. 38 b. The source process for a BL-type event at 14 h 56 m March 13, 1983. Comparison of observed seismograms with the synthetic ones at station MAE for a tensile crack model.

ones at station MAE. A cylindrical model gives the minimum squared residuals and AIC (Fig. 40 a). The cumulative source time function shows that the expansion component is dominant at first and the contraction component appears later. A tensile crack model gives the second minimum AIC (Fig. 40 b). Fig. 41 shows a comparison of the observed seismograms from eight seismic stations of AVO with the synthetic ones of a cylindrical model.

6.2.4.3 Example 3: of a BL-type event at 3 h 1 m March 17, 1983

A comparison between the observed seismograms and the synthetic ones at station MAE is shown in Fig. 42. A cylindrical model gives the minimum squared residuals and the minimum AIC (Fig. 42 a). The cumulative source time function shows that the expansion component is dominant at first and the contraction component become dominant later. A tensile crack model gives the second mini-

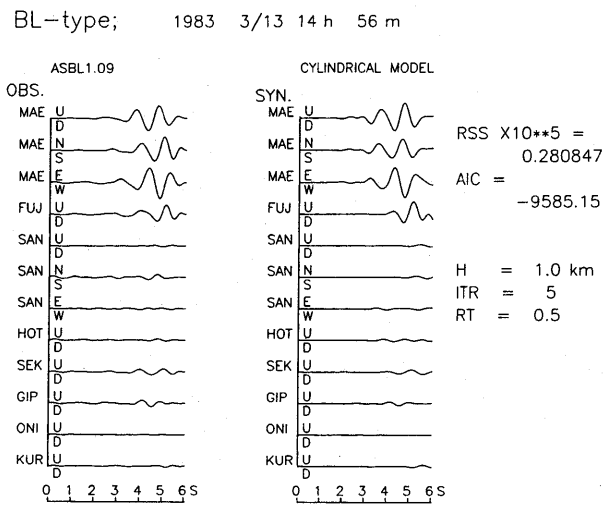

Fig. 39. The source process for a BL-type event at 14 h 56 m March 13, 1983. Comparison of observed seismograms with the synthetic ones for a cylindrical source model. A parabolic triangle function is assumed for the source time function.

mum AIC (Fig. 42 b). Fig. 43 shows a comparison of the observed seismograms from eight seismic stations of AVO with the synthetic ones of the cylindrical model.

In the cases of BL-type events, we can cull the prospects to two source models: 1) the cylindrical model, 2) the tensile crack model. A source model that gives the minimum AIC is the cylindrical model (cf. Table 10). Locations of hypocenters of the source ranged from 0.5 km to 1.0 km (cf. Table 10). Locations of synthetic BL-type events seem to be shallower than those of BM-type events. The results are consistent with those obtained from the waveform analysis. The source time function for the cylindrical model shows that the seismic signals of BL-type events are the results of vibrations excited by not only the pressure increase but also the pressure decrease.

6.3 Source mechanism of the explosion event at April 26, 1982

We analyzed the initial phase of the explosion event on April 26, 1982 which was recorded by 1 s short period velocity-type seismographs (Fig. 24). First, we verified the validity of explosive source and single force models.

Figure 44 a shows a comparison of the observed seismograms and the synthetic ones from the isotropic explosive source at station MAE. The displacement amplitude of the N-S component from synthetic seismograms is much smaller than those of observed seismograms. Because the waveform match is not good, we rejected the explosive source model from among the candidates.

Fig. 44 b shows a comparison of the observed seismograms and the synthetic ones from an inclined vertical single force model at station MAE. In Fig. 44 a parabolic triangle function is assumed for the source time function. As mentioned

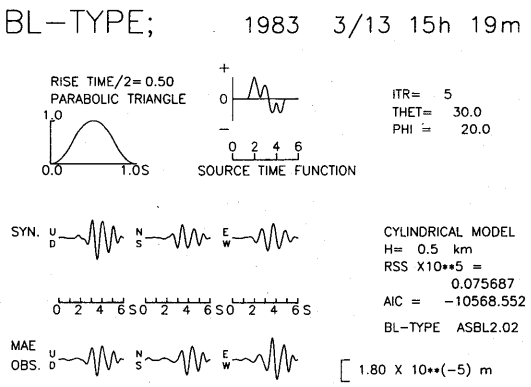

Fig. 40 a. The source process for a BL-type event at 15 h 19 m March 14, 1983. Comparison of observed seismograms with the synthetic ones at station MAE for a cylindrical model.

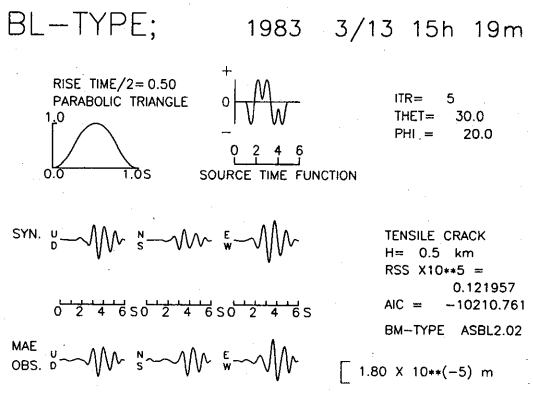

Fig. 40 b. The source process for a BL-type event at 15 h 19 m March 14, 1983. Comparison of observed seismograms with the synthetic ones at station MAE for a tensile crack model.

earlier, THET and PHI denote the dip angle and the azimuth of the source, respectively (Fig. 29). The cumulative source time function shows that the upward component is dominant in the initial phase of the explosion earthquake. Therefore, we do not adopt the single force model.

We chose three examples of time windows, i.e., a 3 sec, a 6 sec, and a 12 sec time window for the assumed source time function. We further assumed that the hypocenter of the explosion earthquake was located under the crater and three source depths of 0 km, 0.5 km, and 1.0 km beneath sea level. We used a Chebyshev band-pass filter whose passband was 0.5 to 2 Hz and stop band of 4 Hz for 5 s seismograms and passband of 1.0 to 3 Hz and stop band of 5 Hz for 1 s short period seismograms, respectively. A zero-phase shift filter was used.

We calculated the residuals of the four source models: 1) cylindrical model, 2)

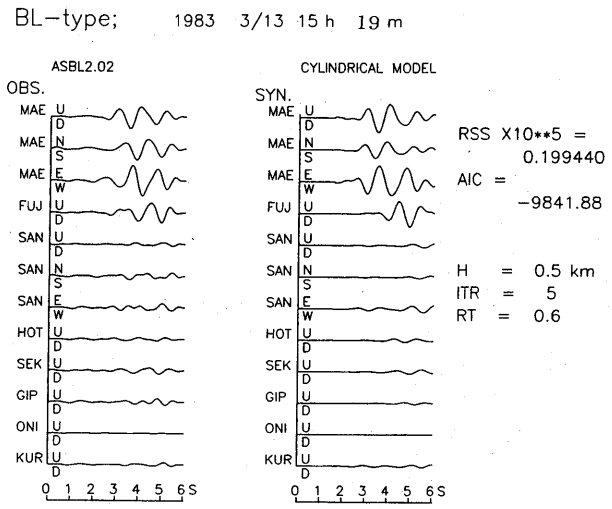

Fig. 41. The source process for a BL-type event at 15 h 19 m March 14, 1983. Comparison of observed seismograms with the synthetic ones for a cylindrical source model. A parabolic triangle function is assumed for the source time function.

tensile crack model, 3) moment tensor component M_{zz}, and 4) CLVD source model. The source model that gives minimum residuals and AIC is the moment tensor M_{zz} component (Fig. 45 a) and those of the second minimum is the cylindrical model (Fig. 45 b). Fig. 46 shows a comparison of observed seismograms from eight seismic stations of AVO with the synthetic seismograms of the M_{zz} component of moment tensor.

6.4 Source size

A volume source is represented by a point source whose dimensions should satisfy the following conditions,

$$\frac{l^2}{r_{\min}\lambda_{\min}} << 1,$$

where, l, $r_{\min}$ and $\lambda_{\min}$ are the source dimensions, the minimum epicentral distance, and the minimum wavelength, respectively (AKI and RICHARDS, 1980). $r_{\min}$ and $\lambda_{\min}$ for B-type and explosion events from station MAE and NAK are listed in Table 11. B-type and explosion events presumably occur in the vent. Therefore, $r_{\min}$ at station MAE and NAK for B-type and explosion events are approximately 1.3 km and 4.2 km respectively. If we assume wave velocity of 2.4 km, and the dominant frequency of 1 or 2 Hz for BM-type and BL events, $\lambda_{\min}$ is estimated to be in the order of kilometers. As for the source size, we may think that the source size of B-type and explosion events is comparable to the vent size. The radius of the vent is considered to be less than one hundred meters at Asama volcano (SHIMOZURU *et al.*,

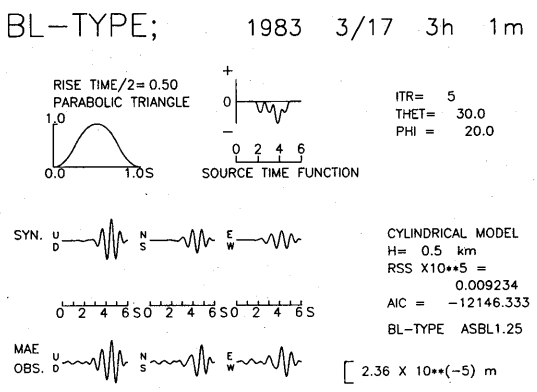

Fig. 42a. The source process for a BL-type event at 3h 1m March 17, 1983. Comparison of observed seismograms with the synthetic ones at station MAE for a cylindrical model.

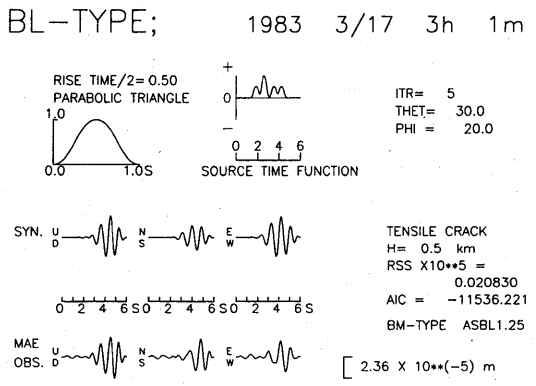

Fig. 42b. The source process for a BL-type event at 3h 1m March 17, 1983. Comparison of observed seismograms with the synthetic ones at station MAE for a tensile crack model.

1982). SHIMOZURU *et al.* (1982) found that the radius of lava is approximately 60 m, which filled up the vent at the time of the 1973 eruption. Therefore, we think that the point source approximation holds good.

6.5 Source process of B-type events

We have discussed the model of equivalent body-force of BM-, BL-, and explosion events. In this section we discuss the substance of B-type earthquakes. More than three decades ago, MINAKAMI (1960) successfully predictited explosive volcanic eruptions of Asama volcano. His prediction of volcanic eruptions was based on the simple empirical formula that B-type earthquakes increased in number before the eruption of Asama volcano. Furthermore, he suggested that there were two kinds of B-type event; one is correlated with eruptive phenomena of Asama volcano, and the other has no relation with them. B-type events related to the Asama activity

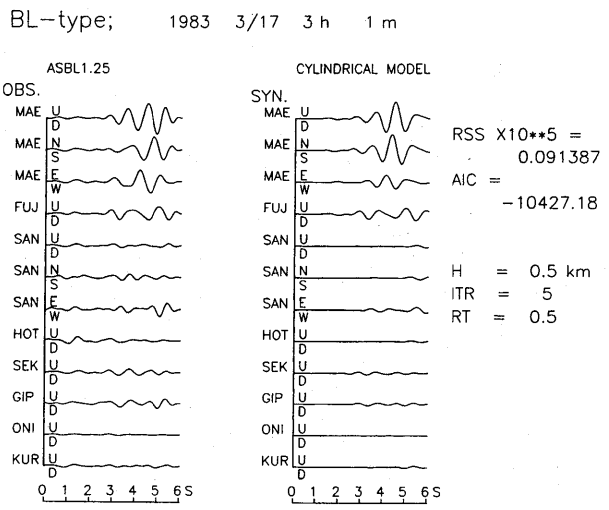

Fig. 43. The source process for a BL-type event at 3 h 1 m March 17, 1983. Comparison of observed seismograms with the synthetic ones for a cylindrical source model. A parabolic triangle function is assumed for the source time function.

have similar waveforms to those of explosion events. He also found that the minimum amplitude of explosion events corresponds to the maximum amplitude of B-type events related to eruptive phenomena. As cited earlier, ISHIHARA and IGUCHI (1989) found that BH-type swarms occurred during the inflation stage with no significant changes of eruptive activity of Sakurajima volcano and swarms of BL-type events took place during the period of rapid deflation of the summit area with the successive emission of volcanic ash and gases. Thus, according to ISHIHARA and IGUCHI (1989) we can understand MINAKAMI's description by replacing the words "B-type events related to eruptive phenomena" and "B-type events with no relation to those" with "typical BL-type" and "BH-type events", respectively.

As was shown in Sec. 6.2 a cylindrical model gives the minimum residuals and the minimum AIC for BM- and BL-type events. Moreover, the results of an analysis using the cylindrical model suggest that volume changes in the source region of BM- and BL-type correspond not only to expansion but also to contraction (e.g., UHIRA and TAKEO, 1994). Here we estimate the strain in the source region of BM- and BL-type events (c.f. FUKUYAMA and TAKEO, 1990; UHIRA and TAKEO, 1994). We assume that a finite cylinder filled with liquid is located in the source region of BM- and BL-type events. Assuming the radius of the cylinder is much smaller than the seismic wavelength, the volumetric source is represented by the moment density tensor (cf. Table 6)

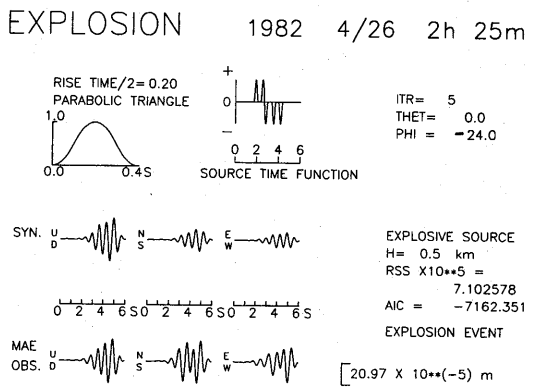

Fig. 44a. Model check for the explosive source model. Comparison of observed seismograms of the explosion event at 2 h 25 m April 26, 1982 with synthetic ones at station MAE for an explosive source model. We can see that the amplitude of the N-S component of synthetic seismograms is smaller than that of observed ones.

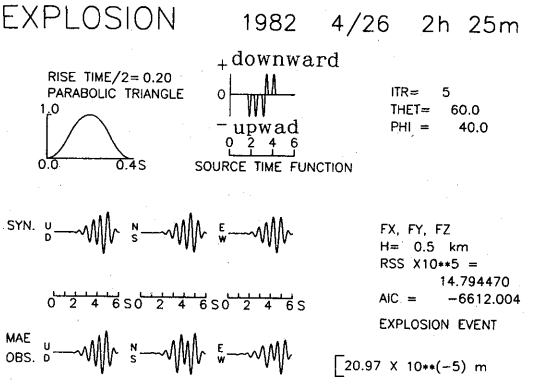

Fig. 44b. Model check of the vertical single force model. Comparison of observed seismograms of the explosion event at 2 h 25 m April 26, 1982 with synthetic ones at station MAE for an explosive source model. Initial motion is an upward vertical force.

$$M=\begin{pmatrix}2&0&0\\0&2&0\\0&0&1\end{pmatrix}V\mu\delta,$$

where V, μ, δ, denote volume change of a cylinder, rigidity ($\lambda=\mu$ is assumed), strain in the radial component of a cylinder, respectively. We assumed P wave velocity of 2.4 km/s and density 2.0 kg/m^3, $\lambda=\mu=4\times10^9$N/m^2. If we assume seismic

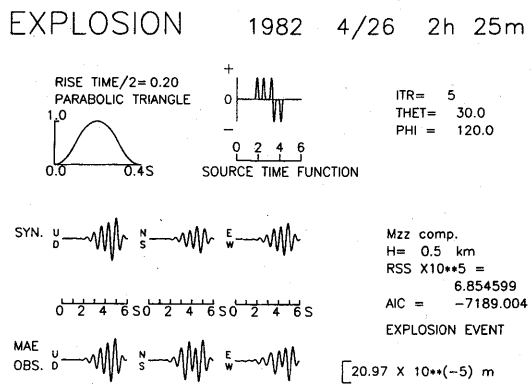

Fig. 45 a. The source process for the explosion event at 2 h 25 m April 26, 1982. Comparison of observed seismograms with synthetic ones for a moment tensor *Mzz* component model. A parabolic triangle function is assumed for the source time function.

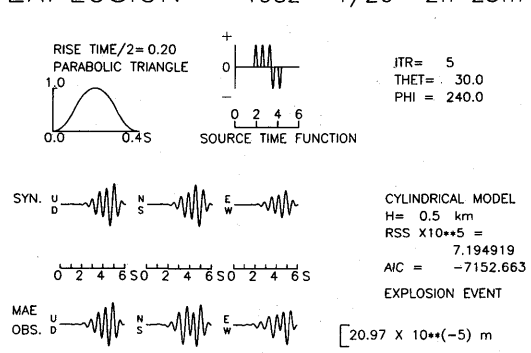

Fig. 45 b. The source process for the explosion event at 2 h 25 m April 26, 1982. Comparison of observed seismograms with synthetic ones for a cylindrical model. A parabolic triangle function is assumed for the source time function.

moment tensor of M_{xx} or M_{yy} to be range from -10^{11} Nm to -10^{12} Nm, then $V\delta$ becomes from 6 m^3 to 60 m^3. Assuming the radius of a cylinder to be 60 m and the effective length of a cylinder to be 10 m, δ is ranging from -5×10^{-4} to -5×10^{-3}. These values are approximately one-tenth to one-hundredth in the case of the 1987 eruption of Izu-Oshima volcano.

7. N-type earthquakes at Asama volcano

CHOUET *et al.* (1994) and CHOUET (1996 a) discussed the source mechanism of long-period events at Redoubt volcano and concluded that long-period events were

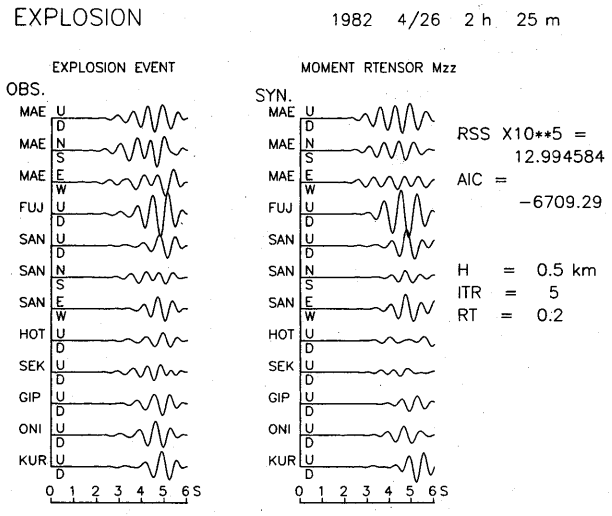

Fig. 46. Comparison of observed seismograms with synthetic ones at station MAE for a cylindrical model. a. Left shows an assumed source time function. We used a parabolic triangle function. At right is cumulative source time function obtained with 25 iterations. b. RSS shows squared error. THET and PHI indicate best-fit angle of the dip and the azimuth which was measured clockwise, respectively (cf. Fig. 29). Unit of the angle is degree.

Table 11. The source dimensions.

$r_{min} \times \lambda_{min} \gg d^2$

r_{min} : the minimum epicentral distance

λ_{min} : the minimum wave length

d: the source dimension

Vp=2.40 km/s

Station: MAE (r_{min}=1.3 km)

Frequency (Hz)	λ_{min}	$r_{min} \times \lambda_{min}$	d (km)
1	2.40	3.12	1.77 >>
2	1.20	1.56	1.25 >>
3	0.80	1.04	1.02 >>
5	0.48	0.62	0.79 >>
10	0.24	0.31	0.56 >>

Station: NAK (r_{min}=4.2 km)

Frequency (Hz)	λ_{min}	$r_{min} \times \lambda_{min}$	d (km)
0.5	4.80	20.16	5.49 >>
1	2.40	10.08	3.17 >>
2	1.20	5.04	2.24 >>

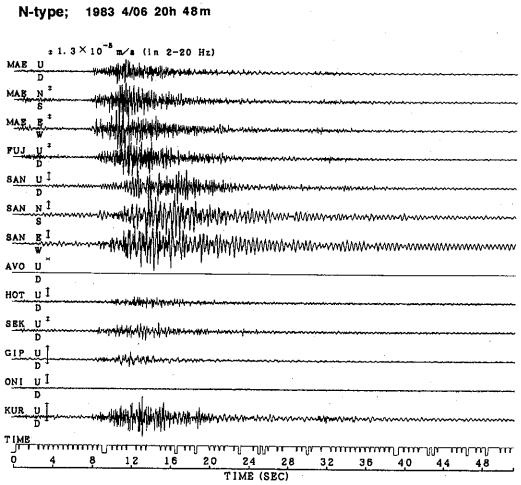

Fig. 47. An example of seismograms of a N-type earthquake (cf. Fig. 5).

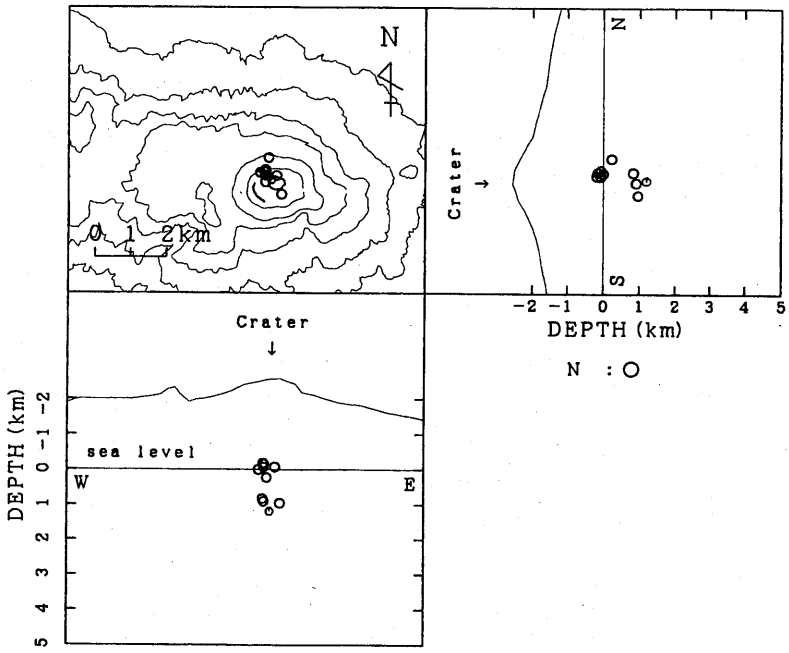

Fig. 48. Hypocenter locations determined from initial motions of N-type events (cf. Fig. 26).

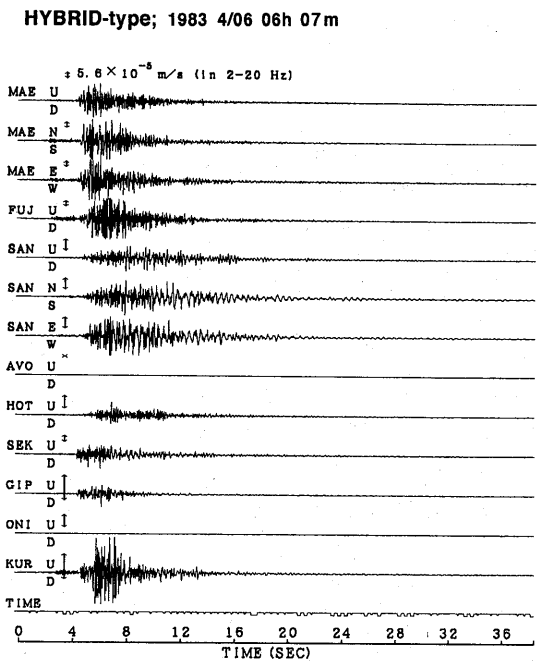

Fig. 49a. An example of seismograms of hybrid earthquakes. The tail parts of seismograms at station SAN slightly become longer than that of BH-type events (cf. Figs. 7 and 9).

triggered by A-type earthquakes and that they were precursors to eruptive activity. This study presents a different idea on the possible origins of N-type events.

7.1 Seismic features of N-type earthquakes

7.1.1 Seismograms of N-type events

Fig. 47 shows seismograms of N-type earthquakes. Seismograms of N-type events begin with relatively high-frequency (5-9 Hz) waves and are followed by quasi-monochromatic low-frequency (approximately 2 Hz) waves (cf. Fig. 47 and Fig. 5). Waveforms similar to N-type events are observed at various volcanoes, e.g., Kuchinoerabu (HAMADA *et al.*, 1975), Kusatsu-Shirane (UEKI, *et al.*, 1985; FUJITA *et al.*, 1995), Tokachi (e.g., MATSHUSHIMA *et al.*, 1987), Galeras, St. Helens, Pinatsubo and Redoubt volcanoes. They are active andesitic and dacite volcanoes. CHOUET *et al.* (1994) called this type of earthquake a long-period earthquake. Although in Japan N-type events are observed at various andesitic volcanoes, they are not observed at Sakurajima volcano, which is a typical active andesitic volcano. Hence we may think that the occurrence of N-type events depends on the structure of the volcano. N-type events appeared before the 1958 and the 1983 eruptions of Asama volcano. Before the 1958 eruption N-type events having a duration of approximately 10 minutes were recorded at Asama Volcano Observatory. However, as mentioned earlier, TANAKA and JINGU (1979) found that N-type events could not be regarded as precursors to the eruptive stage of Asama volcano, because they are often observed

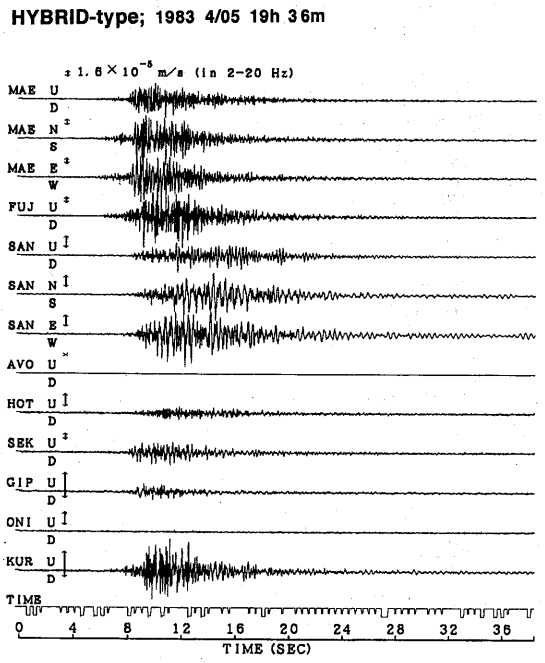

Fig. 49 b. An example of seismograms of hybrid earthquakes. The tail parts of seismograms at station SAN slightly become longer than that of BH-type events (cf. Figs. 7 and 9).

at the calm stage.

Seismograms of N-type events indicate that amplitude and duration become maximum at station SAN. In the cases of B-type events the maximum amplitude and duration are recorded at station MAE (cf. Figs. 47 and 5).

7.1.2 Hypocenters of N-type events

Hypocenters of N-type events are located beneath the vent of Asama volcano (Fig. 48). Focal depths of N-type events range approximately from 0 to 1 km beneath sea level. A-type events do not occur at these places at Asama volcano (cf. Fig. 26).

7.1.3 Seismograms of N′-type events

Before the occurrence of typical N-type events "the hybrid" events that share both wave characteristics of B-type and N-type events appear. Hereafter, we call this type of event a N′-type event. Fig. 49 shows seismograms of a N′-type event. Seismograms of a hybrid event show that waveforms are very similar to those of BH- or BM-type events except with coda parts of seismograms at station SAN. Fig. 49 shows that the coda parts of hybrid events at station SAN extend slightly and share the waveforms of N-type events. Hybrid events also tend to swarm.

7.1.4 Peculiarity of N-type events

As was shown in Fig. 48 hypocenters are determined from initial motions locate beneath the vent. Important features of N-type events are that the maximum

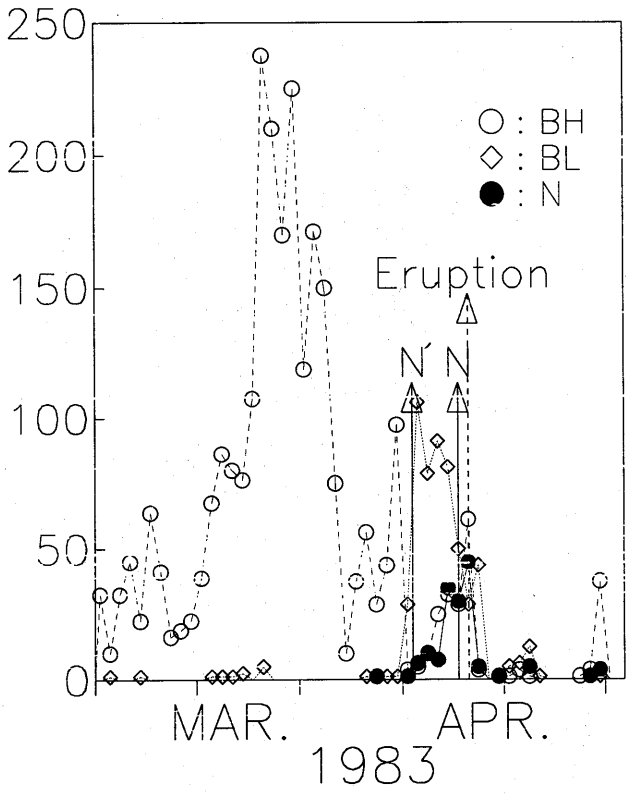

Fig. 50. The daily number of earthquakes at station MAE in March and April of 1983. The swarm of B-type events are followed by the occurrence of N-type events. (Modified SHIMOZURU and KAGIYAMA (1989)).

amplitude and duration of the main monochromatic oscillations are not recorded at station MAE closer to the epicenter than station SAN. The amplitude and the duration of N-type events are maximum at station SAN, which is located 2.6 km east of the vent. This is in contrast to the B-type events in which the maximum amplitude and duration are recorded at station MAE. This strongly suggests that the main motion of N-type event is not generated at the initial source (i.e., near the vent), but elsewhere near station SAN.

7.2 Time sequence of N-type events

In Fig. 50 N′ and N indicate the first occurrence time of hybrid and typical N-type events following the swarm of B-type events, respectively. After the swarm of B-type events hybrid events appear at first, then N-type events appear and begin to increase. As mentioned earlier, N-type events tend to swarm. These observational facts are very important when discussing the origins of N-type events. Here, we summarize the occurrence of N-type events. N-type events occur in the following time sequence:

1) N-type events follow the swarm of B-type events (cf. Fig. 47);

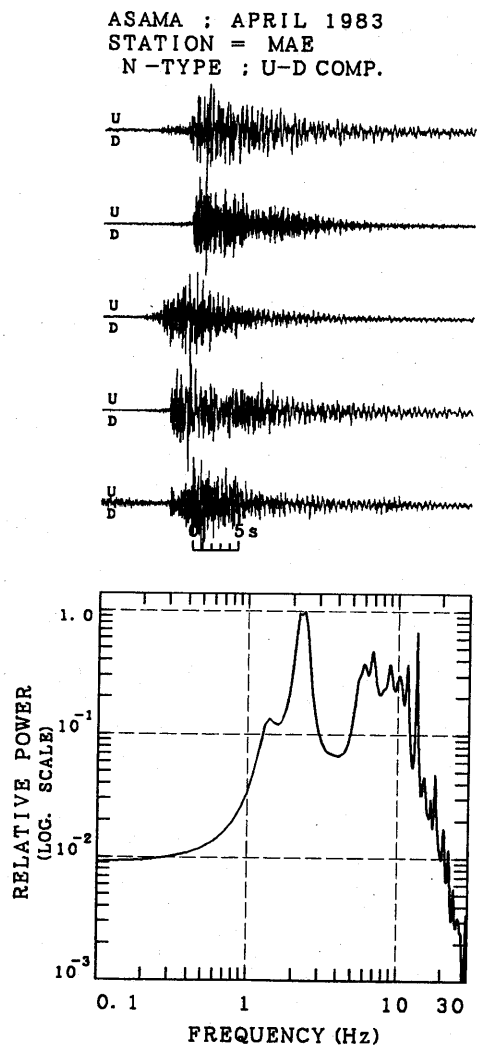

Fig. 51 a. Five stacked velocity spectra of N-type events from the vertical component at station MAE and individual seismograms of N-type events used for velocity spectra.

2) Hybrid events of B-type and N-type events appear at first. Hybrid events are characterized by similar waveforms to B-type events having small tails with a frequency of approximately 2 or 3 Hz;

3) Then typical N-type events appear. N-type events tend to swarm (cf. Fig. 47).

7.3 Wave characteristics of N-type and hybrid events

7.3.1 Spectral analysis

Figure 51 a shows the stacked spectra and individual seismograms of N-type

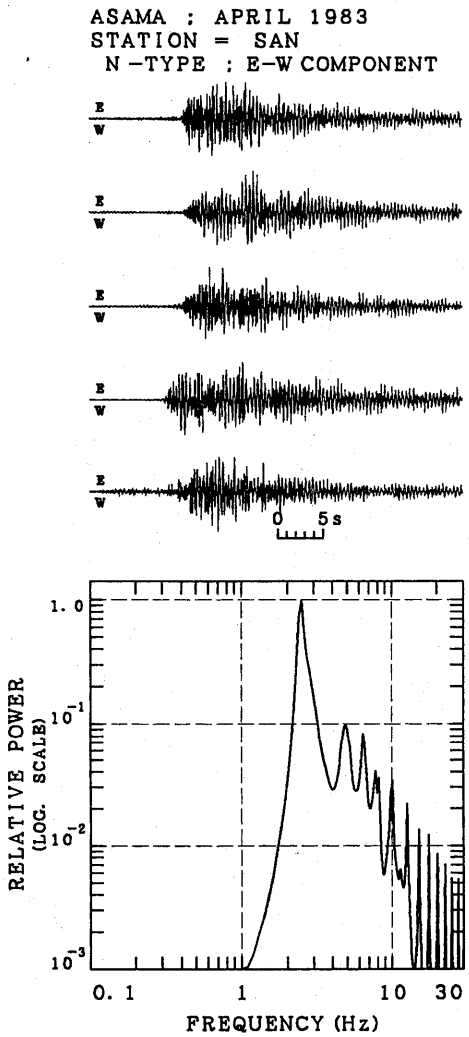

Fig. 51 b. Five stacked velocity spectra of N-type events from the vertical component at station SAN and individual seismograms of N-type events used for velocity spectra.

events at station MAE. We can distinguish five prominent peaks at about 2, 6, 7, 9, and approximately 1 Hz for a N-type event at station MAE (Fig. 51 a). Conversely, the stacked spectra of N-type events from station SAN show five or six strong peaks. The peak frequencies seem to have even harmonics (Fig. 51 b). The spectral peaks at SAN are much stronger than those at station MAE. This suggests that the locations of main motions of N-type events are near station SAN. Figure 52 a shows stacked spectra and individual seismograms of hybrid events at station MAE. Stacked spectra are very similar to those of BH-type events. We can distinguish five

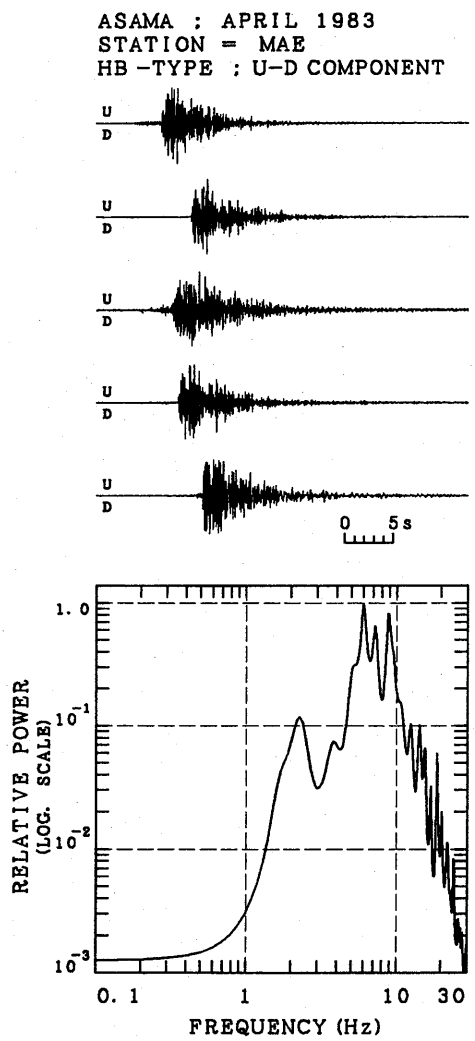

Fig. 52 a. Five stacked velocity spectra of hybrid events from the vertical component at station MAE and individual seismograms of hybrid type events used for velocity spectra.

prominent peaks at about 6, 7, 9, 2, and 4 Hz for hybrid events at station MAE. The stacked spectra of hybrid events from station SAN show a very strong peak at 4 Hz (Fig. 52 b). The stacked spectra of hybrid events from station SAN are also very similar to those of BH-type events (cf. Fig. 15 a-4).

Running spectra of N-type and hybrid events are also examined. Fig. 53 a shows the running spectra of N-type events from station MAE. Except for the coda part (between solid arrows in Fig. 53 a), the running spectra are similar to those of BM-type events (cf. Fig. 16 c). Fig. 53 b shows the running spectra of a N-type event

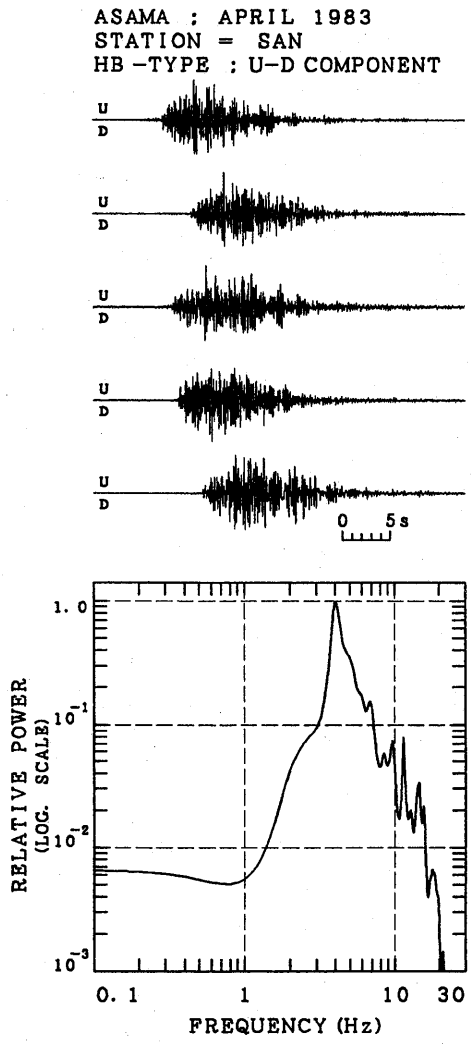

Fig. 52 b. Five stacked velocity spectra of hybrid events from the vertical component at station SAN and individual seismograms of hybrid type events used for velocity spectra.

from station SAN. We can recognize a strong, stable peak at approximately 4 Hz. Fig. 54 a shows the running spectra of a hybrid events from station MAE. Except for the coda part, the running spectra are similar to those of BH-type events (cf. Fig. 16 a). Fig. 54 b exhibits running spectra of a hybrid event from stations SAN. To analyze the initial phases of N-type events, the MEM method does not give high enough resolution. Therefore, we introduced the Sompi method as mentioned in the Appendix. Fig. 55 shows running spectra of a N-type event from station SAN obtained by the Sompi method. In Fig. 55 spectral peaks are represented by solid

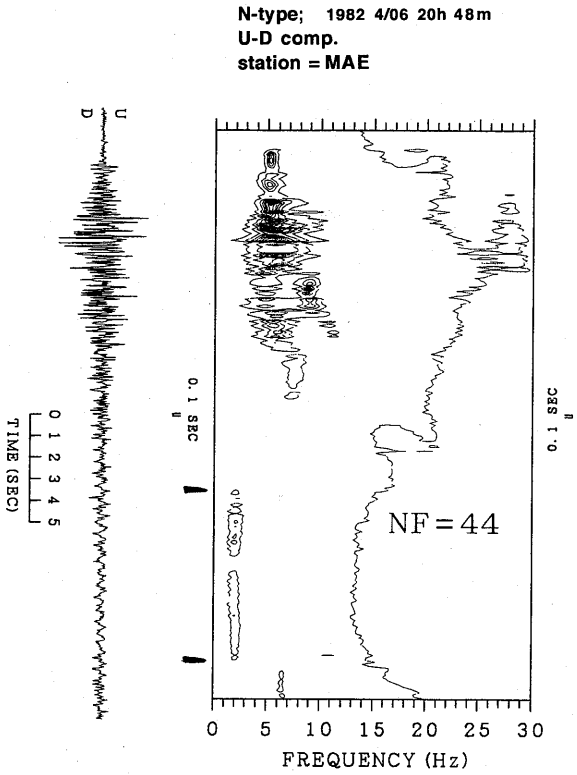

Fig. 53 a. Running spectra of a N-type event recorded at station MAE. The spectra were calculated for a 3-s time window at 0.1 s time intervals. Power spectral density is graded into ten classes on a linear scale.

and open bars, which indicate increasing and decreasing amplitude in the time window of 0.5 sec, respectively. The power spectral density is graded into 10 classes on a linear scale. The spectral peaks of high frequency portions represent the spectral features of BH-type events. We can see that a stable peak at approximately 2-3 Hz lasted for a long time.

From a pectral analysis we may conclude that spectra from high-frequency portions of N-type or hybrid events are very similar to those of BH- or BM-type events.

7.3.2 Polarization analysis

Figure 56 shows a low-frequency portion (1-4 Hz) of particle motion diagrams for a N-type event. The amplitude of the horizontal component of N-type events is about two times larger than that of the vertical component. A particle motion diagram at station MAE starts with prograde motions (solid arrow at approximately 6 sec in the time axis in Fig. 56 a). Retrograde and prograde motions appear alternately at station MAE. Fig. 56 b shows that the prograde motion is dominant at

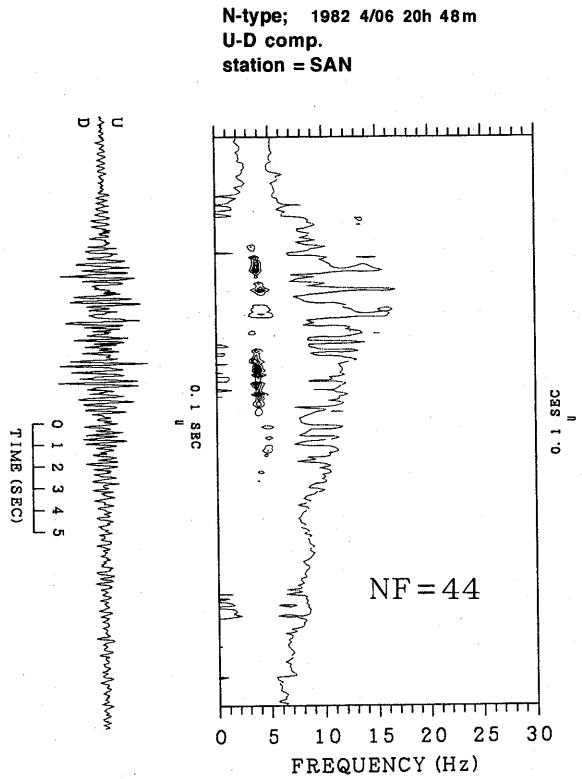

Fig. 53 b. Running spectra of a N-type event recorded at station SAN. The spectra were calculated for a 3-s time window at 0.1 s time intervals. Power spectral density is graded into ten classes on a linear scale.

station SAN. This implies that the source of N-type events is located near station SAN. Because station SAN is located 1.4 km east of station MAE, the locations of the source are considered to be in west toward station SAN. Namely, the sources of N-type events are located between stations MAE and SAN.

7.4 Summary of the seismic features of N-type events

The seismic features of N-type events are summarized as follows:

1) N-type events start with high-frequencies (5-9 Hz) and are followed by quasi-monochromatic oscillations of frequencies of approximately 2-4 Hz (cf. Fig. 47);

2) The hypocenters of N-type events are determined to be under the crater of Asama volcano. The focal depths of N-type events range from 0 to 1 km beneath sea level. The amplitude of initial phase seems to be proportional to the distance from the crater; The amplitude of the initial phase of N-type events recorded at station MAE is larger than that recorded at station SAN;

3) The amplitude and the duration of N-type events reach their maximum at

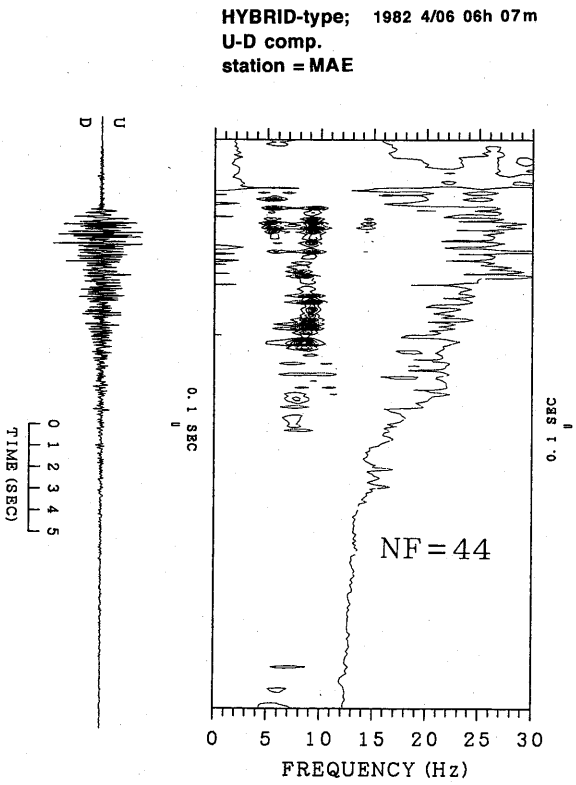

Fig. 54a. Running spectra of a hybrid event at station MAE. The spectra were calculated for a 3-s time window at every 0.1 s time interval. Power spectral density is graded into ten classes on a linear scale.

station SAN located 2.6 km east of the crater. Those recorded at station MAE located at 1.3 km east of the crater are smaller than those at station SAN. The spectral analysis of N-type events suggests that the source of the main motions of N-type events is located near station SAN. A polarization analysis of N-type events supports the view that the source of N-type events is near station SAN;

4) Running spectra of N-type events show that initial motions of N-type events are very similar to those of BH-type or BM-type events.

7.5 Possible mechanism of N-type events

As mentioned earlier, HIRABAYASHI (1982) and OHTA *et al.* (1988) carried out measurements of emission rates of sulfur-dioxide (SO_2) from various volcanoes using a correlation spectrometer (COSPEC). Figure 57 shows the relation between emission rates of SO_2 and monthly frequency of volcanic earthquakes at Asama volcano. We can recognize the correlation between SO_2 emission rates and eruptive activity of Asama volcano. In Fig. 57, volcanic explosions number three. In April 1982 and 1983 we observed two minor volcanic explosions associated with explosion earth-

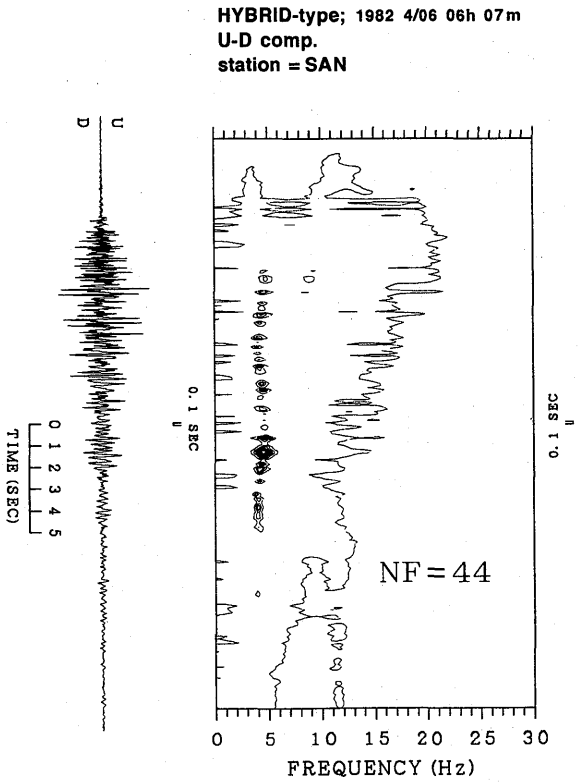

Fig. 54 b. Running spectra of a hybrid event at station SAN. The spectra were calculated for a 3-s time window at 0.1 s time intervals. Power spectral density is graded into ten classes on a linear scale.

quakes after the 1973 eruptions of Asama volcano. In addition to these, on Oct. 2, 1982 Asama volcano emitted a small quantity of volcanic ashes associated with a weak volcanic tremor. At that time an explosion earthquake was not observed (EARTHQUAKE RESEARCH INSTITUTE, 1983 a). Therefore, we did not classify this event as a volcanic explosion. However, OHTA *et al.* (1988) categorized this event as a volcanic explosion. Returning to the real subject, we may conclude that the occurrence of B-type events has a good correlation with the emission of volcanic gases at Asama and Sakurajima volcanoes. Furthermore, explosion earthquakes are followed by large emissions of volcanic gases (e.g., ISHIHARA *et al.*, 1983; ISHIHARA, 1990).

The occurrence of hybrid events suggests that B-type events become N-type events under some conditions. In other words, the existence of hybrid events supports the view that N-type events are triggered by BM- or BH-type events. We may conclude that N-type events are triggered by B-type events. Therefore, we will discuss the trigger mechanism of N-type events. When we discuss the mechanism of N-type events we must explain: 1) driving force of N-type events, and 2)

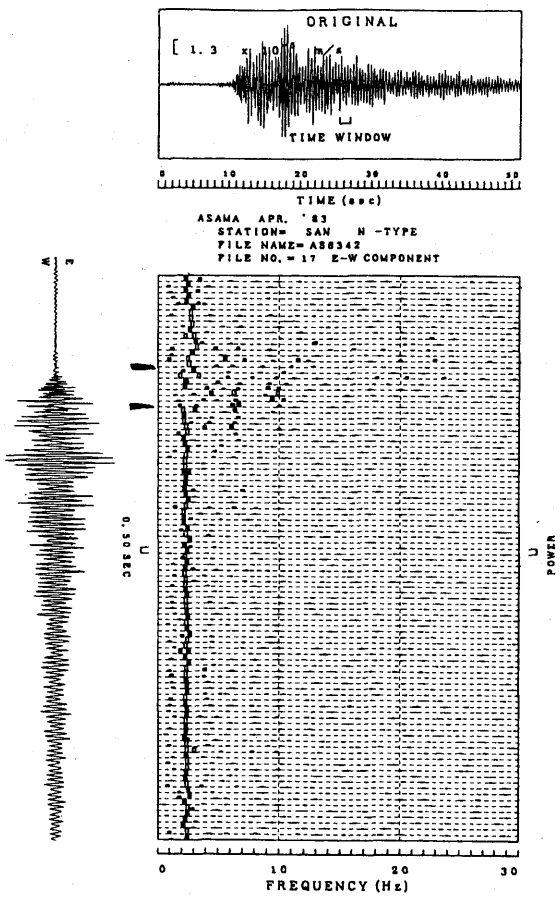

Fig. 55. Running spectra of a N-type event at station SAN by the Sompi method. The spectra were calculated for a 1.5-s time window at 0.5 s time intervals. Power spectral density is graded into ten classes on a linear scale.

energy balance to maintain the duration of N-type events. The distance from the crater to station SAN is approximately 2.6 km. The duration of N-type events was 10 minutes before the eruption of 1958. What is the driving force of N-type events that vibrates the ground for as long as 10 minutes with frequencies of approximately 2 to 4 Hz? The idea that N-type events are results of eigen vibrations of an elastic body triggered by a physical external force has difficulty in explaining the maintenance system of the oscillations over a long time with high frequencies of 2 or 4 Hz. B-type events having durations of approximately 15 to 30 s cannot maintain the 5 or 10 minutes of oscillations associated with N-type events. Moreover, the maximum amplitude of N-type events at station SAN is much larger than that at station MAE.

Fig. 58 shows a conceptual model of the Asama volcano magma system. At this point, we adopt the idea that the substance of B-type events are high-temperature

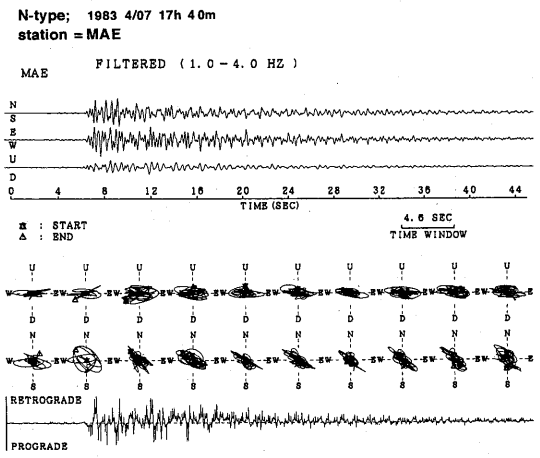

Fig. 56a. Particle motion diagram for the low-frequency portion (1-4 Hz) of a N-type event at station MAE.

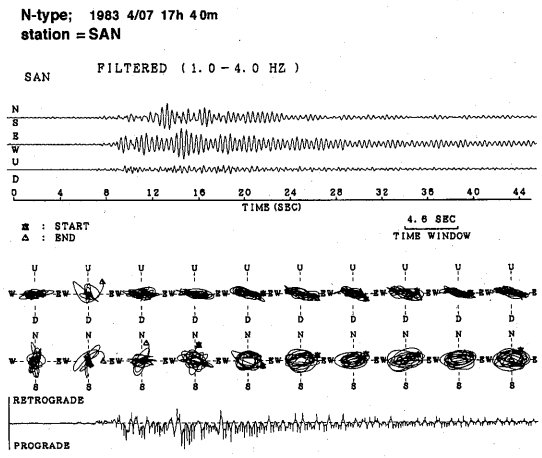

Fig. 56b. Particle motion diagram for the low-frequency portion (1-4 Hz) of a N-type event at station SAN.

volcanic gases and that there is a sub-vent or a crack under the crater extending near station SAN. The location of sub-vent or crack is inferred to be in the range of about 0 to 1 km beneath the vent from the distribution of focal depths of N-type events. B-type events occurred in the depth range of 0 to 1 km reaching ground water near the station SAN via a sub-vent or a crack. The edifice of the Asama volcano is probably very porous. This is why the sporadic occurrence of B-type events does not trigger N-type events and that hybrid events follow swarms of B-type events.

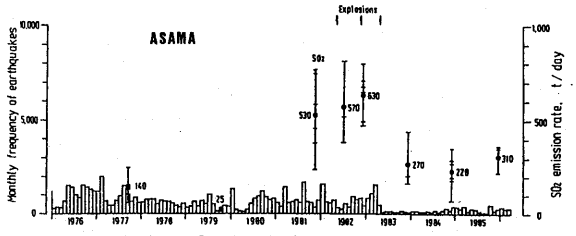

Fig.3 Variations of SO2 emission rates at Asama volcano.
Earthquake data from Asama V.O., ERI, Univ. Tokyo.

Fig. 57. Variations of SO_2 emission rates and monthly frequency of volcanic earthquakes at Asama volcano (After OHTA *et al.*, 1988).

8. Discussion

8.1 Source of B-type and explosion events

The source mechanism of explosion earthquakes at Sakurajima volcano were investigated in detail by IGUCHI (1994), UHIRA and TAKEO (1994) and UHIRA *et al.* (1995 a). UHIRA and TAKEO (1994) and UHIRA *et al.* (1995 a) investigated the force system equivalent to the volcanic eruptions using the waveform inversion method. Important results obtained by them were: 1) the estimated source time function showed that rapid expansion and subsequent contraction occurred in the source region at the initial stage of the eruption, 2) a vertical force dipole M_{zz} was the largest of the diagonal elements of the moment tensor in the initial expansion of the source region. Although only one example of the explosion event was analyzed in this study, the result is consistent with them.

Hypocenter distribution of B-type and explosion events implies that they probably occur in the vent. The source model of BM-type and BL-type events at Asama volcano obtained in this study shows that the initial stage of these events is excited by pressure changes in the source region of cylindrical form. The spectra of BM-type and BL-type events have approximately common prominent peaks (Fig. 14). The difference between the dominant frequencies of BM-type events and those of BL-type events can be explained by the difference of focal depths. Hypocenter depths of BM-type events seem to be deeper than those of BL-type events. Because the source mechanism of BL-type events is similar to BM-type events and the locations of BL-type events are shallower than those of BM-type events, attenuation of the high-frequency parts of BL-type events is much stronger than that of BM-type events due to path effects. This may be the reason why the spectra of BL-type events are dominant at low frequencies than those of BM-type events.

As shown in Figs. 26 and 28, the hypocenters of BH-type events are located deeper than those of BL-type and BM-type events. Increases in the number of the daily frequencies of BH-type events also have a close relation to the volcanic activity of Asama volcano. Although we omitted showning the results of an analysis of BH-type events because we could not obtain reliable results in comparison with those of BM-type and BL-type events, a tentative analysis of the waveform inversion of BH-

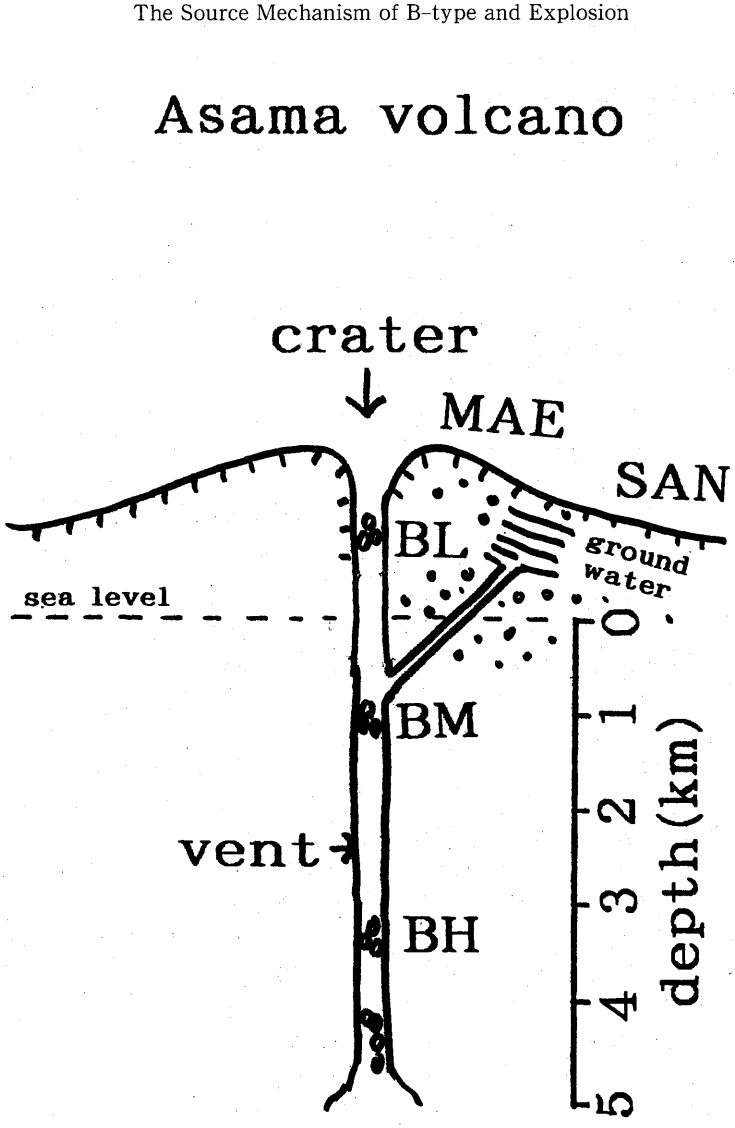

Fig. 58. Conceptual model of the Asama volcano magma system inferred from seismic data.

type events suggests that the source mechanism of BH-type events may be similar to that of BM-type and BL-type events. Moreover, both BM-type and BH-type events could trigger N-type events. Therefore, we may think that the source mechanism of BH-type events is also similar to that of BM-type and BL-type events.

As for BH-type events, the dominant frequencies of BH-type events are different from those of BL-type and BM-type events. An approximately 1 Hz peak is found in the spectral peaks of BL-type events. However, the peak frequency of 1 Hz is not recognized among the spectral peaks of BH-type events. The fundamental frequen-

cy of BH-type events is approximately 2 Hz (cf. Fig. 14). If the source of B-type is represented by pressure changes of a fluid-filled cylinder with finite length, the dominant frequencies are expressed as (cf. FERRICK *et al.*, 1982),

$$f = \frac{na}{4L} \quad n = 1, 2, 3, 4, \cdots\cdots$$

where f is frequencies, a is the pressure wave speed in the fluid and L is the cylinder length. The frequencies are the odd harmonics or the even harmonics as a cylinder responds as if it were a closed (or open) pipe or a one open at one end. If the pressure wave speed and pipe length are not so different between the top of the vent and the bottom, the discrepancy in the dominant frequencies may be explained by difference in pipe conditions. BH-type events are triggered by pressure changes of an open or closed cylinder. Conversely, BM-type and BL-type events are triggered by pressure changes of a cylinder that is open at one end. If the cylinder length of the BL-type event is approximately the same as that of BH-type events, then the fundamental frequency of BH-type events becomes bimodal compared to that of BL-type events. However, if this is only one of the BH-type events, then the fundamental frequency of BH-type becomes bimodal compared to that of BL-type events. However, this may be only possibility which explains why the fundamental frequency of BM-type and BL-type events is approximately 1 Hz and that of BH-type events is approximately 2 Hz. It is not clear whether the spectra of each type of event are excited by odd harmonics or even harmonics. Another idea is based on experimental data that the sound speed of water-steam rich vapor is sensible to changes in pressure and temperature (KIEFFER, 1984). If the cylindrical pipe is filled with water-steam rich volcanic gases, volcanic gases which trigger BH-type events have much higher pressures and temperatures than those of BM-type and BL-type events.

8.2 Long-period events at Redoubt volcano and N-type events at Asama volcano

Seismograms of N-type events at Asama volcano are very similar to those of long-period events at Redoubt volcano. As mentioned earlier, CHOUET *et al.* (1994) and CHOUET (1996) proposed a source model of long-period earthquakes at Redoubt volcano. They occur in the following process: 1) there are a shallow hydrothermal system and a magma chamber at Redoubt volcano; long-period event source is located between two reservoirs; shallow magma chamber is located 2.5 km beneath

Table 12. Comparison of sources of long-period earthquakes.

volcano	Asama volcano	Redoubt volcano
trigger	B-type events	A-type events
hypocenters of long-period events	outside the vent	beneath the vent
location of trigger	beneath the vent	beneath the vent
time sequence of which long-period events appear	the results of swarms of B-type events	precursor of eruptive activity

the crater and 1-2 km north of the vent, 2) a fluid-filled crack is excited by a supersonic magmatic steam flow from the shallow magma chamber, 3) then long-period events are produced by the resonant vibrations of a fluid-driven crack under the crater, 4) long-period event activity is triggered by an unsteady choked flow response to fluctuations of outlet pressure associated with the reaction of the upper reservoir to the injection of mass and heat from below, 5) thus long-period events appear as a precursor to the eruptive activity of Redoubt volcano.

A comparison of this study with CHOUET's model is summarized in Table 12. CHOUET's model is based on the earthquake classification of LAHR *et al.* (1994). LAHR *et al.* (1994) and POWER *et al.* (1994) classified volcanic earthquakes at Redoubt volcano into five types: 1) volcano-tectonic earthquakes that have clear high-frequency P and S arrivals, 2) long-period earthquakes that have quasi-monochromatic waveforms and high-frequency onset phases, 3) hybrid events that share both characteristics of volcano-tectonic events and long-period events; hybrid events that have high-frequency onsets, clear P and S phases, and an extended coda, 4) explosion events, 5) volcanic tremors. In their earthquake classification volcano-tectonic events represent a brittle failure resulting from strain induced by a volcanic process, and volcano-tectonic events include both A-type and B-type earthquakes. LAHR *et al.* (1994) and POWER *et al.* (1994) consider that B-type events occur due to a brittle failure in the edifice and that emergent low-frequency waveforms of B-type events are due to the attenuation of high-frequency energy along the propagation path.

Major differences between the results obtained at Asama volcano and those of Redoubt volcano are: 1) an earthquake type which triggers N-type or long-period events, 2) volcanic gases which excite N-type or long-period events are primary magma origin or secondary magma origin, 3) location of the source of N-type or long-period events.

As mentioned in Chap. 3, we distinguished B-type earthquakes from A-type events at Asama volcano (cf. MINAKAMI, 1960, 1974; SAWADA, 1994). The locations of A-type events are different from those of B-type events (cf. Fig. 26). A-type events at Asama volcano do not occur under the vent. The occurrence of B-type events has a close relation to the volcanic activity of Asama volcano. Moreover, we can discriminate the spectra of B-type events from those of A-type events at Asama volcano using the Sompi spectral analysis. CHOUET *et al.* (1994) and CHOUET (1996) start from an earthquake classification obtained at Redoubt volcano. They assumed a fluid-filled crack under the crater. In the case of Asama volcano, B-type events occur under the crater. We think that the vent is a stable pipe which transfers a large quantity of volcanic gases and that B-type events occur in the vent. As shown in Chap. 6, the source mechanism of B-type events was different from that driven by a tensile crack or a brittle failure. We analyzed the high-frequency beginnings of N-type events and found that spectral structures of these parts are very similar to those of B-type events. Therefore, we may conclude that N-type events at Asama volcano are triggered by B-type events.

Locations of long-period events at Redoubt volcano are determined to be under

the vent while the source of the main motions of N-type events at Asama volcano is located near station SAN, which is located 2.6 km east of the crater. Therefore, we consider that N-type events are triggered by B-type events and then excited by a secondary source, which is located near station SAN. If N-type events at Asama volcano are excited by volcanic gases of the primary magma origin, N-type events may be precursors to eruptive activity. However, N-type events often occur during a calm stage at Asama volcano (TANAKA and JINGU, 1979). Observations that the locations of the main motions of N-type events are located outside the vent and that N-type events are not precursors to eruptive activity imply that N-type events are excited by volcanic gases of a secondary magma origin.

Discrepancies in the locations of initial motions of N-type events and those of main motions of N-type events strongly suggest that the source of main motions of N-type events is excited by primary source under the vent and that the vent is connected to the secondary source location by a crack or a sub-vent. Travel time at which the initial motions of N-type events at station MAE transfer until the onset of main motions of N-type events at station SAN is roughly estimated to be around 2.6 s (cf. Fig. 56). Apparent velocity which triggers the main motion of N-type events from stations MAE to SAN is roughly estimated to be 0.5 km/s. This apparent velocity is much slower than that of the initial motions of N-type events (cf. Figs. 5 and 47). This shows that the primary source is under the vent transfer to station SAN with an apparent velocity of approximately 0.5 km/s and that locations of primary source (i.e., the vent) and locations of secondary source are connected with air or volcanic gases such as vapor rich steam.

9. Summary and conclusions:

(1) B-type events may be classified as high-frequency B-type (BH-type) and low-frequency B-type (BL-type) events. However, there are also medium-frequency B-type (BM-type) events. BM-type events have the wave characteristics of both BH-type and BL-type events.

(2) Focal depths of BH-type events are deeper than those of BL- and BM-type events. Typical BL-type and explosion events predominantly consist of Rayleigh waves.

(3) A cylindrical model gives the minimum residuals and AIC for BM- and BL-type events. The tensile crack model offers the second minimum residuals and AIC for BM- and BL-type events. Distribution of cumulative source time functions suggests that BM- and BL-type events are triggered not only by expansion but also by contraction of a cylindrical form vessel.

(4) Moment tensor M_{zz} component gives the minimum residuals and AIC for the explosion event. The cylindrical model offers second minimum residuals and AIC. This suggests that vibrations of the explosion event are triggered by the emission of volcanic gases both upward and downward.

(5) The observational fact that emissions of volcanic gases at Asama is correlated with the occurrence of B-type events supports the view hat B-type events are

the results of emissions of volcanic gases in the vent.

(6) N-type events are triggered B-type events. Hypocenters of N-type events determined from initial motions are located under the crater. However, the results of polarization and spectral analyses indicate that main motions of N-type events are located near the station SAN.

(7) N-type events occur as the results of B-type earthquake swarms N-type events are not a precursor of eruptive activity of Asama volcano. There are hybrid type events between B-type and typical N-type events. These hybrid events appear before the advent of typical N-type events.

(8) Spectral analyses of high-frequency beginnings of N-type events show that the spectral structures are very similar to those of BH- or BM-type events. These support the view that N-type events are triggered by B-type events.

Acknowledgments

The author is grateful to Prof. M. Takeo and Dr. K. Uhira of Japan Meteorological Agency who kindly provided computer programs of waveform inversion and very valuable advice. Thanks are due to Prof. H. Watanabe and Prof. K. Ishihara of Kyoto Univ. who kindly reviewed this paper and provided very useful advice. Thanks are due to Prof. H. Hamaguchi of Tohoku Univ. and Prof. Y. Hamano and Prof. Y. Sasai who kindly reviewed this paper. Thanks are due to Prof. Y. Tanaka of Kyoto Univ. who kindly constructed an amplifier of 5-sec seismographs, and measured the frequency response. Prof. Kawakatsu critically read the first version of the manuscript. The author is grateful to Dr. H. Mikada and Dr. T. Miyazaki of Tokyo government for valuable information and discussions. Thanks are also due to the staff of AVO, N. Gyoda, E. Koyama and H. Tsuji who were of great help. Thanks are due to Prof. emeritus I. Yokoyama of Hokkaido Univ. who provided constant encouragement me. Thanks are due to Prof. emeritus D. Shimozuru of Tokyo Univ. for his encouragement. The author is also grateful to one of anonymous referees. The manuscript has been much improved by his comments. For this study, the author used the computer system of Earthquake Information Center of Earthquake Research Institute, the University of Tokyo.

References

ABE, K., 1979, Magnitude of major volcanic earthquakes of Japan 1901 to 1925, *J. Fac. Sci., Hokkaido Univ., Ser. VII (Geophys.)*, **6**, 201-212.

AKI, K., 1984, Evidence for magma intrusion during the Mammoth Lakes earthquakes of May 1980 and implications of the absence of volcanic (harmonic) tremor, *J. Geophys. Res.*, **89**, 7689-7696.

AKI, K., 1988, Local site effects on ground motion, in "Earthquake Engineering and Soil Dynamics II: Recent Advances in Ground-Motion Evaluation" edited by J. Lawrence Von Thun, *Am. Soc. Civil Eng. Geotechnical Special Publication* **20**, pp. 103-155.

AKI, K., 1992, State of the art in volcanic seismology, in "Volcanic Seismology", edited by P. Gasparini, R. Scarpa and K. Aki, Springer-Verlag, Berlin, pp. 3-10.

AKI, K. and B.A. CHOUET, 1975, Origin of coda waves: source, attenuation, and scattering effects, *J. Geophys. Res.*, **80**, 3322–3342.

AKI, K. and R.Y. KOYANAGI, 1981, Deep volcanic tremor and magma ascent mechanism under Kilauea, Hawaii, *J. Geophys. Res.*, **86**, 7095–7109.

AKI, K. and P.G. RICHARDS 1980, Quantitative Seismology, W.H. Freeman, San Francisco, California.

AKI, K. and Y.B. TSAI, 1972, Mechanism of Love-wave excitation by explosive sources, *J. Geophys. Res.*, **77**, 1452–1475.

AKI K., M. FEHLER and S. DAS, 1977, Source mechanism of volcanic tremor: fluid-driven crack models and their application to the 1963 Kilauea eruption, *J. Volcanol. Geotherm. Res.*, **2**, 259–287.

ARAMAKI, S., 1963, Geology of Asama Volcano, *J. Fac. Sci. Univ. Tokyo, Sec. 2*, **14**, 229–443.

ASAKAWA, E., H. UTADA and T. YUKUTAKE, 1988, Application of Sompi spectral analysis to the estimation of the geomagnetic transfer function, *J. Geomag. Geoelectr.*, **40**, 447–463.

BOUCHON, M., 1979, Discrete wave number representation of elastic wave fields in three-space dimensions, *J. Geophys. Res.*, **84**, 3609–3614.

BOUCHON, M., 1981, A simple method to calculate Green's function for elastic layered media, *Bull. Seism. Soc. Am.*, **71**, 959–971.

CHIN, B.-H. and K. AKI, 1991, Simultaneous study of the source, path, and site effects on strong ground motion during the 1989 Loma Prieta earthquake: a preliminary result on pervasive nonlinear site effects, *Bull. Seism. Soc. Am.*, **81**, 1859–1884.

CHOUET, B.A., 1985, Excitation of buried magmatic pipe: a seismic source model for volcanic tremor, *J. Geophys. Res.*, **90**, 1881–1893.

CHOUET, B.A., 1986, Dynamics of a fluid-driven crack in three dimensions by the finite difference method, *J. Geophys. Res.*, **91**, 13967–13992.

CHOUET, B.A., 1988, Resonance of a fluid-driven crack: radiation properties and implications for the source of long-period events and harmonic tremor, *J. Geophys. Res.*, **93**, 4375–4400.

CHOUET, B.A., 1996 a, Long-period volcano seismicity: its source and use in eruption forecasting, *Nature*, **380**, 309–316.

CHOUET, B.A., 1996 b, New methods and future trends in seismological volcano monitoring, in "Monitoring and Mitigation of Volcanic Hazards", edited by R. Scarpa, R.I. Tilling, Springer-Verlag, Berlin, pp. 23–97.

CHOUET, B.A., R.Y. KOYANAGI and K. AKI, 1987, Origin of volcanic tremor in Hawaii. Part II: Theory and discussion, *U. S. Geol. Surv. Prof. Pap.*, **1350**, 1259–1280.

EARTHQUAKE RESEARCH INSTITUTE, UNIV. of TOKYO, 1983 a, Seismic activity of Asama Volcano during the period Jan. 1–Oct. 24, 1982 and topographic change inside the crater after the April 26 eruption, Rep. Coord. Comm. *Pred. of Volcanic Erupt.*, No. 26, pp. 22–24.

EARTHQUAKE RESEARCH INSTITUTE, UNIV. of TOKYO, 1983 b, A small eruption on October 2, 1982 of Asama Volcano, Rep. Coord. Comm. *Pred. of Volcanic Erupt.*, No. 26, pp. 25.

ENDO, E.T., S.D. MALONE, L.L. NOSON and C.S. WEAVER, 1981, Locations, magnitudes, and statistics of the March 20–May 18 earthquake sequence, *U.S. Geol. Surv. Prof. Pap.*, **1250**, 93–107.

FERRAZZINI, V. and K. AKI, 1987, Slow waves trapped in a fluid-filled infinite crack: implication for volcanic tremor, *J. Geophys. Res.*, **92**, 9215–9223.

FERRAZZINI, V. and K. AKI, 1992, Preliminary results from a field experiment on volcanic events at Kilauea using an array of digital seismographs. in "Volcanic Seismology", edited by P. Gasparini R. Scarpa and K. Aki, Springer-Verlag, Berlin, pp. 168-189.

FERRICK, M.G., A. QAMAR and W.F. ST. LAWRENCE, 1982, Source mechanism of volcanic tremor, *J. Geophys. Res.*, **87**, 8675-8683.

FOULGER, G.R. and R.E. LONG, 1992, Non-double couple earthquake focal mechanisms and the accretionary tectonic cycle, in "Volcanic Seismology", edited by P. Gasparini, R. Scarpa and K. Aki, Springer-Verlag, Berlin, pp. 223-234.

FUJITA, E, Y. IDA and J. OIKAWA, 1995, Eigen oscillation of a fluid sphere and source mechanism of harmonic tremor, *J. Volcanol. Geotherm. Res.*, **69**, 365-378.

FUKUYAMA, E. and M. TAKEO, 1990, Analysis of the near-field seismogram observed during the eruption of Izu-Oshima volcano on November 16, 1987, *Bull. Volcanol. Soc. Japan*, **35**, 283-0297 (in Japanese with English abstract).

GORDEEV, E.I., 1992, Modelling of volcanic tremor wave fields, *J. Volcanol. Geotherm. Res.*, **51**, 145-160.

HAMADA, N., H. JINGU and K. IKUMOTO, 1976, On the volcanic earthquakes with slowly decaying coda wave, *Bull. Volcanol, Soc. Japan*, **21**, 167-183 (in Japanese with English abstract).

HAMAGUCHI, H., T. NISHIMURA and N. ZANA, 1992, Process of the 1977 Nyiragongo eruption inferred from the analysis of long-period earthquakes and volcanic tremors, *Tectonophysics*, **209**, 241-254.

HIRABAYASHI, J., 1982, Geochemical study on the Sakurajima Volcano, *Bull. Volcanol. Soc. Japan*, **27**, 293-309 (in Japanese with English abstract).

HORI, S., Y. FUKAO, M. KUMAZAWA, M. FURUMOTO and A. YAMAMOTO, 1989, A new method of spectral analysis and its application to the earth's free oscillations: The Sompi method, *J. Geophys. Res.*, **94**, 7535-7553.

IGUCHI, M., 1989, Distribution of the initial motions of volcanic micro-earthquakes (B-type) at Sakurajima Volcano, *Ann. Disast. Prevent. Res. Inst. Kyoto Univ.*, **32** (B-1), 13-22 (in Japanese with English abstract).

IGUCHI, M., 1991, Geophysical data collection using an interactive personal computer system (Part 1)-Experimental monitoring of Suwanosejima Volcano-, *Bull. Volcanol. Soc. Japan*, **36**, 335-343.

IGUCHI, M., 1994, A vertical expansion source model for the mechanisms of earthquakes originated in the magma conduit of an andesitic volcano: Sakurajima, Japan, *Bull. Volcanol. Soc. Japan*, **39**, 49-67.

IGUCHI, M., 1995, Source mechanism of volcanic earthquakes and tremors and their field of origin, *Bull. Volcanol. Soc. Japan*, **40**, S47-S57.

IGUCHI, M. and K. ISHIHARA, 1990, Comparison of earthquakes and air-shocks associated with explosive eruptions at Sakurajima and Suwanosejima volcanoes, *Ann. Disast. Prevent. Res. Inst. Kyoto Univ.*, **33** (B-1), 1-12 (in Japanese with English abstract).

IMAI, H., 1980, Explosion earthquakes associated with the 1973 eruptions of Asama Volcano. (Part 2) The summary of studies on explosion earthquakes and a model of explosions inferred from seismic data, *Bull. Earthq. Res. Inst., Univ. Tokyo*, **55**, 537-576 (in Japanese with English abstract).

IMAI, H., 1983 a, A short comment on the 1982 explosive eruption of Asama Volcano, central Honshu, Japan, *Bull. Earthq. Res. Inst., Univ. Tokyo*, **58**, 401–409.

IMAI, H., 1983 b, A mechanism of successive eruption as inferred from seismic data associated with the 1973 eruptive stage of Asama Volcano, in "Arc Volcanism: Physics and Tectonics", edited by D. Shimozuru and I. Yokoyama, Terra Science Publishing Company, Tokyo, pp. 63–80.

IMAI, H., N. GYODA and E. KOYAMA, 1979, Explosion earthquakes associated with the 1973 eruptions of Asama Volcano. (Part 1) Spectral studies, *Bull. Earthq. Res. Inst., Univ. Tokyo*, **54**, 161–186 (in Japanese with English abstract).

INOUE, M. (Editor), 1987, The Chronicles of Japan (Translated into Modern Japanese), Chuo-koron-sha Inc., Tokyo, Vol. **2**, PP. 353.

ISHIHARA, K., 1990, The pressure sources and induced ground deformation associated with explosive eruptions at an andesitic volcano: Sakurajima volcano, Japan, in "Magma Transport and Storage", edited by M.P. Ryan, John Wiley, New York, pp. 336–356.

ISHIHARA, K. and M. IGUCHI, 1989, The relationship between micro-earthquake swarms and volcanic activity at Sakurajima Volcano, *Ann. Disast. Prevent. Res. Inst. Kyoto Univ.*, **32** (B-1), 1–11 (in Japanese with English abstract).

ISHIHARA, K., M. IGUCHI and K. KAMO, 1983, Emission of volcanic cloud and gases on the process of a volcanic explosion, *Ann. Disast. Prevent. Res. Inst. Kyoto Univ.*, **26** (B-1), 1–7 (in Japanese with English abstract)

JULIAN, B. and S.T. SIPKIN, 1985, Earthquake processes in the Long Valley caldera area, California, *J. Geophys. Res.*, **90**, 11155–11169.

KAGIYAMA, T., N. GYODA, E. KOYAMA and H. TSUJI, 1982, Seismic activities at the flank of the volcano Asama, *Bull. Volcanol. Soc. Japan*, 27, 311–313 (in Japanese).

KAGIYAMA, T., N. GYODA, E. KOYAMA and H. TSUJI, 1985, Geological meanings of minor eruptions of the volcano Asama and their precursor phenomena, in "Comparative Studies of Physical Background of Volcanic Activity and its Relation to Eruption Disasters", edited by H. Okada, Hokkaido Univ., pp. 92–101.

KAKUTA, T. and Z. IDEGAMI, 1970, The volcanic tremors of "C-type" at the Sakurajima Volcano, *Bull. Volcanol. Soc. Japan*, **15**, 61–74 (in Japanese with English abstract).

KAKUTA, T. and Y. NONAKA, 1979, Spectra of volcanic earthquakes related to the eruptions of Sakurajima Volcano in February, 1975, *Bull. Volcanol. Soc. Japan*, **24**, 213–222 (in Japanese with English abstract).

KAMO, K., 1978, Some phenomena before the summit eruptions at Sakura-jima Volcano, *Bull. Volcanol. Soc. Japan*, **23**, 53–64 (in Japanese with English abstract).

KAMO, K., T. FURUSAWA and J. AKAMATSU, 1977, Some nature of the volcanic tremors at Sakura-jima Volcano, *Bull. Volcanol. Soc. Japan*, **22**, 41–58 (in Japanese with English abstract).

KANAMORI, H. and J.W. GIVEN, 1982, Analysis of long-period seismic waves excited by the May 18, 1980 eruption of Mount St. Helens–A terrestrial monopole?, *J. Geophys. Res.*, **87**, 5422–5432.

KANAMORI, H. and J. MORI, 1992, Harmonic excitation of mantle Rayleigh waves by the 1991 eruption of Mount Pinatubo, Philippines, *Geophys. Res. Lett.*, **19**, 721–724.

KANAMORI, H., J. MORI and D.G. HARKRIDER, 1994, Excitation of atmospheric oscillations by volcanic eruption, *J. Geophys. Res.*, **99**, 21947–21961.

KANAMORI, H., J.W. GIVEN and T. LAY, 1984, Analysis of seismic body waves excited by the Mount St. Helens eruption of May 18, 1980, *J. Geophys. Res.*, **89**, 1856-1866.

KANASEWICH, E.R., 1981, Time Sequence Analysis in Geophysics, 3rd ed., The Univ. of Alberta Press, Edmonton, Alberta, Canada, pp. 162-164.

KANESHIMA, S., H. KAWAKATSU, H. MATSUBAYASHI, Y. SUDO, T. TSUTSUI, T. OHMINATO, H. ITO, K. UHIRA, H. YAMAMOTO, J. OIKAWA, M. TAKEO, and T. IIDAKA, 1996, Mechanism of phreatic eruptions at Aso volcano inferred from near-field broadband seismic observations, *Science*, **272**, 642-645.

KAWAKATSU, H., 1991, Earthquake size and varieties determined by moment tensor inversions, *Zisin*, **44**, 265-277 (in Japanese with English abstract).

KAWAKATSU, H., T. OHMINATO, H. ITO, Y. KUWAHARA, T. KATO, K. TSURUGA, S. HONDA and K. YOMOGIDA, 1992, Broadband seismic observation at the Sakurajima volcano, *Japan, Geophys. Res. Lett.*, 19, 1959-1962.

KENNETT, B.L.N. and N.J. KERRY, 1979, Seismic waves in a stratified half space, *Geophys. J.R. Astr. Soc.*, **57**, 557-583.

KIEFFER, S.W., 1984, Seismicity at Old Faithful Geyser: an isolated source of geothermal noise and possible analogue of volcanic seismicity, *J. Volcanol. Geotherm. Res.*, **22**, 59-95.

KIKUCHI, S., 1962, On the short period volcanic micro-tremors at Mt. Aso, *Bull. Volcanol. Soc. Japan*, **7**, 1-16 (in Japanese with English abstract).

KIKUCHI, S., 1964, On the short period volcanic micro-tremors at Mt. Aso (II), *Bull. Volcanol. Soc. Japan*, **9**, 91-16 (in Japanese with English abstract).

KIKUCHI, M. and H. KANAMORI, 1982, Inversion of complex body waves, *Bull. Seism. Soc. Am.*, **72**, 491-506.

KIKUCHI, M. and H. KANAMORI, 1991, Inversion of complex body waves-III, *Bull. Seism. Soc. Am.*, **81**, 2335-2350.

KNOPOFF, L. and M.J. RANDALL, 1970, The compensated linear vector dipole, a possible mechanism for deep earthquakes, *J. Geophys. Res.*, **75**, 4957-4963.

KOYANAGI, R.Y., B.A. CHOUET and K. AKI, 1987, Origin of volcanic trmor In Hawaii. Part I Data from the Hawaii Volcano Observatory 1969-1985, *U.S. Geol. Surv. Prof. Pap.*, **1350**, 1221-1257.

KUBOTERA, A., 1964, Volcanic micro-tremor of the Volcano Aso (I)-Nature of the volcanic micro-tremor of the second kind and its source condition-, *Bull. Volcanol Soc. Japan*, **9**, 87-98 (in Japanese with English abstract).

KUBOTERA, A., 1974, Volcanic tremors at Aso Volcano, in "Physical Volcanology", edited by L. Civetta, P. Gasparini, G. Luongo and A. Rapolla, Elsevier, New York, pp. 29-48.

KUDO, K., M. SAWADA, M. SAKAUE, T. MIYAZAKI and S. OSHIMA, 1991, Volcanic tremor associated with the 1989 submarine eruption off Ito, Japan, *J. Phys. Earth*, **39**, 27-45.

KUMAZAWA, M., M. FURUMOTO, Y. FUKAO, A. YAMAMOTO and H. MIZUTANI, 1983, The Sompi method: Its principle and merits, *Programme Abstr. Seismol. Soc. Japan*, I, pp.137.

KUMAZAWA, M., Y. IMANISHI, Y. FUKAO, M. FURUMOTO and A. YAMAMOTO, 1990, A theory of spectral analysis based on the characteristic property of a linear dynamic system, *Geophys. J. Int.*, **101**, 613-630.

LAHR, J.C., B.A. CHOUET, C.D. STEPHENS, J.C. POWER and R.A. PAGE, 1994, Earthquake classification, location, and error analysis in a volcanic environment: implications for the magmatic

system of the 1989–1990 eruptions at Redoubt volcano, Alaska, *J. Volcanol. Geotherm. Res.*, **62**, 137–151.

LATTER, J.H., 1981, Volcanic earthquakes, and their relationship to eruptions at Ruapehu and Ngauruhoem volcanoes, *J. Volcanol. Geotherm. Res.*, **9**, 293–309.

LIU, H., D.L. ANDERSON and H. KANAMORI, 1976, Velocity dispersion due to an elasti-city; implica tions for seismology and mantle composition, *Geophys. J.R. Astr. Soc.*, **47**, 41–58.

MALONE, S.D., 1983, Volcanic earthquakes, examples from Mt. St. Helens, in "Earthquakes, Observation, Theory and Interpretation", edited by H. Kanamori, Elsevier/North-Holland, Amsterdam, pp. 435–455.

MATSUSHIMA, N., Y. NISHIMURA, A. SUZUKI and H. OKADA, 1987, Spectral analysis of volcanic earthquakes observed at Mt. Tokachi, *Bull. Volcanol. Soc. Japan*, **32**, 317–328 (in Japanese with English abstract).

MCNUTT, S.R., 1986, Observation and analysis of B-type earthquakes, explosions, and volcanic tremor at Pavlof Volcano, Alaska, *Bull. Seism. Soc. Am.*, **76**, 153–175.

MENKE, W., 1984, Geophysical Data Analysis: Discrete Inverse Theory, Academic Press, New York, pp. 1–260.

MIKADA, H., 1992, On the volcanic tremor originating from Asama Volcano–Interpretation of tremor associated with the 1973 and the 1982 activity–, *Bull. Volcanol. Soc. Japan*, **37**, 21–33 (in Japanese with English abstract).

MINAKAMI, T., 1935 a, Changes in the relative height to the cone of Volcano Asama, *Bull. Earthq. Res. Inst., Univ. Tokyo*, **13**, 318–327 (in Japanese with French abstract).

MINAKAMI, T., 1935 b, The explosive activities of Volcano Asama in 1935. (Part 1), *Bull. Earthq. Res. Inst., Univ. Tokyo*, **13**, 629–644.

MINAKAMI, T., 1935 c, The explosion activities of Volcano Asama in 1935. (Part 2), *Bull. Earthq. Res. Inst., Univ. Tokyo*, **13**, 790–800.

MINAKAMI, T., 1936, Changes in the height of Volcano Asama caused by eruptions in 1935, *Bull. Earthq. Res. Inst., Univ. Tokyo*, **14**, 222–234.

MINAKAMI, T., 1937, Changes in the depth of the crater floor of Volcano Asama in the recent activities, *Bull. Earthq. Res, Inst., Univ. Tokyo*, **15**, 492–496.

MINAKAMI, T., 1942 a, On the distribution of volcanic ejecta. (Part 1) The distribution of volcanic bomb ejected by the recent explosions of Asama, *Bull. Earthq. Res. Inst., Univ. Tokyo*, **20**, 65–92.

MINAKAMI, T., 1942 b, On the distribution of volcanic ejecta. (Part 2) The distribution of Mt. Asama pumice in 1783, *Bull. Earthq. Res. Inst., Univ. Tokyo*, **20**, 93–106.

MINAKAMI, T., 1950 a, Report on the volcanic activities in Japan during 1939–1947, *Bull. Volcanol.*, **10**, 45–58.

MINAKAMI, T., 1950 b, On explosive activities of andesitic volcanoes and their forerunning phenomena, *Bull. Volcanol.*, **10**, 59–87.

MINAKAMI, T., 1956, Report on volcanic activities and volcanological studies in Japan for the period from 1951 to 1954, *Bull. Volcanol.*, **18**, 39–76.

MINAKAMI, T., 1959, The study of eruptions and earthquakes originating from volcanoes. (Part 1) Some statistical relations between explosive eruptions and earthquakes of Volcano Asama, *Bull Volcanol. Soc. Japan*, **4**, 104–114 (in Japanese with English abstract).

MINAKAMI, T., 1960, Fundamental research for predicting volcanic eruptions. (Part 1) Earthquakes and crustal deformations originating from volcanic activities, *Bull. Earthq. Res. Inst., Univ. Tokyo*, **38**, 497–544.

MINAKAMI, T., 1974, Seismology of volcanoes in Japan, in "Physical Volcanology", edited by L. Civetta, P. Gasparini, G. Luongo and A. Rapolla Elsevier, New York, pp. 1–27.

MINAKAMI, T. and K. MOGI, 1959, Report on volcanic activities in Japan for the period from 1954 to 1957, *Bull Volcanol.*, **21**, 127–151.

MINAKAMI, T. and S. SAKUMA, 1953, Report on volcanic activities and volcanological studies concerning them in Japan during 1948–1951, *Bull Volcanol.*, **14**, 79–130.

MINAKAMI, T., K. MOGI, S. HIRAGA and T. MIYAZAKI, 1957, On the investigation of explosive activities of Sakura-jima and various earthquakes originating from the volcano. (Part 1), *Bull. Volcanol. Soc. Japan*, **2**, 77–90 (in Japanese with English abstract).

MINAKAMI, T., S. HIRAGA, S. UTIBORI, and T. MIYAZAKI, 1959, The study of eruptions and earthquakes originating from volcanoes. (Part 2) Some contribution to prediction of explosive eruption of Volcano Asama, *Bull. Volcanol. Soc. Japan*, **4**, 115–130 (in Japanese with English abstract).

MINAKAMI, T., S. SAKUMA, K. MOGI and S. HIRAGA, 1960, The study of eruptions and earthquakes originating from volcanoes. (Part 3) Relation between depth of volcanic earthquakes and subsequent volcanic phenomena, *Bull. Volcanol. Soc. Japan*, **5**, 133–151 (in Japanese with English abstract).

MINAKAMI, T., S. UTIBORI, S. HIRAGA, T. MIYAZAKI, N. GYODA and T. UTSUNOMIYA, 1970 a, Seismometrical studies of Volcano Asama. Part 1. Seismic and volcanic activities of Asama during 1934–1969, *Bull. Earthq. Res. Inst., Univ. Tokyo*, **48**, 235–301.

MINAKAMI, T., S. UTIBORI, T. MIYAZAKI, S. HIRAGA, H. TERAO and K. HIRAI, 1970 b, Seismometrical studies of Volcano Asama. Part 2. Anomalous distribution of the P arrival times and some information of the velocity of the P wave propagating through the volcano, *Bull. Earthq. Res. Inst.., Univ. Tokyo*, **48**, 431–489.

MIYAZAKI, T., 1990, Recent crustal movement of active volcanoes in Japan as revealed by leveling survey, *Bull. Earthq. Res. Inst., Univ. Tokyo*, **65**, 665–807 (in Japanese with English abstract).

MORI, J., H. PATIA, C. MCKEE, I. ITIKARAI, P. LOWENSTEIN, P. DE SAINT OURS and B. TALAI, 1989, Seismicity associated with eruptive activity at Langila volcano, Papua New Guinea, *J. Volcanol. Geotherm. Res.*, **38**, 243–255.

NAGAMUNE, T., 1975, Volcanic tremors of C type observed at Sakurajima, *Bull. Volcanol. Soc. Japan*, **20**, 157–168 (in Japanese with English abstract).

NAKAGAWA, T. and Y. OYANAGI, 1982, Experimental Data Analysis with Least Squares-Program SALS, Univ. of Tokyo Press, Tokyo, pp. 1– 206 (in Japanese).

NISHI, K., 1966, High sensitivity seismometric observation near the crater of Volcano Sakurajima (Part I)-On the initial motion of B-type volcanic micro-earthquake-, *Bull. Volcanol. Soc. Japan*, **11**, 84–92 (in Japanese with English abstract).

NISHI, K., 1980, Spectral study on the volcanic earthquake (I)-explosion earthquake-, *Ann. Disast. Prevent. Res. Inst. Kyoto Univ.*, **23** (B-1), 29–35 (in Japanese with English abstract).

NISHI, K., T. ETO, M. IGUCHI, T. TAKAYAMA, Y. NISHIMURA, H. HAMAGUCHI, T. NISHIMURA, M. SAWADA

and M. SUDO, 1991, Seismic activity at Suwanosejima Volcano in October, 1989, Report of the 2nd Joint Observation at Suwanosejima Volcano, 3–11 (in Japanese).

NISHIMURA, T., 1995, Source parameters of the volcanic eruption earthquakes at Mount Tokachi, Hokkaido, Japan, and a magma ascending model, *J. Geophys. Res.*, **100**, 12465–12473.

NISHIMURA, T. and H. HAMAGUCHI, 1993, Scaling law of volcanic explosion earthquake, *Geophys. Res. Lett.*, **20**, 2479–2482.

NISHIMURA, T., H. HAMAGUCHI and S. UEKI, 1994, Source mechanisms of volcanic tremor and low-frequency earthquakes associated with the 1988–89 eruptive activity of Mt. Tokachi, Hokkaido, Japan, *Geophys. J. Int.*, **121**, 444–458.

NISHIMURA, Y., H. MIYAMACHI, S. UEKI, T. NISHIMURA, H. SHIMIZU, S. OHMI and H. OKADA, 1990, Joint seismometrical observations by the national university team during the 1988–1989 eruptive activity of Mt. Tokachi, Hokkaido, *Bull. Volcanol. Soc. Japan*, **35**, 163–173.

OHTA, K., N. MATSUO, H. SHIMIZU, M. KAMADA and T. KAGIYAMA, 1988, Emission rates of sulfur-dioxide from some volcanoes in Japan, in "Kagoshima International Conference on Volcanoes Proceedings", pp. 420–423.

OKADA, H., Y. NISHIMURA, H. MIYAMACHI, H. MORI and K. ISHIHARA, 1990, Geophysical significance of the 1988–1989 explosive eruption of Mt. Tokachi, Hokkaido, Japan, *Bull. Volcanol. Soc. Japan*, **35**, 175–203.

OKITA, T. and D. SHIMOZURU, 1975, Remote sensing measurements of mass flow of sulfur dioxide gas from volcanoes, *Bull. Volcanol, Soc. Japan*, **19**, 151–157 (in Japanese with English abstract).

OMORI, F., 1912, The eruptions and earthquakes of the Asama-yama, *Bull. Imp. Earthq. Inv. Comm.*, **6**, 1–147.

OMORI, F., 1914 a, The eruptions and earthquakes of the Asama- yama II. (List of the volcanic earthquakes instrumentally registered at the Asama-yama (Yuno-taira) observatory in 1911 and 1912), *Bull. Imp. Earthq. Inv. Comm.*, **6**, 149–226.

OMORI, F., 1914 b, The eruptions and earthquakes of the Asama-yama III. (Remarks on the seismographical observations at Yuno-taira in 1911 and 1912), *Bull. Imp. Earthq. Inv. Comm.*, 6, 227–257.

OMORI, F., 1914 c, The eruptions and earthquakes of the Asama-yama IV. (Strong Asama-yama outbursts, Dec. 1912 to May 1914), *Bull. Imp. Earthq. Inv. Comm.*, **7**, 1–215.

OMORI, F., 1917, The eruptions and earthquakes of the Asama-yama V. (List of the volcanic disturbances instrumentally registered at the Asama-yama seismological station, 1913 to 1916), *Bull. Imp. Earthq. Inv. Comm.*, **7**, 217–326.

OMORI, F., 1919, The eruptions and earthquakes of the Asama-yama VI, *Bull. Imp. Earthq. Inv. Comm.*, **7**, 327–456.

POWER, J.A., J.C. LAHR, R.A. PAGE, B.A. CHOUET, C.D. STEPHENS, D.H. HARLOW, T.L. MURRAY and J. N. DAVIES, 1994, Seismic evolution of the 1989–1990 eruption sequence of Redoubt volcano, Alaska, *J. Volcanol. Geotherm. Res.*, **62**, 69–94.

QAMAR, A., W. ST LAWRENCE, J.N. MOORE and G. KENDRICK, 1983, Seismic signals preceding the explosive eruption of Mount St. Helens, Washington, on 18 May 1980, *Bull. Seismol. Soc. Am.*, **73**, 1797–1813.

RADOSKI, H.R., E.J. ZAWALICK and P.F. FOUGERE, 1976, The superiority of maximum entropy

power spectrum techniques applied to geomagnetic micropulsations, *Phys. Earth Planet. Interiors*, **12**, 208–216.

SAITO, M., 1975, An automatic design algorithm for band selective recursive digital filters, *Geophys. Explor.*, **31**, 240–263 (in Japanese with English abstract).

SAITO, M., 1978, Possible instability in the Burg maximum entropy method, *J. Phys. Earth*, **26**, 123–128.

SAKUMA, S., 1951, Damage on window-panes by the air-waves of explosion of Volcano Asama on Sept. 23, 1950, *Bull. Earthq. Res. Inst., Univ. Tokyo*, **29**, 605–615.

SASSA, K., 1935, Volcanic micro-tremor and eruption-earthquakes (Part I of the geophysical studies on the volcano Aso), *Mem. Coll. Sci. Kyoto Univ.*, **18**, 255–293.

SASSA, K., 1936a, Micro-seismometric study on eruptions of the Volcano Aso (Part II of the geophysical studies on the volcano Aso), *Mem. Coll. Sci. Kyoto Univ.*, **19**, 11–56.

SASSA, K., 1936b, Anomalous deflection of seismic rays in volcanic districts (Part III of the geophysical studies on the volcano Aso), *Mem. Coll. Sci. Kyoto Univ.*, **19**, 65–78.

SAWADA, M., 1994, B-type and explosion earthquakes observed at Asama volcano, central Japan, *J. Volcanol. Geotherm. Res.*, **63**, 111–126.

SAWADA, M., N. GYODA, N. OSADA, E. KOYAMA, H. TSUJI, T. KAGIYAMA and T. MIYAZAKI, 1983, P wave velocity structure of Asama Volcano, *Bull. Volcanol. Soc. Japan*, **28**, 301–304 (in Japanese).

SAWADA, M., N. GYODA, E. KOYAMA and H. TSUJI, 1989, Spectral analysis of volcanic earthquakes observed at Asama volcano II, *Bull. Volcanol. Soc. Japan*, **34**, 163–164 (in Japanese).

SCHICK, R., G. LOMBARDO and G. PATANE, 1982, Volcanic tremors and shocks associated with Etna (Sicily), September 1980, *J. Volcanol. Geotherm. Res.*, **14**, 261–279.

SEIDEL, D., R. SCHICK and M. RIUSETTI, 1981, Volcanic tremors at Etna: a model for hydraulic origin, *Bull. Volcanol.*, **44**, 43–56.

SEKIYA, H., 1961, A study of volcanic activity of Mt. Asama, *Bull. Volcanol. Soc. Japan*, **6**, 13–28 (in Japanese with English abstract).

SHERBURN, S. and B.J. SCOTT, 1993, B-type volcanic earthquakes at White Island volcano, New Zealand, *J. Volcanol. Geotherm. Res.*, **56**, 351–355.

SHIMA, M., 1958, On the second volcanic micro-tremor at the volcano Aso, *Ann. Disast. Prevent. Res. Inst. Kyoto Univ.*, **22**, 1–6.

SHIMIZU, H., S. UEKI and T. KOYAMA, 1987, A tensile-shear crack model for the mechanism of volcanic earthquakes, *Tectonophysics*, **144**, 287–300.

SHIMOZURU, D., 1979, Estimation of the superficial structure of volcanoes by the use of air gun, *Bull. Volcanol. Soc. Japan*, **24**, 25–26 (in Japanese).

SHIMOZURU, D. and T. KAGIYAMA, 1989, Some significant features of pre-eruption volcanic earthquakes, in "Volcanic Hazards", edited by J.H. Latter, Springer-Verlag, Berlin, Heidelberg, pp. 504–512.

SHIMOZURU, D., K. KAMO and W.T. KINOSHITA, 1966, Volcanic tremor of Kilauea Volcano, Hawaii, during July-December, 1963, *Bull. Earthq. Res. Inst., Univ. Tokyo*, 44, 1093–1133.

SHIMOZURU, D., S. UTIBORI, N. GYODA, E. KOYAMA, T. MIYAZAKI, T. MATSUMOTO, N. OSADA and H. TERAO, 1975, The 1973 explosive activity of Asama Volcano. General description of volcanic and seismic events, *Bull. Earthq. Res. Inst., Univ. Tokyo*, **50**, 115–151 (in Japanese with English abstract).

SHIMOZURU, D., N. GYODA, T. KAGIYAMA, E. KOYAMA, M. HAGIWARA, and H. TSUJI, 1982, The 1982 eruption of Asama Volcano, *Bull. Earthq. Res. Inst., Univ. Tokyo*, **57**, 537–559 (in Japanese with English abstract).

SUDO, Y., 1991, An attenuating structure beneath the Aso Caldera determined from the propagation of seismic waves, *Bull. Volcanol.*, **53**, 99–111.

TAKAHASHI, H. and Y. HOSOYA, 1978, Variation in chemical species in the groundwater around the Asama volcano–Relation of the explosive activity in 1973–, *Bull. Earthq. Res. Inst., Univ. Tokyo*, **53**, 551–568 (in Japanese with English abstract).

TAKEO, M., 1985, Near-field synthetic seismograms taking into account of the effects of anelasticity–The effects of anelastic attenuation on seismograms caused by a sedimentary layer, *Pap. Meteorol. Geophys.*, **36**, 245–257 (in Japanese with English abstract).

TAKEO, M., 1987, An inversion method to analyze the rupture process of earthquakes using near-field seismograms, *Bull. Seism. Soc. Am.*, **77**, 490–513.

TAKEO, M., 1992, The rupture process of the 1989 offshore Ito earthquakes preceding a submarine volcanic eruption, *J. Geophys. Res.*, **97**, 6613–6627.

TAKEO, M. and K. ABE, 1981, Analysis of accelerograms by recursive-filter method, *Zisin*, **34**, 351–364 (in Japanese with English abstract).

TAKEO, M., N. HAMADA, S. KASHIWABARA and K. UHIRA, 1984, Analysis of long-period seismic waves excited by the explosive eruption of Mt. Asama on April 8, 1983, *Bull. Volcanol. Soc. Japan*, **29**, 31–44 (in Japanese with English abstract).

TAKEO, M., H. YAMASATO, I. FURUYA and M. SEINO, 1990, Analysis of long-period seismic waves excited by the November 1987 eruption of Izu-Oshima volcano, *J. Geophys. Res.*, **95**, 19377–19393.

TAKEYAMA, I., Y. TANAKA, E. KOBAYASHI and Y. ISONO, 1959, On the seismic waves and air-shocks caused by the explosion of volcano Asamayama, Nov. 10, 1958, *Quart. J. Seism.*, **25**, 45–53 (in Japanese with English abstract).

TANAKA, H. and H. JINGU, 1979, On the type of volcanic earthquakes, at Asamayama Volcano, *Pap. Meteorol. Geophys.*, **30**, 61–74 (in Japanese with English abstract).

TOKAREV, P.I., 1971, Forecasting volcanic eruptions from seismic data, *Bull. Volcanol.*, **35**, 243–250.

TOKAREV, P.I., 1983, Experience in predicting volcanic eruptions in the USSR, in "Forecasting Volcanic Events", edited by H. Tazieff and J.C. Sabroux, Elsevier, New York, pp. 267–270.

TSUJI, H., N. GYODA, E. KOYAMA, Y. IDA, T. KAGIYAMA and M. HAGIWARA, 1990, Seismic velocity and distribution of volcanic earthquakes at Asama Volcano, *Programme and Abstracts of the Volcanol. Soc. Japan*, Fall meeting of 1990, pp. 70 (in Japanese).

UEKI, S., H. SHIMIZU and T. KONO, 1982, Seismograms of volcanic and non-volcanic earthquakes observed at volcano Asama, *Bull. Volcanol. Soc. Japan*, **27**, 328–329 (in Japanese).

UHIRA, K., 1993, Velocity structure beneath Kagoshima, deduced from explosion earthquakes of Sakurajima volcano–Rayleigh wave prograde sense rotation–, *Bull. Volcanol. Soc. Japan*, **38**, 213–217.

UHIRA, K. and M. TAKEO, 1994, The source of explosive eruption of Sakurajima volcano, Japan, *J. Geophys. Res.*, **99**, 17775–177789.

UHIRA, K., T. YAMASATO and M. TAKEO, 1994, Source mechanism of seismic waves excited by pyroclastic flows observed at Unzen volcano, Japan, *J. Geophys. Res.*, **96**, 17757–17773.

UHIRA, K., S. IKEDA, and M. TAKEO, 1995 a, Source process of explosion earthquakes deduced from short-period records at Sakurajima volcano, *Bull. Volcanol. Soc. Japan*, **40**, 295–310.

UHIRA, K., H. YAMASATO, T. HASHIMOTO, K. FUKUI, and M. TAKEO, 1995 b, Source mechanism of low-frequency seismic events at Unzen volcano, Kyushu, Japan–Volcanic tremor on May 10 and explosive earthquake of June 11, 1991–, *Bull. Volcanol. Soc. Japan*, **40**, 311–327.

UKAWA, M. and M. OHTAKE, 1987, A monochromatic earthquake suggesting deep-seated magmatic activity beneath the Izu-Oshima volcano, Japan, *J. Geophys. Res.*, **92**, 12649–12663.

WADA, T. and H. ONO, 1963, Spectral study of volcanic micro-tremors (1) Propagation of the micro-tremors of the 1st kind observed at Volcano Aso, *Bull. Volcanol. Soc. Japan*, **8**, 1–10 (in Japanese with English abstract).

YAMASATO, H., 1987, Distribution of the initial motions of explosion earthquakes at Sakurajima Volcano, *Bull. Volcanol. Soc. Japan*, **32**, 289–300 (in Japanese with English abstract).

ZHAO, L.S. and D.G. HARKRIDER, 1992, Wave fields from an off-center explosion in an embedded solid sphere, *Bull. Seism. Soc. Amer.*, **82**, 1927–1955.

(Received May 15, 1998)
(Accepted February 1, 1999)

Appendix: The Sompi method

1. Theory

The Sompi method was proposed by KUMAZAWA *et al.* (1983, 1990). The Sompi spectral analysis gives a higher frequency resolution and a more reliable power amplitude than the conventional spectral analysis (e.g., the MEM or FFT method). ASAKAWA *et al.* (1988) estimated the geomagnetic transfer function using the Sompi method. HORI *et al.* (1989) discussed the Earth's free oscillations using the Sompi spectral analysis. The principle and the procedure of the Sompi method are described in ASAKAWA *et al.* (1988) and HORI *et al.* (1989). The Sompi spectral analysis is very useful for obtaining descriptions of seismograms of volcanic earthquakes in the requency domain. An outline of the principle and the procedure of the Sompi method is given by ASAKAWA *et al.* (1988), HORI *et al.* (1989) and KUMAZAWA *et al.* (1990). Here we mention only the main features of the Sompi method following the work of ASAKAWA *et al.* (1988). The Sompi method breakes time series data down into white noise plus a signal. The signal is assumed to apply the autoregressive (AR) process, and it is represented by the sum of finite numbers of wave elements of a complex amplitude and a complex frequency:

$$y_l = x_l + \mathrm{n}_l, \tag{A 1}$$

where y_l, x_l and n_l denote the observable time series data, the signal, and observation error. n_l is assumed to be random noise with a normal distribution $N(0, \sigma^2)$. The AR coefficients are determined by the least squares method to obtain the following S minimum,

$$S = \frac{1}{N-2m} \sum_{l=m+1}^{N-m} \left(\sum_{i=-m}^{m} a_i \cdot y_{l-i} \right)^2 = minimum, \tag{A 2}$$

under the condition that $\sum_{i=-m}^{m} a_i^2$ is 1. At this point we should specify the number of AR coefficients, i.e., AR order. We use the method of Lagrange's undetermined multiplier and obtain the following equation.

$$\sum_{k=-m}^{m} P_{jk} a_k = \lambda a_j \ (j = -m, \ -m+1, \cdots, \ m-1, \ m), \tag{A 3}$$

where

$$P_{jk} = \frac{1}{N-2m} \sum_{l=m+1}^{N-m} y_{l-j} \cdot y_{l-k} = P_{kj} \cdot$$

Under the condition that $\sum_{j=-m}^{m} a_i^2$ is 1, the eigen value λ gives an estimate of σ^2. The autocovariance matrix **P** in the Eq. (A 3) is the non-Toeplitz, positive definite and symmetric matrix.

The time series x_l is expressed as a sum of finite numbers of wave elements. KUMAZAWA *et al.* (1983) named the wave element Namiso. One Namiso or one wave element $W(t, f)$ can be represented as

$$W(t.f)=A(f)\cdot\exp(2\pi ift), \tag{A 4}$$

where $A(f)$ is complex amplitude and f is a complex frequency.

$A(f)$ and f are defined by

$$A(f)=|A(f)|\cdot\exp(i\phi),$$

$$f=f_{re}+if_{im},$$

where $|A(f)|$ and ϕ denote initial amplitude and phase, respectively.

Eq. (A 1) is rewritten as

$$W(t,f)=|A(f)|\cdot\exp(i\phi)\cdot\exp(-2\pi f_{im}t)\cdot\exp(2\pi if_{re}t),$$

where f_{im} denotes attenuation factor. Complex amplitude has information on initial amplitude ($|A(f)|$) and phase (ϕ) and complex frequency has information on frequency (f_{re}) and attenuation factor (f_{im}). The Sompi method represents line spectra.

There are two main differences between the Sompi method and the conventional method: 1) AR coefficients are determined by solving an eigen equation (A 3). The Sompi method determines a_i from Eq. (A 2) under the condition $\sum_{i=-m}^{m} a_i^2=1$, whereas the conventional AR method or the MEM method solves the normal equation (e.g., Yule-Walker equation) and gives a solution of a_i to minimize the prediction error with the condition that a_{-m} is 1; 2) the autocovariance matrix **P** in Eq. (A 3) is non-Toeplitz, positive-definite and symmetric matrix. The use of an autocovariance matrix of the non-Toeplitz type can describe the decay rate of a signal. While the autocovariance matrix in conventional AR models is of the Toeplitz type, which treats only a stationary signal.

2. Comparison of the Sompi method and the conventional method

Before we make a comparison of resolution between the Sompi method and the conventional method for seismograms of volcanic earthquakes, we calculate the power spectral density of synthetic time series.

Example 1. Sampling interval and total data are assumed to be unity and 50, respectively. Synthetic time series consists of two different time series. One is f1(t) $=2.5\cdot\cos(0.25\cdot2\pi t)$ and the other is f2(t)$=1.0\cdot\exp(-0.001)\cdot\cos(2.0\cdot2\pi t)$. These data contain no white noise. Fig. A-1 a, 1 b show that the Sompi method resolved two spectral peaks. The AR order is assumed to be 4. However, both the FFT and the MEM exhibit broad peaks around 0.1 Hz and do not give good resolution (Fig. A-1 c).

Example 2. Sampling interval and total data are assumed to be unity and 50, respectively. Synthetic time series is the sum of two time series. One is f1(t)$=2.5\cdot$

exp $(-0.001)\cdot\cos(25.0\cdot 2\pi t)$ and the other is $f2(t)=1.0\cdot\exp(0.0025)\cdot\sin(25.0\cdot 2\pi t)$. The Sompi method exactly resolved the two spectral peaks. Attenuation factors were also determined (Fig. A-2 a, 2 b), while the FFT and MEM method could resolve only one peak at approximately 25 Hz (Fig. A-2 c).

Example 3. Seismogram of an explosion event. Fig. A-3 shows a comparison of the spectral estimate provided by the Sompi method, the FFT and the MEM method for a seismogram of an explosion event. Sampling interval and total number of data are 0.1 s and 200. The Sompi method broke the seismogram down into 9 Namisos assuming the AR order to be 18. Approximately 0.2 and 2 Hz peaks are predominant (Fig. A-3 a, 3 b). The FFT and MEM methods provided a resolution of approximately a 0.5 Hz peak (Fig. A-3 c).

Thus the Sompi spectral analysis gives a higher frequency resolution and a more reliable power amplitude than the FFT or MEM method.

3. Running spectra of volcanic earthquakes using the Sompi method

We applied the Sompi method to the running spectra for volcanic earthquakes (SAWADA *et al.*, 1989). The spectra were calculated for a 1.5 sec time window at 0.5 sec time intervals. The power spectral density is scaled on a linear scale and normalized by the maximum power density at every time window. AR order is assumed to be 20 in a 1.5 sec time window. The open bar indicates decaying Namiso in the time window. The solid bar shows an increasing one in the same time window. Fig. A-4 shows the running power spectra of the vertical component of a BH-type event from station MAE. The characteristic of running spectra of BH- and BM-type events is that the maximum peak frequency changes randomly with time (cf. MORI *et al.*, 1989). In Fig. A-4 we can see that the maximum peak frequency changes randomly with time (between solid arrow in Fig. A-4). Frequency range of BH-type events is dominant at a high frequency of approximately 20 Hz.

Fig. A-5 indicates running power spectra of the vertical component of a BH-type event from station SAN. In Fig. A-5 between the solid arrow, the peak frequency also changes randomly with time. However, the duration is much shorter than that from station MAE. Fig. A-6 shows the running spectra of a BM-type event from station MAE. A tendency that the peak frequency changes randomly with time is also recognized (between solid arrow in Fig. A-6). Discrepancy with the running spectra of BH-type event from station SAN is that high-frequency waves are much more dominant in the seismograms of a BM-type event from station MAE than that of a BH-type event from station SAN. Fig. A-7 shows running spectra of the vertical component of a BL-type event from station MAE. Duration at approximately 1 Hz peak frequency was several sec in the initial phase (between solid arrow). Thus we can clearly distinguish the three sub-groups of the B-type event.

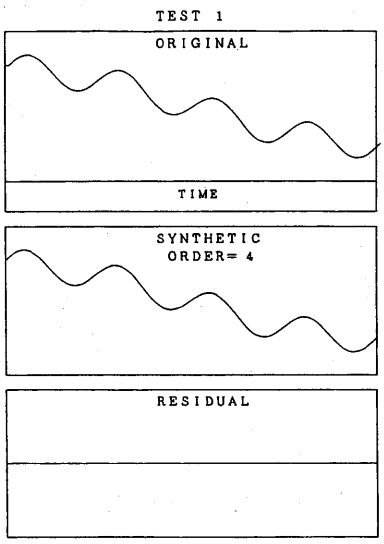

a.

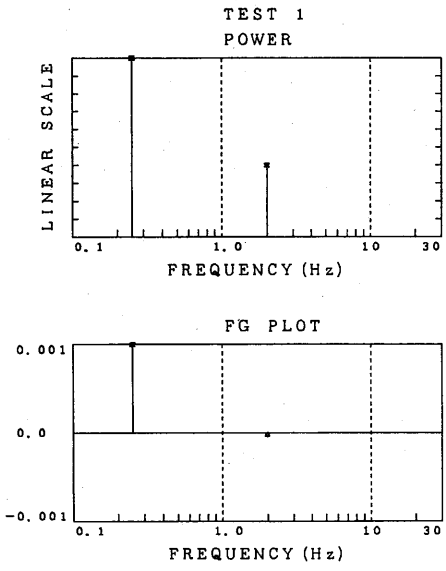

b.

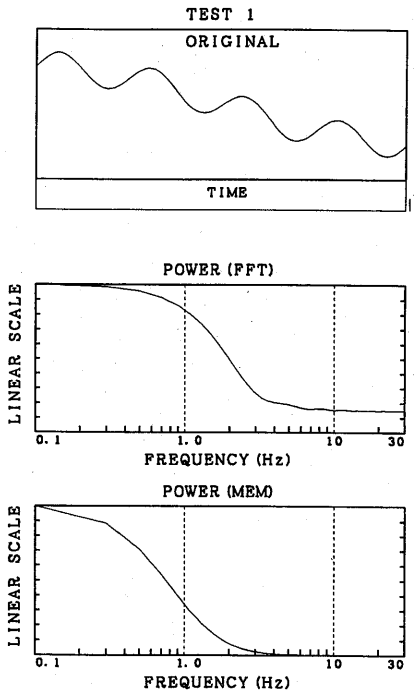

c.

Fig. A-1. Comparison of spectral estimates obtained by the Sompi method, the FFT, and the MEM method for synthetic time series.

a. The top shows synthetic time series of
$F(t)=2.5\cdot\cos(0.25\cdot 2\pi t)+1.0\cdot\exp(-0.001)\cdot\cos(2.0\cdot 2\pi t)$.
Sampling interval is taken as unity and total number of data is 50. At middle is synthetic time series calculated from Namisos obtained by the Sompi method. We assumed AR order to be four. At bottom are the residuals that subtract the synthetic time series by the Sompi method from the original one.

b. At top is the power spectral density estimated by the Sompi method. At bottom is the decaying rate of Namisos. Two Namiso are obtained by the Sompi method. The frequencies and the amplitude of Namisos estimated by the Sompi method are 0.25 Hz, 1 Hz and 1.0 and 0.4. Decaying rate of Namiso at a frequency of 0.25 Hz and 1 Hz are 0.001 and 0. Thus the Sompi method gives good resolution.

c. Comparison of power spectral density estimated by the MEM and the FFT. Neither method gives good resolution.

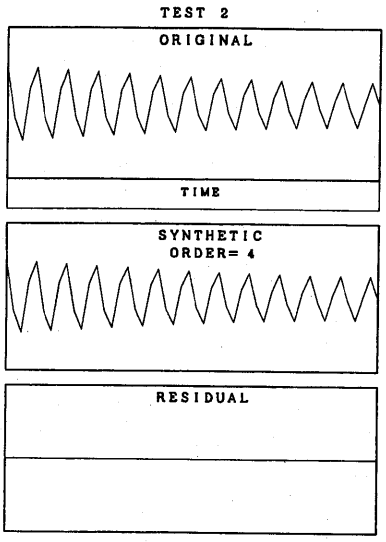

a.

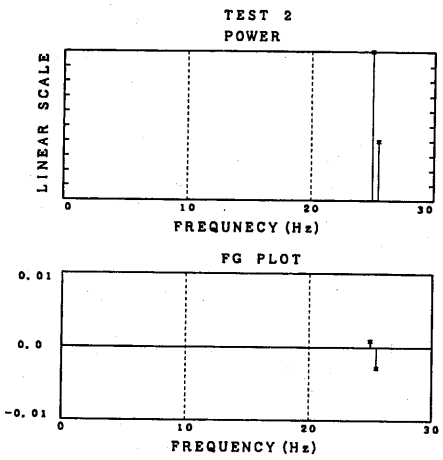

b.

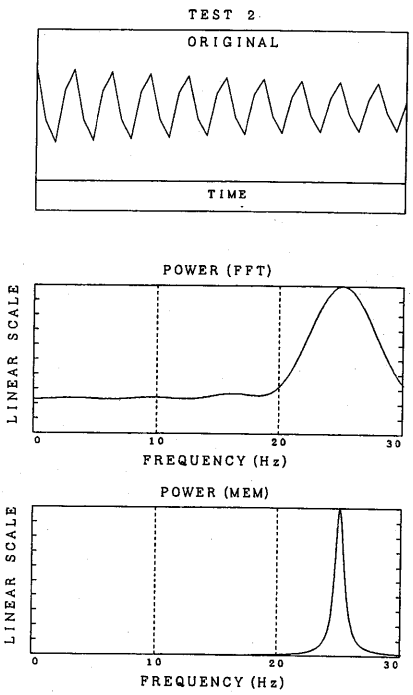

c.

Fig. A-2. Comparison of spectral estimates obtained by the Sompi method, the FFT and the MEM method for synthetic time series.

a. At top is synthetic time series of $F(t) = 1.0 \cdot \exp(0.001) \cdot \cos(25.0 \cdot 2\pi t) + 0.4 \cdot \exp(0.0025) \cdot \sin(25.0 \cdot 2\pi t)$. Sampling interval is taken as unity and total number of data are 50. At middle is synthetic time series calculated from Namisos obtained by the Sompi method. We assumed AR order to be four. At bottom are the residuals that subtract the synthetic time series by the Sompi method from the original one.

b. At top is the power spectral density estimated by the Sompi method. At bottom is the decaying rate of Namisos. Two Namiso are obtained by the Sompi method. The frequencies and the amplitude of Namiso estimated by the Sompi method are 25 Hz, 25.2 Hz and 1.0 and 0.4. Decaying rate of Namiso at a frequency of 25 Hz and 25.2 Hz are 0.001 and -0.0025. The Sompi method gives good resolution.

c. Comparison of the spectral estimates obtained by the FFT method and the MEM method for synthetic time series.

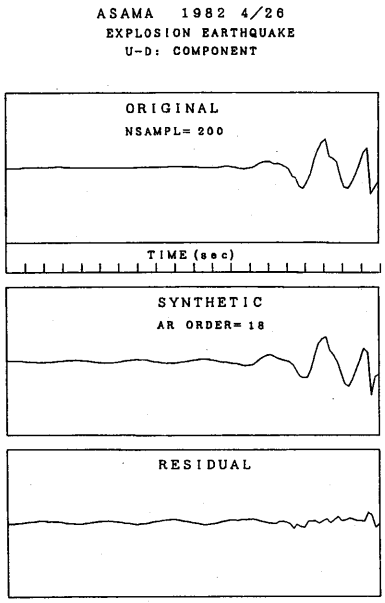

a.

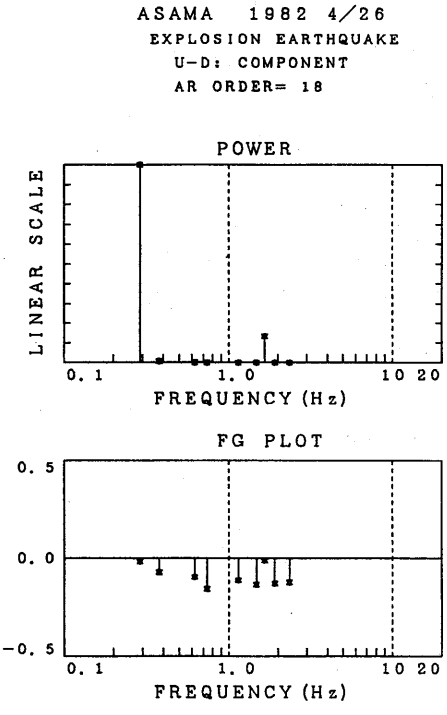

b.

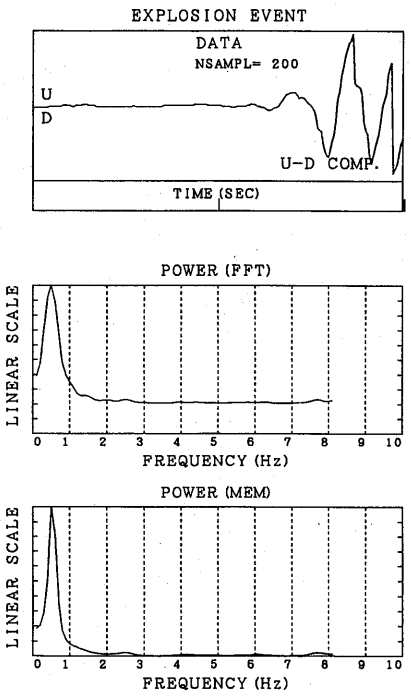

c.

Fig. A-3. Comparison of the spectral estimates obtained by the Sompi method, the FFT and the MEM method for seismogram of an explosion earthquake.
a. At top are seismograms of the vertical component of the explosion event on April 26, 1982 recorded by 5 s seismographs (cf. Fig. 22). At middle are synthetic seismograms calculated from Namisos obtained by the Sompi method. At bottom are the residuals that subtract the synthetic seismogram by the Sompi method from the observed one. AR order is assumed to be 18.
b. At top is the power spectral density estimated by the Sompi method. Approximately 0.2 and 2 Hz peaks are dominant. At bottom is the decaying rate of Namisos. Nine Namiso are obtained by the Sompi method. All Namiso are increasing waves in approximately 20 s time window (cf. Fig. A-3 a).
c. Comparison of power spectral density estimated by the MEM and the FFT methods. Both methods resolve only one peak of spectral power density of approximately 0.5 Hz.

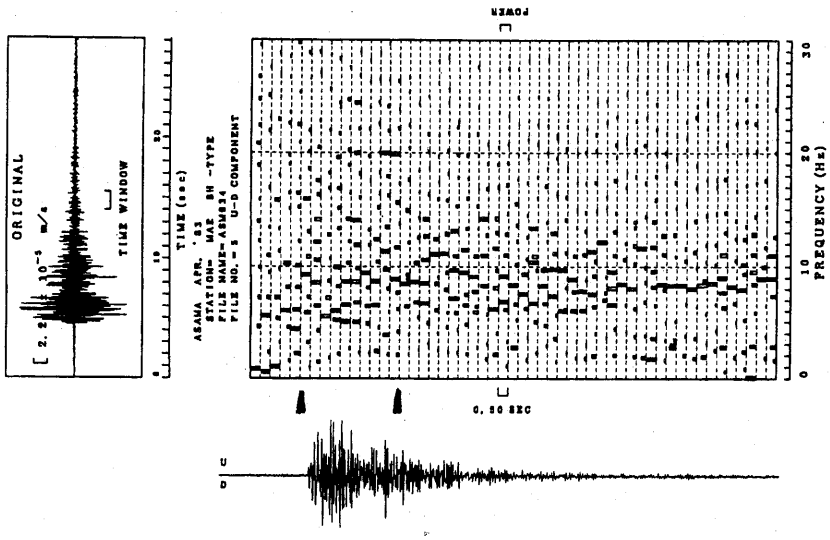

Fig. A-4. Running spectra obtained by the Sompi method for the vertical component of a BH-type event from station MAE. The spectra were calculated for a 1.5-s time windows at 0.5 s time intervals.
AR order is assumed to be 20 at each window. Power spectral density is depicted on a linear scale. The open bar indicates decaying Namiso in a 1.5-s time window. The solid bar shows an increasing one in the same time window.

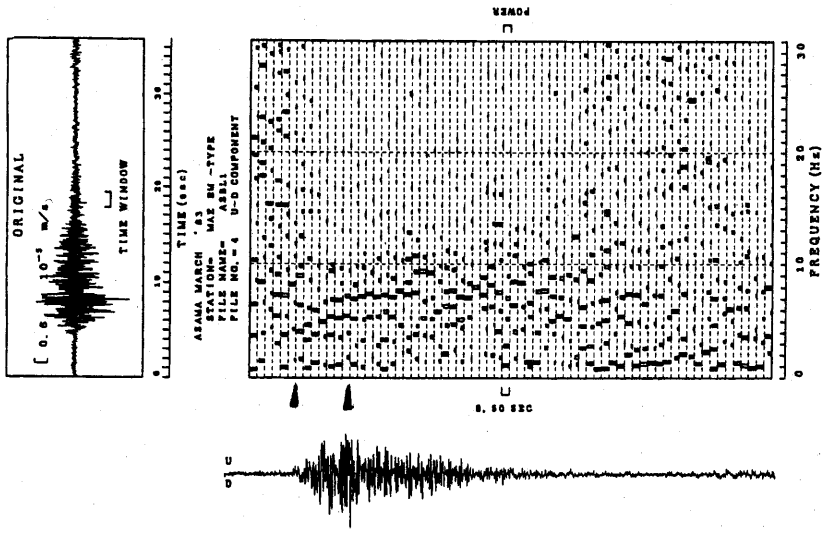

Fig. A-5. Running spectra obtained by the Sompi method for the vertical component of a BH-type event from station SAN.

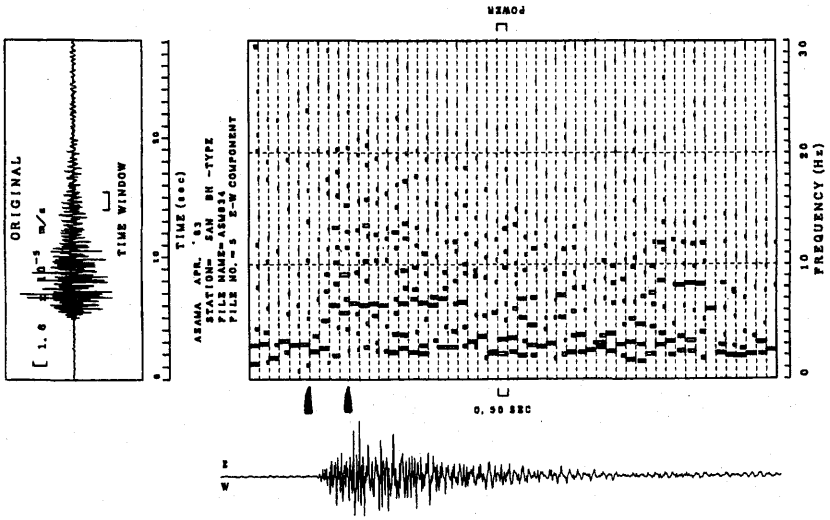

Fig. A-6. Running spectra obtained by the Sompi method for the vertical component of a BM-type event from station MAE.

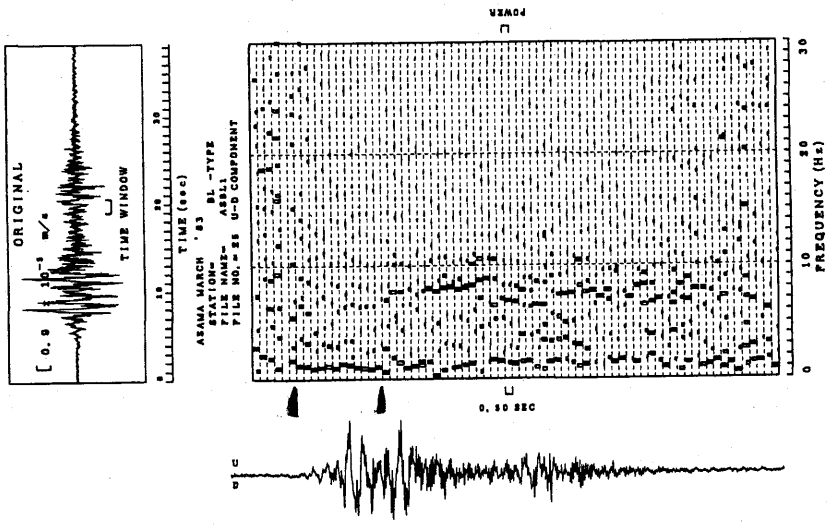

Fig. A-7. Running spectra obtained by the Sompi method for the vertical component of a BL-type event from station MAE.

Munehisa SAWADA

浅間火山で観測されるB型地震と爆発地震の震源メカニズムとN型地震の起源

沢 田 宗 久*

東京大学地震研究所

*現在メキシコ国立防災センター

浅間火山の火山性地震の観測は1910年にOMORI (1912) により開始された．浅間火山は桜島火山・十勝岳と同様の安山岩質の活火山であり，ブルカノ式の爆発的な噴火をする火山として知られている．1910年から1960年代のはじめにかけて，浅間火山は活発な噴火活動を繰り返した．最近では，1982年1983年に2回の噴火活動を行った後，静穏な状態が続いている．浅間火山に発生する火山性地震は，1) 通常の構造性の地震に波形が似たP相・S相の比較的明瞭なA型地震，2) 初動の立ち上がりも，S相も不明瞭でenvelopeが紡錘形の，安山岩質の火山に特徴的なB型地震，3) 5-9 Hzの比較的高周波で始まり，2-4 Hzのmonochromaticな波が長時間継続し，時には振動継続時間が10分間にも及ぶことのあるN型（T型）地震，4) 火山の爆発に伴って発生する爆発地震，5) 火山性微動，の5種類に大別される．A型地震は浅間火山の火口の西側山体の海水面下1-4 kmの範囲と火口の東側約2.6 kmにある観測点SAN付近を震央とし，震源の深さが海水面付近の山体に発生する．それ以外の2)-5)の火山性地震はマグマが地表に流出する経路となる火道にその振動の起源を持つ．MINAKAMI (1960) はB型地震の日別発生頻度から，浅間火山の噴火の確率的な予測を行う事に成功した．これは，浅間火山の活動とB型地震の発生頻度との相関が極めて良く，B型地震の発生頻度がある程度増加すると，浅間火山が必ず噴火するという単純明快な観測事実に基礎を置いている．ところで，浅間火山・桜島・十勝岳のB型地震は互いに波形は良く似ている．しかし，N型地震は浅間火山と十勝岳には発生するが，桜島火山には発生しない．これはN型地震の発生が火山体の構造に依存することを意味する．本研究では，浅間火山の火道に発生の起源を持つと思われるB型地震・N型地震・爆発地震の波形解析とB型地震のうちのBM (Medium-frequency B-type) とBL (Low-frequency B-type) 爆発地震についてのソース・モデルの検討を行い，以下の結論を得た．

1) 浅間火山に発生するB型地震は定性的には安山岩質マグマの発泡あるいは火道内での火山ガスの分離に伴う振動であると考えると，浅間火山のB型地震の発生頻度と火山ガスSO_2の放出量との相関，N型地震の発生原因などを合理的に説明できる．また，この考えはB型地震の発生頻度が浅間火山の火山活動の推移を推定する上で極めて良い指標となっていることを支持する．

2) 浅間火山で発生するB型地震は5-9 Hzの波が卓越するBH (High-frequency B-type) と1-4 Hzの波の卓越するBL (Low-frequency B-type) の他にBM (Medium-frequency B-type) と呼ぶべきB型地震が存在する．BMのスペクトルは低周波部分がBL，高周波部分がBHのスペクトル構造と酷似する．言い換えると，BMはBHとBMが重畳したようなスペクトル構造を持つ．

3) BL-BM—爆発地震の震源位置はBHに比べ相対的に浅い．BLと爆発地震の波形はRayleigh波が卓越しているものと思われる．

4) N型地震は初動から震源を求めると火口の下，海水面下0-1 km近辺に決まる．しかし，N型地震の主要動は火口の東約2.6 kmの位置にある観測点SANで振幅・振動継続時間とも最大となる．またスペクトルも観測点SANで最もシャープとなる．これはN型地震の主要動が観測点SAN付近にあることを意味する．更にparticle motionの解析結果もN型地震の主要動が観測点SAN付近にあることを支持する．

5) N型地震の発生過程を調べると，まずB型地震が群発する．そのあとにB型地震の尾部のやや延びたB型地震とN型地震とのhybrid型と呼ぶべき地震が発生する．つぎに尾部が十分に延びた典型的なN型地震が出現する，という経過をたどる．典型なN型地震の振動の初動のhigh-frequency部分のランニング・スペクトルはB型地震-BMかBHのランニング・スペクトルに酷似する．

6) 従って，N型地震はB型地震によってtriggerされて発生すると考えて良い．B型地震の振動を起こす実体が高温の火山ガスであり，この高温の火山ガスが火口の下の割れ目かあるいは火道の支脈を通り，観測点SAN付近の地下水と接触し，高温の火山ガスによって加熱された地下水から高圧の水蒸気が発生して振動源となり，N型地震が発生すると考えると4) 5)を合理的に説明しうる．これは，N型地震の長時間の振動エネルギーが熱エネルギーによって補給されることを意味する．

7) B型地震のsource mechanismの検討をTAKEO (1987)，UHIRA and TAKEO (1994)のプログラムを用いて行った．BH型地震についてはhigh-frequencyのためsource mechanismの推定が困難である．BMとBLの低周波部分と爆発地震の初相（いずれも1 Hz近辺）について，1) explosive source，2) 円筒状の圧力源，3) tensile crack，4) moment tensor M_{zz} 成分，5) 鉛直方向のsingle force，6) CLVDの6つの候補のうちから妥当と思われるものを推定することを試みた．このうち，explosive sourceはBM・BL・爆発地震とも理論波形は観測波形に比べてN-S成分の振幅が小さすぎて，観測波形を全く説明できない．また，single force modelは観測波形に合うような力源を考えるためには，上向きの力が卓越するようなモデルにする必要がある．上向きの力が卓越するということは，火山ガス等が下向きに噴出することを意味し，これも採用しがたい．BM・BLの低周波部分については結局2)のcylindricl modelに絞られる．ただし，cylinderの膨張だけではなくて，収縮も考慮しなければ観測波形を説明できない．爆発地震の初相に関しては一例のみの解析であるが，4)のmoment tensorの M_{zz} 成分が観測波形との対応が一番良い．これは，爆発地震の振動が火山ガスの上下方向への噴出に伴って励起される振動であることを示唆する．